

Fall 2013

Fabricating Complex-Shaped Components by Room-Temperature Injection Molding of Aqueous Ceramic Suspension Gels

Valerie Lynn Wiesner
Purdue University

Follow this and additional works at: https://docs.lib.purdue.edu/open_access_dissertations



Part of the [Mechanics of Materials Commons](#)

Recommended Citation

Wiesner, Valerie Lynn, "Fabricating Complex-Shaped Components by Room-Temperature Injection Molding of Aqueous Ceramic Suspension Gels" (2013). *Open Access Dissertations*. 22.
https://docs.lib.purdue.edu/open_access_dissertations/22


This document has been made available through Purdue e-Pubs, a service of the Purdue University Libraries. Please contact epubs@purdue.edu for additional information.

**PURDUE UNIVERSITY
GRADUATE SCHOOL
Thesis/Dissertation Acceptance**

This is to certify that the thesis/dissertation prepared

By Valerie L. Wiesner

Entitled
Fabricating Complex-Shaped Components by Room-Temperature Injection Molding of Aqueous Ceramic Suspension Gels

For the degree of Doctor of Philosophy 

Is approved by the final examining committee:

Rodney Trice _____
Chair

Jeffrey Youngblood _____

Elliott Slamovich _____

Carlos Martinez _____

To the best of my knowledge and as understood by the student in the *Research Integrity and Copyright Disclaimer (Graduate School Form 20)*, this thesis/dissertation adheres to the provisions of Purdue University's "Policy on Integrity in Research" and the use of copyrighted material.

Approved by Major Professor(s): Rodney Trice _____

Jeffrey Youngblood _____

Approved by: David Bahr _____ 12/02/2013 _____
Head of the Graduate Program Date

FABRICATING COMPLEX-SHAPED COMPONENTS BY ROOM-TEMPERATURE
INJECTION MOLDING OF AQUEOUS CERAMIC SUSPENSION GELS

A Dissertation

Submitted to the Faculty

of

Purdue University

by

Valerie Wiesner

In Partial Fulfillment of the

Requirements for the Degree

of

Doctor of Philosophy

December 2013

Purdue University

West Lafayette, Indiana

For my mom and dad

ACKNOWLEDGEMENTS

This work was funded by National Science Foundation Materials and Surface Engineering CMMI Grant 0726304 and U.S. Department of Education GAANN Grant P200A10036. Additional support and access to resources at NASA Glenn Research Center were provided through the NASA Pathways Program. I would like to thank Dr. Joe Grady for his support and valuable discussions, Dr. Bryan Harder for XRD assistance, Bob Angus for sintering work and the rest of the Ceramic Branch and the Durability & Protective Coatings Branch at NASA Glenn Research Center for their support.

I am truly grateful to my advisors, Prof. Rodney Trice and Prof. Jeffrey Youngblood, for their guidance and support ever since my first materials research experience in 2005. I am also grateful to a number of professors, staff and students within Purdue MSE that provided invaluable input, assistance and training throughout my time at Purdue. I would like to recognize Prof. Carlos Martinez, Prof. Elliott Slamovich, Prof. Kendra Erk, Patti Metcalf, Dave Meyer, Patti Finney, Vicki Cline, Donna Bystrom as well as the Trice and Youngblood research groups for their help and advice in and out of the lab. I would also like to thank Prof. Alyssa Panitch and her group in the Weldon School of Biomedical Engineering at Purdue University for training and use of rheometric equipment along with Dr. Jennifer Groh and the Graduate Mentoring Program Leadership Team for their invaluable support.

My graduate experience has been positive, rewarding and incredibly enjoyable, thanks especially to the following for their help and friendship: Manuel Acosta, WinnieTan, Stephanie Gong, Jen-Chieh Liu, Jui-Hsun Sherry Lu, Colton Steiner, James Fleetwood, Kristin Paulson, Jairo Diaz, Lisa Rueschhoff, Andrés Díaz Cano, Andrew Rosenberger, Lisa Murray, Alex Bruce, Sammy Saber, Pylin Sarobol, Luthfia Syarbaini, Lea Marlor, Kera Lovell, Chelsea Stripe, Christy Lowney, Dorothée Bouquet, Sergii Kravchenko and Oleksandr Kravchenko. I am also appreciative of Cherrale Ricks, Elina Alterman, Kelly Jacob, Jessica Austin, Hana Podhoretz and Olivia Jee for their friendship and support.

I owe all of my success to my mom as well as to my dad and family for their unwavering support and encouragement, which continues to motivate me to achieve my goals and realize my dreams.

TABLE OF CONTENTS

	Page
LIST OF TABLES	ix
LIST OF FIGURES	x
ABSTRACT	xiv
CHAPTER 1. INTRODUCTION.....	1
1.1 Ultra-High Temperature Ceramics.....	1
1.2 Densification and Processing of Zirconium Diboride.....	2
1.3 Powder Injection Molding.....	5
1.3.1 Material Selection and Feedstock Preparation for Traditional Ceramic Injection Molding	6
1.3.2 Conventional Ceramic Injection Molding Procedure.....	9
1.3.3 Binder Burnout and Sintering	11
1.3.4 Current Status of Ceramic Injection Molding.....	13
1.4 Alternative Room-Temperature Injection Molding Method for Zirconium Diboride	14
CHAPTER 2. DEVELOPMENT OF ALUMINA CERAMIC SUSPENSION GELS FOR ROOM-TEMPERATURE INJECTION MOLDING	16
2.1 Utilizing Unique Flow Properties of Alumina-Polymer Suspensions for Room-Temperature Injection Molding.....	16
2.1.1 Alumina-PVP Suspension Preparation.....	17
2.2 Design and Approach of Room-Temperature Injection Molding.....	22
2.2.1 Room-Temperature Injection Molding Procedure.....	22
2.2.2 Previous Modifications to Room-Temperature Injection Molding Process	26
2.2.2.1 Eliminating Crack Formation during Drying.....	27
2.2.2.2 Preventing Closed Pore Formation.....	29
2.2.3 Binder Burnout and Pressureless Sintering of Injection Molded Alumina Rings	32

2.2.4	Preparation of Alumina Specimens for Mechanical Characterization	33
2.3	Experimental Approach for Characterization of Alumina Rings Produced by Room-Temperature Injection Molding of Alumina CeraSGels	34
2.3.1	Rheology of Alumina CeraSGels with Varying PVP Content	35
2.3.2	Machinability in Green State	36
2.3.3	Density and Internal Porosity of Sintered Specimens	37
2.3.4	Ultimate Strength of Sintered Alumina C-Ring Samples.....	38
2.3.5	Statistical Analysis of Density, Grain Size and Ultimate Strength of Sintered Alumina C-Ring Samples.....	40
2.4	Results and Discussion of Alumina CeraSGels for Room-Temperature Injection Molding.....	41
2.4.1	Rheological Behavior and Processability of Alumina Suspensions with Varying PVP Content.....	41
2.4.2	Green Machinability and Density of Alumina Components	47
2.4.3	Sintered Density and Microstructure of Alumina C-Ring Specimens.....	49
2.4.4	Mechanical Properties of Sintered Alumina C-Ring Specimens...	51
2.4.5	Varying Molecular Weight at Optimal PVP Concentration.....	53
2.5	Summary and Conclusions of Room-Temperature Injection Molding of Alumina-PVP Suspensions	57
2.6	Perspectives on Improving and Optimizing Room-Temperature Injection Molding for Manufacturing Alumina Ring-Shaped Specimens	59
2.6.1	Reducing Drying Time of Formed CeraSGel Samples	59
2.6.2	Improving Sintered Mechanical Properties of Alumina Rings.....	60
CHAPTER 3. EXPERIMENTAL AND ANALYTICAL INVESTIGATION OF THE RHEOLOGY AND STABILITY OF ALUMINA-PVP SUSPENSIONS.....		61
3.1	Understanding Dispersion and Stability in Colloidal Systems	62
3.1.1	Colloidal Stability	62
3.2	Experimental Investigation of Room-Temperature Rheology of Alumina-PVP Suspensions.....	66
3.2.1	Formulating Alumina-PVP Suspensions.....	66
3.2.2	Rheological Characterization of Dispersed Alumina-PVP Suspensions	71
3.3	Results and Discussion of the Experimental Characterization of Alumina-PVP Suspensions.....	71
3.3.1	Polymer-Dispersant Interactions with Alumina.....	71
3.3.2	Effect of PVP Concentration and Average Molecular Weight	72
3.3.3	Stress and Frequency Response of Alumina-PVP Suspensions	74
3.3.4	Thixotropy Investigations of Alumina/Dolapix CE64/PVP Aqueous Suspensions.....	78

	Page
3.3.5 Rheological Influence of Polymer Solutions	80
3.3.6 Implications of Experimental Evaluation of the Rheological Properties of Aqueous Alumina-PVP Suspensions	80
3.4 Analytical Study of Alumina/DI Water/Dolapix CE64/PVP Suspensions through Modeling of Potential Interactions	82
3.4.1 Modeling Potential Interactions of Alumina/DI Water/Dolapix CE64/PVP Suspensions	82
3.5 Summary and Conclusions of Ascertaining the Rheology and Potential Interactions of Aqueous, Highly Loaded Alumina-Polyvinylpyrrolidone Suspensions.....	90
 CHAPTER 4. ADAPTING ROOM-TEMPERATURE INJECTION MOLDING TO ZIRCONIUM DIBORIDE-POLYVINYLPIRROLIDONE SUSPENSIONS	 93
4.1 Producing Dense Zirconium Diboride Rings by Room-Temperature Injection Molding.....	93
4.1.1 Formulation of ZrB ₂ -PVP Suspension Gels	93
4.1.2 Modifications of Room-Temperature Injection Molding for ZrB ₂ -Based Suspensions	97
4.1.3 Binder Burnout and Pressureless Sintering of Injection Molded ZrB ₂ Rings	98
4.1.4 Preparation of ZrB ₂ Specimens for Mechanical Characterization	98
4.2 Characterizing ZrB ₂ /B ₄ C/WC-PVP Suspensions for Room-Temperature Injection Molding.....	100
4.2.1 Characterization of ZrB ₂ /B ₄ C/WC-PVP Suspensions Rheology and pH	100
4.2.2 Density and Material Composition of Sintered Specimens.....	100
4.2.3 Ultimate Strength of Sintered ZrB ₂ C-Ring Samples.....	101
4.3 Determining the Optimal ZrB ₂ /B ₄ C/WC-PVP Suspension for Room- Temperature Injection Molding	102
4.3.1 Rheological Behavior and Processability of ZrB ₂ /B ₄ C/WC Suspensions with Varying PVP Content.....	102
4.3.2 Green Machinability of Room-Temperature Injection Molded ZrB ₂ Specimens	106
4.3.3 Sintered Density, Microstructure and Composition of Room- Temperature Injection Molded ZrB ₂ Specimens	106
4.3.4 Mechanical Properties of Sintered ZrB ₂ C-Ring Specimens.....	111
4.4 Summary and Conclusions of Room-Temperature Injection Molding of ZrB ₂ -Based CeraSGels	112
4.5 Recommendations for Future Work.....	114
4.5.1 High-Temperature Mechanical Testing of ZrB ₂ -Based C-Rings	114

	Page
4.5.2 Silicon Carbide Particulate Reinforcing Phase for ZrB ₂ Prepared by Room-Temperature Injection Molding.....	114
CHAPTER 5. CONCLUSIONS AND FUTURE WORK.....	117
LIST OF REFERENCES.....	123
VITA.....	133
PUBLICATIONS	135

LIST OF TABLES

Table	Page
Table 2.1 Compositions of alumina-PVP suspensions with corresponding curve-fit parameters using the Herschel-Bulkley equation for yield-pseudoplastic fluids, average green and sintered densities and C-ring strength values for sintered samples prepared by room-temperature injection molding of suspensions with varying content of PVP with molecular weight of 55,000 g/mol.....	20
Table 2.2 Alumina suspension compositions with corresponding Herschel-Bulkley curve-fit parameters, average green and sintered densities and C-ring strength values for sintered samples prepared by room-temperature injection molding of suspensions with 2.5 vol.% PVP of varying molecular weights.....	21
Table 3.1 Compositions of A16 SG alumina suspensions fabricated without PVP and with increasing inorganic content (30-54.7 vol.% alumina).	67
Table 3.2 Compositions and calculated curve fit parameters from the Herschel-Bulkley model used in flow curves ($R=0.99$) of A16 SG alumina suspensions fabricated with PVP contents of 1, 2.6 and 5.1 vol.% PVP as well as PVP solutions without alumina or dispersant. P_r represents the ratio of the lowest molecular weight PVP to the total amount of PVP in the formulation.	69
Table 4.1 Compositions of zirconium diboride-based CeraSGels with effective yield stress and pH values for suspensions with varying amounts of PVP with molecular weight of 10,000 g/mol as well as average grain size and C-ring strengths for specimens prepared by room-temperature injection molding.....	96

LIST OF FIGURES

Figure	Page
Figure 1.1 Reciprocating screw-type injection molding machine.....	10
Figure 1.2 Reciprocating screw-type injection molding machine.....	11
Figure 2.1 Flow curves of Newtonian, pseudoplastic and yield-pseudoplastic fluids.	17
Figure 2.2 a) Chemical structure of Darvan 821A (ammonium polyacrylate) and b) polyvinylpyrrolidone (PVP).....	18
Figure 2.3 Schematic of room-temperature injection mold device.	23
Figure 2.4 a) Ring-shaped mold with EPDM foam centerpiece and three escape ports adjacent and across from the injection port. b) The injection mold setup between two compression platens of the load frame prior to the injection molding operation. A pneumatic vibrator with dimensions of 5.5 cm × 1.6 cm × 2.3 cm was fixed on top of the ring-shaped mold using cable ties (not pictured) during forming.....	24
Figure 2.5 Final sintered alumina specimen after machining.	26
Figure 2.6 An alumina CeraSGel specimen exhibiting crack and air bubble formation a) before binder burnout and b) after binder burnout and sintering.	27
Figure 2.7 Ring-shaped mold with tapered Plexiglas centerpiece with formed alumina part immediately after injection molding.	28
Figure 2.8 An injection molded alumina CeraSGel part that was formed using an EPDM foam insert and exhibited no cracking after binder burnout and sintering.....	28
Figure 2.9 A valve was fitted to a ball mill bottle to evacuate using a vacuum pump.....	30
Figure 2.10 Injection mold setup with pneumatic vibrator.....	31

Figure	Page
Figure 2.11 An alumina ring was formed using the pneumatic vibrator during injection molding and did not develop closed pores due to air bubble formation. Specimen a) prior to and b) after binder burnout and sintering. ...	32
Figure 2.12 Thermogravimetric analysis revealed that PVP thermally decomposed by 500°C.....	33
Figure 2.13 Evening out surfaces of an alumina ring in the green state using a polishing wheel.....	34
Figure 2.14 Polishing mount used to even out surfaces of CeraSGel samples in the green state using a polish wheel.	37
Figure 2.15 P is the compressive force, r_o is the outer radius and r_i is the inner radius, and b is the width. Thickness t is r_o-r_i	38
Figure 2.16 Flow curves of alumina suspensions with 0, 1 and 5 vol.% PVP (MW = 55,000 g/mol). Curve fits to the Herschel–Bulkley fluid model are shown as black continuous lines with $R > 0.99$	42
Figure 2.17 Log viscosity against log shear rate plots of alumina suspensions prepared with varying contents of PVP with molecular weight of 55,000 g/mol. Increasing PVP content resulted in higher apparent viscosities of suspensions.....	44
Figure 2.18 Oscillatory stress plot of alumina CeraSGels with 2 and 5 vol.% PVP. The higher polymer content corresponds to a high storage modulus, G'	45
Figure 2.19 The storage modulus, G' , is greater than the loss modulus, G'' , for stress oscillations <100 Pa for CeraSGel compositions of 2 and 5 vol.% PVP.....	46
Figure 2.20 Images of alumina parts with a) 1, b) 2.5 and c) 5 vol.% PVP content after machining in the green state using a polishing mount. Samples with less than 2.5 vol.% PVP chipped during machining suggesting a lower green strength when compared with samples with higher binder content.	48
Figure 2.21 SEM micrographs of polished and thermally etched surfaces of alumina samples prepared with suspensions containing a) 1 vol.%, b) 2.5 vol.%, c) 4 vol.% and d) 5 vol.% PVP. All samples were sintered at 1620°C.	50

Figure	Page
Figure 2.22 Plot of average C-ring strength data for sintered specimens prepared with suspensions containing 1, 2.5, 4 and 5 vol.% PVP (MW = 55,000 g/mol). Specimens of 2.5 vol.% PVP exhibited the highest average C-strength. ** p -Values for specimens prepared with 2.5 vol.% PVP were less than 0.05 indicating a statistically significant peak in strength for these specimens.	52
Figure 2.23 Plots of log viscosity vs. log shear rate of alumina suspensions prepared with 2.5 vol.% PVP of varying molecular weights.	55
Figure 3.1 Schematic of a charged ceramic particle in solution with associated charge distribution for its diffuse double layer.	63
Figure 3.2 Schematic of a) steric stabilization, b) bridging flocculation, c) depletion flocculation and d) depletion stabilization.	65
Figure 3.3 Structure of Dolapix CE64 poly(methacrylic acid) used in fabrication of alumina suspensions.	66
Figure 3.4 Flow behavior of alumina suspensions containing 5.1 vol.% PVP of 10,000 g/mol, 55,000 g/mol, 360,000 g/mol, and 1,300,000 g/mol average molecular weights (suspensions listed in Table 2). The black continuous lines are curve fits to the Herschel-Bulkley fluid model ($R \sim 0.99$). Increasing average molecular weight directly affects the consistency (k) and yield stress (σ_y) of the suspensions. Parameters calculated using the Herschel-Bulkley model are listed in Table 2.2.	74
Figure 3.5 Multiple experimental hysteresis loops performed on a) suspension 6A and b) suspension 15A from Table 3.2. The resultant loops are very narrow since the response of the suspensions is not thixotropic (i.e. no time dependence).	76
Figure 3.6 Oscillation stress sweep on alumina a) suspensions 3A and 13A (Table 3.2) and b) suspensions 6A and 10A (Table 3.2) showing a linear viscoelastic region <10 Pa. In both cases, the range of the linear viscoelastic region is independent of polymer concentration and molecular weight.	77
Figure 3.7 Total interaction potential curve for alumina-Dolapix CE64 suspensions without PVP additions exhibits a shallow potential minimum indicating weak flocculation of the suspension.	87

Figure	Page
Figure 3.8 Depletion interaction potential curves for alumina-Dolapix® CE64 suspensions with 5.1 vol.% PVP of varying molecular weights. (Inset depicts total interaction potential curve.)	88
Figure 4.1 Ring-shaped mold with foam centerpiece and three overflow ports.	97
Figure 4.2 Preparing ZrB ₂ -based green body for mechanical testing.	99
Figure 4.3 Final sintered C-shaped ZrB ₂ sample.	99
Figure 4.4 Flow startups (constant shear rate) revealed transient (time-dependent) response of ZrB ₂ -based CeraSGels containing 3 vol.% PVP.....	103
Figure 4.5 Creep plots of shear rate vs. time at stresses of a) 400 Pa, b) 410 Pa and c) 420 Pa. Identical creep data plotted in terms of viscosity vs. time for d) 400 Pa, e) 410 Pa and f) 420 Pa. Blue arrows, green arrows and red arrows indicate Newtonian, shear-thinning shear-thickening behaviors, respectively.....	104
Figure 4.6 SEM micrographs of ZrB ₂ cross-sections of ZrB ₂ specimens prepared by room-temperature injection molding of suspensions with a) 1 vol.%, b) 2 vol.% and c) 3 vol.% PVP contents.....	108
Figure 4.7 Cross section of specimen prepared with 1 vol.% PVP CeraSGel evaluated by EDS showed B ₄ C grains surrounded by ZrB ₂ grains.	109
Figure 4.8 XRD spectra of sintered ZrB ₂ specimens prepared with 1, 2 and 3 vol.% PVP CeraSGels along with spectrum from starting attrition milled ZrB ₂ /B ₄ C/WC powders.	110

ABSTRACT

Wiesner, Valerie L. Ph.D., Purdue University, December 2013. Fabricating Complex-Shaped Components by Room-Temperature Injection Molding of Aqueous Ceramic Suspension Gels. Major Professors: Rodney W. Trice and Jeffrey P. Youngblood

Water-based ceramic suspension gels (CeraSGels) effectively produced dense, near-net shape ceramic parts by room-temperature injection molding, a novel processing method based on traditional ceramic injection molding. This alternative method eliminated the need for heating and cooling feedstocks to process, as is required in conventional injection molding, through control of the rheological response of the CeraSGels by simply varying polymer content without the use of any harsh crosslinking or curing agents or further chemical processes. The development of room-temperature injection molding initially focused on forming CeraSGels based on alumina, a readily available model material, in order to optimize suspension preparation and processing prior to tailoring the process to zirconium diboride (ZrB_2), an ultra-high temperature ceramic (UHTC) system.

CeraSGels were highly loaded (>50 vol.%) with alumina powder and had a minimal amount (≤ 5 vol.%) of water-soluble polyvinylpyrrolidone (PVP). Rheological study of alumina CeraSGels using parallel plate rheometry revealed that suspensions containing PVP as a viscosity modifier behaved like yield-pseudoplastic fluids at room temperature. Because understanding flow properties of CeraSGels was vital to enable

fabrication of ceramic components into useful geometries, estimations of the interparticle interactions, which qualitatively reflected the colloidal stability, of the alumina-PVP suspensions were modeled to correlate with experimental rheological observations.

Alumina ring-shaped samples were successfully injection molded at room temperature using CeraSGels containing 1 to 5 vol.% PVP with molecular weight of 55,000 g/mol. Alumina samples could not be produced by room-temperature injection molding using suspensions without PVP additions. Specimens prepared using PVP-containing alumina CeraSGels exhibited high green body strength and machinability prior to binder removal and sintering, and increasing PVP content was observed to enhance green machinability. Alumina rings with high green densities (60-63% true density (TD)) as found using Archimedes technique were obtained after binder removal, which was accomplished by heating specimens at a rate of 2°C/min to 700°C with an isothermal hold for 1h. In a subsequent heat treatment, specimens were pressureless sintered by heating at a rate of 5°C/min to 1620°C and holding for 1.5h. Bulk density of sintered samples using the Archimedes technique was found to reach 98%TD with linear shrinkage of <16%. Microstructural characterization revealed minimal pore formation within sintered samples regardless of initial PVP content, and average grain sizes were ~3.4 μm. Ultimate strength of the sintered alumina samples was determined using the ASTM C1323-10 compressive C-ring test, and C-strength values were comparable to values found in literature for specimens prepared by conventional processing methods. A minimum strength value of 192 ± 27.2 MPa was found for specimens prepared with CeraSGels containing 5 vol.% PVP, and a maximum of 261 ± 57.6 MPa was obtained for rings produced using CeraSGels with 2.5 vol.% PVP, suggesting it was the optimal

concentration. Alumina CeraSGels containing 2.5 vol.% PVP of varying molecular weights of 10,000, 360,000 and 1,300,000 g/mol were prepared to determine if molecular weight affected the resulting ring-shaped specimens. Despite similar mechanical and microstructural properties, the favorable flow properties as well as high green and sintered densities distinguished CeraSGels containing 2.5 vol.% PVP with a molecular weight of 55,000 g/mol from all other suspensions examined in this study as the optimal PVP molecular weight and concentration to be incorporated into alumina suspensions for room-temperature injection molding.

The room-temperature injection molding technique was later adapted to ZrB_2 , a leading UHTC material that was difficult to fabricate into complex shapes due to its high melting temperature ($>3000^\circ\text{C}$) and sensitivity to impurities during sintering. ZrB_2 -based CeraSGels containing 3.5 wt.% boron carbide (B_4C) and 10.5 wt.% tungsten carbide (WC) sintering aids as well as 1 to 3 vol.% PVP with molecular weight 10,000 g/mol exhibited a time-dependent rheological response. Although the shear stress required to initiate flow for ZrB_2 -based CeraSGels was observed to decrease with increasing PVP content, all suspensions flowed at room temperature to successfully yield dense ring-shaped specimens after binder burnout and sintering. The polymer binder and impurities were removed by a series of heat treatments, which involved heating at a rate of $4^\circ\text{C}/\text{min}$ to 600°C held for 1h in medium vacuum ($\sim 10^{-5}$ Torr) followed by heating at $10^\circ\text{C}/\text{min}$ to 1650°C for a 1-h hold at which point argon was flowed into the system and a final ramp at $10^\circ\text{C}/\text{min}$ to 1850°C for 1.5h that was performed in an inert argon environment, to facilitate pressureless sintering of $\text{ZrB}_2/\text{B}_4\text{C}/\text{WC}$ rings to full density ($>98\%TD$). Microstructural and elemental analysis suggested that the binders did not affect the

resulting composition or microstructure of the ZrB₂-based specimens as no oxide-containing phase were present. Room-temperature mechanical properties were determined using the ASTM C1323-10 compression test. C-strength values ranged from 30.7 ± 12.0 MPa to 75.1 ± 26.7 MPa for specimens prepared by CeraSGels containing 1 and 3 vol.% PVP, respectively. Further processing improvements will likely enhance the resulting mechanical and microstructural properties of ZrB₂ specimens prepared using CeraSGels. Room-temperature injection molding of CeraSGels proved to be a viable, environmentally friendly processing alternative to fabricate dense, complex-shaped ceramic components.

CHAPTER 1. INTRODUCTION

1.1 Ultra-High Temperature Ceramics

New technologies, particularly in aerospace, that involve the design and manufacture of complex-shaped ceramic components have burgeoned in recent decades.¹ ² The development of advanced hypersonic and re-entry vehicles requires materials resistant to erosion and oxidation along with the ability to withstand operating temperatures well above 2000°C that are routinely encountered in the severe re-entry environment.³ Ultra-high temperature ceramics (UHTCs) are ideal candidates for these particular applications, due to their combination of high melting temperature (>3000°C), oxidation and erosion resistance, high thermal conductivity, low density and exceptional strength.^{4,5}

Due to their unique material properties, manufacturing UHTC components is a complex and challenging process that necessitates the use of sintering aids, which may compromise their oxidation resistance and mechanical strength. Conventional processing methods of UHTCs, like hot pressing⁶ or spark plasma sintering,⁷ can form somewhat dense UHTC parts, but these approaches cannot economically produce the complex-shaped components, namely highly curved leading wing-edges for hypersonic vehicles, rocket nozzle-inserts and re-entry vehicle nose cones, needed for aerospace applications without extensive machining.⁴ The capability to form components with complex

geometries is the next step in the development of UHTCs for employment in aerospace and beyond.

UHTC material systems are comprised mostly of the transition metal borides and carbides, including zirconium diboride (ZrB_2), zirconium carbide (ZrC), hafnium diboride (HfB_2) and hafnium carbide (HfC).⁸ HfB_2 and ZrB_2 both exhibit very high thermal conductivities for ceramic materials.^{9, 10} Compared with non-oxide structural ceramics, they have high thermal shock and oxidation resistance coupled with high melting temperatures ($>3000^\circ\text{C}$).¹¹ ZrB_2 in particular has the lowest theoretical density of the UHTC class, making it an incredibly appealing contender for high-temperature structural applications.^{4, 8} This blank thesis is designed to be as self-supporting as possible, and to conform to the Purdue University Style Guidelines. The template has been built with very basic formatting guidelines to acquire Purdue style; therefore, if your department has additional formatting requirements, you may have to adjust a few styles such as subheading numberings or endnotes.

1.2 Densification and Processing of Zirconium Diboride

Zirconium diboride (ZrB_2) is considered to be a leading UHTC material for incorporation into a variety of extreme environment applications, most notably hypersonic aircraft. Because ZrB_2 typically exhibits low volume and grain boundary diffusion rates, high temperatures are required to sinter to full density without the introduction of sintering aids. As a result, a major impetus in the study of sintering of ZrB_2 is underway in order to reduce the temperature needed to densify ZrB_2 , especially without requiring pressure to densify.

Dense zirconium diboride components have been traditionally prepared by hot-pressing at high temperatures ($>2000^{\circ}\text{C}$) with moderate pressures (~ 30 MPa) or at lower temperatures (1800°C) with very high pressures (>800 MPa).¹² Although an effective and repeatable densification method, hot-pressing cannot effectively sinter ceramic components with complex geometries in a high-throughput manner suitable for widespread application.¹³ Recent employment of spark plasma sintering (SPS) to densify UHTC materials, including ZrB_2 , has yielded relative success.^{14,15} SPS entails applying a high, pulsed DC current to a ceramic specimen for rapid heating in combination with uniaxial pressing. The major advantage to applying SPS is that densification can be achieved within minutes of applying current and pressure.¹⁶ ZrB_2 -based ceramics have been spark plasma sintered to full density at 1900°C and at a pressure of 30 MPa for 5 min.¹⁷ However, as with hot-pressing, a notable disadvantage is that complex-shape component production is incredibly challenging by SPS.¹⁸

With pressureless sintering, reduction in post-processing costs as well as near-net shape production of complex-shaped parts is possible, making pressureless sintering a more appealing densification method. Pressureless sintering of zirconium diboride (ZrB_2) and boride ceramics in general has proven to be a challenge in the development and application of these advanced materials mainly due to the unavoidable oxygen impurities that exist on the surface of starting powders that has hindered other sintering procedures previously.¹² These oxygen impurities manifest themselves in the form of boria (B_2O_3) and zirconia (ZrO_2) in the case of ZrB_2 , and in their liquid and vapor form at relatively low temperatures ($\sim 1750^{\circ}\text{C}$). Their presence enhances grain coarsening by increasing

surface diffusion paths. As a result, these surface oxides reduce the driving force to sinter in ZrB_2 samples preventing full densification.¹⁹

The effects of these surface impurities have been somewhat mitigated by incorporating a low-temperature heat treatment ($\sim 1340^\circ\text{C}$) during the pressureless sintering procedure to remove the boria phase under vacuum. This allows the B_2O_3 gas to boil off of the powders preventing any grain growth. In order to remove the more complicated metal oxide, a secondary phase that preferentially reacts with ZrO_2 is added. A successful approach to pressureless sinter ZrB_2 has involved adding a secondary phase to preferentially react with ZrO_2 . Zhang et al.²⁰ and Fahrenholtz et al.²¹ used an attrition milling method with tungsten carbide (WC) milling media to reduce the starting ZrB_2 powder size as well as introduce ~ 8 wt.% WC into the system. 4 wt.% boron carbide (B_4C) was also added to favorably react with ZrO_2 on the surface of ZrB_2 . As a result, they were able to achieve $>98\%$ dense ZrB_2 billets after pressureless sintering for only 1 h at 1850°C ²⁰ and $\sim 100\%$ relative density in ZrB_2 pellets after 2 h at 1850°C ,²¹ both in an argon atmosphere. Processing methods that employ sintering aids, including boron carbide (B_4C),²² tungsten carbide (WC)²⁰ as well as carbon coating of ZrB_2 powders,²³ have effectively reduced the pressureless sintering temperatures ($<2000^\circ\text{C}$) required to densify ZrB_2 composites without significant mechanical property losses.²¹

These breakthroughs in pressureless sintering over the past few decades have paved the way for ZrB_2 production via colloidal shaping methods, like extrusion, tape casting and gelcasting. Extrusion and tape casting have found relative success in producing dense ZrB_2 components; however, the geometries have been restricted by use of hot pressing to achieve densification.^{8,24} These methods traditionally employ complex

binders based on harsh chemical solvents, like toluene and methyl ethyl ketone, in combination with multiple plasticizers.^{25, 26} Although aqueous-based systems for tape casting and gelcasting of ZrB_2 have been studied recently, these processes require multi-component binders and have not produced dense components without hot pressing or pressureless sintering at temperatures $>2000^\circ C$.²⁷⁻²⁹ There is a definite need for complex-shaped UHTC parts that injection molding can make, yet by a cost-effective, low-energy method.

Ceramic injection molding is an alternative method of producing ceramic parts with complex geometries, and the process can meet the needs of a variety of industries, including aerospace, due to its ability to produce net-shaped parts with fine detail without post-process machining. Currently, ceramic injection molding is a widely accepted processing route to attain near-net shape ceramic components. However, injection molding of UHTC materials has not been previously investigated. Before you start using copy and paste, read the important tips below to minimize your formatting work:

1.3 Powder Injection Molding

Powder injection molding is a well-established, powerful processing alternative that allows for the rapid production of ceramic or metallic components with complex geometries.³⁰ The process has garnered a great deal of attention over the past 30 years, and it has found relative success in industry when compared with other conventional fabrication techniques.³¹ The method borrows from plastic injection molding in that a feedstock consisting of a ceramic or metal powder and polymer is prepared and heated into a flowable state, transferred into a mold, formed into a desired shape, and then

solidified by removing the applied heat and cooling.³²⁻³⁴ In ceramic injection molding, the polymer must be removed from the formed part and then sintered to near full density.³⁵

1.3.1 Material Selection and Feedstock Preparation for Traditional Ceramic Injection Molding

The feedstock is a suspension that is prepared for injection molding, and it consists of a powder combined with a polymer binder. The type of powder material selected dictates what binder is used in feedstock preparation. Almost any material in powder form can be incorporated into an injection moldable feedstock provided it falls within a certain size range. Feedstocks for injection molding require powders with particle diameters less than 20 to 30 μm that are spherical or nearly spherical in shape.³⁵ As a result, most metal, ceramic, or ceramic-metallic composite materials that are available in the appropriate powder form can be incorporated into a feedstock for injection molding.

The optimal rheology of a feedstock for injection molding is typically pseudoplastic, also referred to as shear thinning, or of a Bingham-type behavior, such that the feedstock does not flow at low shear stresses.^{36, 37} Since the binder influences the ultimate rheological behavior of the suspension, it is arguably the most important factor in feedstock material selection and preparation. In order to make a feedstock, the ceramic powder is combined with the binder, which controls the overall rheology of the feedstock. The two main elements of a binder system include the polymeric component and processing aids.³⁵

The polymer is often either a thermoplastic or thermosetting polymer and has the greatest influence on the fluidity of the feedstock. The polymer type is primarily selected according to its ability to maintain under certain processing conditions a desired feedstock viscosity that is adequate for the complete filling of the injection mold cavity without introducing defects into the final part. Additionally, the polymer selected should give the formed part enough strength to retain its original injection molded shape during binder removal and leave little to no residue after its extraction.³⁸

Thermoplastic polymers are commonly combined with other substances, such as waxes or oils with low-boiling points, to enhance flow behavior during filling³⁹ and dimensional control during binder removal. Feedstocks of polyethylene and polypropylene, which are thermoplastic polymers, mixed with paraffin wax and stearic acid for silicon carbide⁴⁰ and alumina⁴¹ powders have been successfully injection molded into dense parts with minimal defects. The major advantage of using thermoplastic polymers is that a smaller volume percent of polymer is required in the feedstock, which translates to less volume loss during binder removal. However, components formed using thermoplastic binders tend to be weaker and more fragile prior to binder removal and sintering. Epoxy resins or phenolic resins are the thermoset polymer of choice for feedstocks, and these thermoset binders are combined with waxes or low-boiling oils like their thermoplastic counterparts. Such feedstocks result in sturdy formed parts prior to burnout; however, they often require a larger proportion of resin to achieve the desired rheological properties of the feedstock, ultimately resulting in greater shrinkage of the part.⁴²

One or more processing aids are added to the feedstock in order to uniformly disperse the polymer-powder mixture by altering the adhesive forces between the surfaces of the two. Common surfactants that are combined with polymer binders in ceramic-powder feedstocks include stearic acid and oleic acid.⁴³ Moreover, in ceramic injection molding, sintering aids, like magnesium oxide, are added in small amounts to ceramic feedstocks to improve sintering. Occasionally, glycerin or boric acid is added as a release agent to ensure that the injection molded part does not adhere to the mold. Processing aids are generally added to a feedstock to promote more efficient processing of ceramic parts. However, their use is dictated primarily by availability and cost.⁴²

Initial study and development of ceramic injection molding has relied more heavily on organic solvents.³¹ Because aqueous feedstocks pose significant advantages over the incorporation of more toxic materials and solvents into feedstocks due to their low impact on the environment and on human health,⁴⁴ significant advancement has been made in the development of aqueous injection molding processes. Binders based on methylcellulose⁴⁵ or polysaccharides like agar,⁴⁶ which gel at temperatures at or below 37°C, have been incorporated into water-based feedstocks for injection molding. Feedstocks based on binders that require temperature-induced gelation must be heated to uniformly mix. Additionally, the injection molding operation itself requires heating of the feedstock to decrease viscosity to enter a mold cavity as well as cooling to solidify the part after forming. The binder must give ideal flow properties to a feedstock such that when heated or cooled allow for production of near-net shape parts without defects.⁴⁷ Consequently, binder selection as well as the careful control of feedstock temperatures

during mixing and injection molding is critical to develop a novel suspension suitable for ceramic injection molding.⁴⁸

Preparing a feedstock is a multistep process that first involves the mixing of the binder, followed by blending the binder with the powder. The binder is initially prepared in a conventional worm or rotary-type mixer at room temperature. To expedite and ensure uniform mixing, binders are sometimes mixed at temperatures that are 10 to 20°C higher than the polymer binder melting temperature.³⁵ The binder is then combined with the ceramic powder in the same electric mixer or ball mill. Conventional mixing at elevated temperature takes less than an hour,⁴⁹ whereas ball milling takes on the order of hours but is less energy intensive.⁴²

1.3.2 Conventional Ceramic Injection Molding Procedure

Ceramic injection molding involves first heating the feedstock in order to lower its viscosity and then feeding it under pressure into a metal die cavity. The pressure exerted onto the suspension causes the feedstock to fill the die completely, thus resulting in the feedstock taking the shape of the die cavity. There exists an optimum pressure and temperature at which the feedstock is injection molded resulting in a minimum number of defects in a formed part. Since powder injection molding is considered a low-pressure method, pressures never exceed 200 MPa during molding, and the injection process typically lasts 30 to 90 seconds.³³

The mechanism that causes the molded piece to solidify is directly related to the temperature to which the feedstock is heated. This temperature varies anywhere from 80 to 350°C depending on the melting temperature and type of binder used. In the case of a

thermosetting binder, the piece is heated above its curing temperature, thus causing the polymer to set and irreversibly harden. Cooling below the glass transition temperature of a thermoplastic binder is required to harden components made with thermoplastics. Once the piece hardens, it can then be removed from the mold.³⁵

Ceramic injection molding is an automated process, which is largely based on polymer injection molding. The most widely used types of injection molding devices for ceramics include the plunger-type and reciprocating screw-type machines (refer to Figures 1.1 and 1.2 for schematics of the two instruments).^{35, 42} Although these apparatuses were first developed in the 1940s, they still prove to be commercially viable due to their durability and versatility in handling feedstocks with varying compositions.⁴²

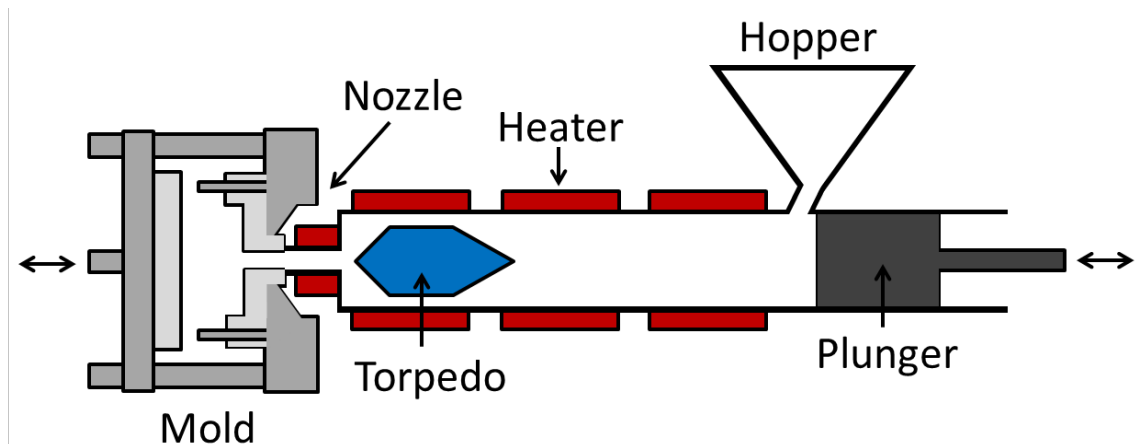


Figure 1.1 Reciprocating screw-type injection molding machine.⁴²

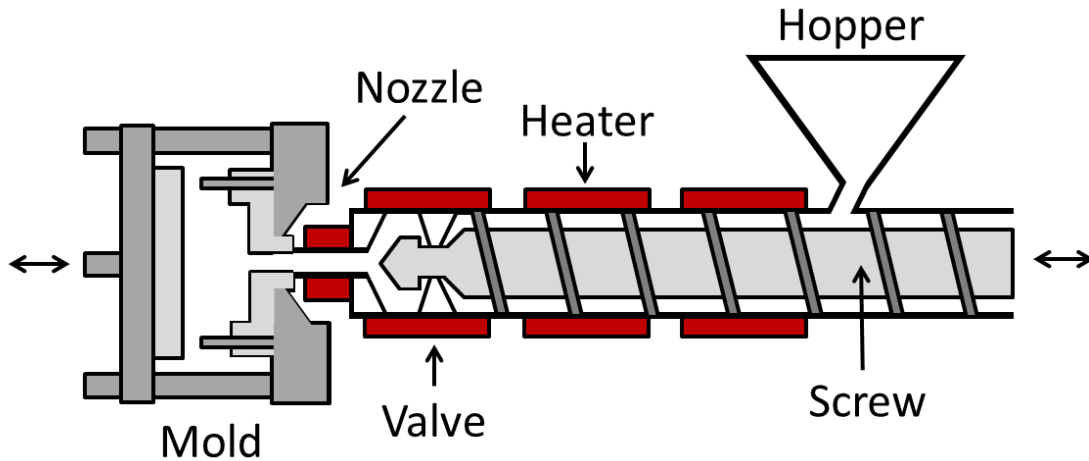


Figure 1.2 Reciprocating screw-type injection molding machine.⁴²

1.3.3 Binder Burnout and Sintering

Binder removal must occur prior to sintering to ensure uniform shrinkage and densification of the ceramic part. Because the removal process predictably depends on the type of binder used in feedstock preparation, binder removal often entails either thermal decomposition, the chemical extraction of the binder using a solvent or a combination of the two techniques.

The most common method of binder removal for thermoplastic binders involves heating the molded part to a temperature between 200 and 400°C, since thermoplastics break down within this temperature range. The binder leaves the sample by gaseous decomposition through pores of the compact upon heating. Heating rate and atmosphere in which thermal decomposition occurs directly influence the ultimate densification of the sample.⁵⁰ Therefore, by slowly heating the sample in an inert or reducing atmosphere at an average rate of around 5°C per minute and isothermally holding a maximum temperature for more than 10 hours, growth and shrinkage, which often lead to cracking,

of the sample are mitigated. Although binder burnout is an effective method of polymer removal, it requires costly heating equipment and a great deal of time (often > 24 hours).⁴²

Thermoset resins can be removed via solvent extraction. This involves immersing the formed part in a solvent, which then breaks down the binder, taking anywhere from 10 minutes to a few hours. Common solvents include ethylene dichloride, hexane, toluene and acetone. After a sample is removed from the solvent, the solvent is evaporated out of the part in air at room temperature or by moderate heating. The advantages to this method of binder removal are that it takes much less time compared with thermal decomposition and costs less since little equipment is required. Additionally, the solvent can be purified and then recycled repeatedly.³¹ However, because harsh solvents are often required, binder removal via solvent extraction is on the decline due to safety and environmental regulations.⁴²

Once the binder has been mostly eliminated from the molded sample, it is then sintered to densify and strengthen the part. Sintering temperatures depend entirely on the ceramic being processed. For example, alumina is usually heat treated in air to approximately 1600°C and cooled over a 10 hour period. Volumetric shrinkage for most injection molded ceramics is on the order of 12 to 22%, which is somewhat greater than other ceramic processing methods.³⁵ Parts formed by powder injection molding reach 96 to 100% of their true density after sintering, which is comparable to other ceramic casting processes. Injection molded ceramic parts have microstructure and mechanical properties, including high hardness and mechanical strength, comparable to ceramics formed by other fabrication methods.³⁰

1.3.4 Current Status of Ceramic Injection Molding

Ceramic injection molding combines the benefits of injection molding plastics with ceramic powder processing, resulting in a manufacturing method with high productivity of complex-shaped ceramic components. A significant hurdle that prevents the wide-spread adoption of injection molding for all ceramics is that very fine powders, which tend to be costly and relatively scarce, are required. Although significant efforts have been made to develop aqueous feedstocks based on more environmentally friendly binders, heating and cooling is required in their preparation and processing. Furthermore, binder removal can be a time- and energy-intensive process. Current research focuses on studying feedstock rheology to better predict the behavior of feedstock in complex-shaped mold cavities^{49, 51} as well as studying different binder systems⁵² in order to minimize defects in molded pieces. Once binder removal is improved through study of new binder systems, ceramic injection molding will be more widely implemented.

Ceramic injection molding is one of a few processing methods that can manufacture complex-shaped ceramic parts that are required in various electronic and aerospace applications without additional machining. Additionally, injection molding can efficiently fabricate ceramic pieces yielding more than 40 parts with high dimensional accuracy per molding operation.³⁵ The method is most cost-effective for ceramics that are difficult to machine, like oxide ceramics or tungsten alloys, into complex shapes that have melting temperatures greater than 1000°C. Non-UHTC materials (alumina, etc.) have been injection molded in the past, but injection molding of UHTCs, particularly ZrB₂ composites, has not been previously attempted. The goal of the present work is to develop a universal room-temperature injection molding method to produce near-net

shape UHTC components, ultimately broadening the number of fields in which ceramics can be employed.

1.4 Alternative Room-Temperature Injection Molding Method for Zirconium Diboride

The goal of this project was to create a low-cost, energy efficient and environmentally friendly processing method capable of forming dense ceramic parts, first of alumina and then of ZrB_2 , with complex geometries by using a ceramic suspension gel (CeraSGel). A CeraSGel is highly loaded with ceramic with minimal binder content (<5 vol.%). To prepare a CeraSGel, micron or nanosized ceramic powders are suspended in a polymer gel prepared by dissolving a polymer mixture in water. The gel-like mixture is fluid enough to injection mold into a complex-shaped component, while maintaining a high enough viscosity to keep its initial shape after formation.

Because of the high material cost and additional sintering additives required to pressureless sinter zirconium diboride, alumina was initially investigated as a model material system. The room-temperature flow behavior of alumina CeraSGels was modified to suit injection molding without the need for heating or cooling of the suspension. The resulting molded alumina CeraSGel part was then dried, and the polymer binder was removed by thermal pyrolysis followed by pressureless sintering to densify the ceramic. Microstructural and mechanical characterization methods were employed to evaluate the efficacy of the resulting alumina components prepared by room-temperature injection molding.

After the novel room-temperature process was successfully applied to alumina CeraSGels, the method was adapted to ZrB_2 CeraSGels containing sintering aids of boron

carbide and tungsten carbide. ZrB_2 parts that were injection molded at room temperature were pressureless sintered to >98% theoretical density after binder burnout in an initial heat treatment step. Microstructural analysis revealed minimal porosity in the formed ZrB_2 pieces. Minute compositional variance resulted, as phase analysis confirmed that little to no oxidization occurred to negatively impact the resulting phases of ZrB_2 after sintering allowing parts to be fully densified.

Advances in processing and fabrication of near-net shape ceramic components in an aqueous, more environmentally prudent manner were accomplished via study and development of room-temperature injection molding. The concept of injection molding alumina and ZrB_2 CeraSGels at room temperature will ultimately allow for faster and less expensive fabrication of ceramic parts, particularly of UHTCs, utilizing this unique “green” gel injection molding process. Through careful design and study of powder loading and polymer additives, the viscosity of a CeraSGel can be optimized to afford room-temperature processing of a variety of near-net shaped ceramics and metal systems. The successful development of the process as applied to alumina and zirconium diboride-based CeraSGels are presented in this work.

CHAPTER 2. DEVELOPMENT OF ALUMINA CERAMIC SUSPENSION GELS FOR ROOM-TEMPERATURE INJECTION MOLDING

Alumina (Al_2O_3) was selected for initial study of ceramic suspension gels as it is a model ceramic material that is inexpensive compared to zirconium diboride (ZrB_2). Once the room-temperature injection molding process was refined and modified for Al_2O_3 CeraSGels, it was then later adapted to a ZrB_2 system. The design and development of room-temperature injection molding of alumina CeraSGels are presented in this section.

2.1 Utilizing Unique Flow Properties of Alumina-Polymer Suspensions for Room-Temperature Injection Molding

Pseudoplastic fluids, also known as shear thinning fluids, demonstrate a decreasing viscosity as shear strain rate is increased. As a result, they flow more easily the faster the flow. Yield-pseudoplastic fluids, sometimes called Ellis fluids, have a yield point, below which they will not flow, and above which they demonstrate shear thinning behavior.⁵³ A flow curve for such a fluid is highlighted in Figure 2.1. Aqueous alumina CeraSGels have been observed to obey a yield-pseudoplastic fluid behavior,⁵⁴ and it is the yield point associated with CeraSGels that will be exploited to injection mold at room temperature in this project.⁵⁵

To use the yield-pseudoplastic behavior of the CeraSGel to full advantage during injection molding, the ceramic-polymer mixture is designed to be in the shear-thinning

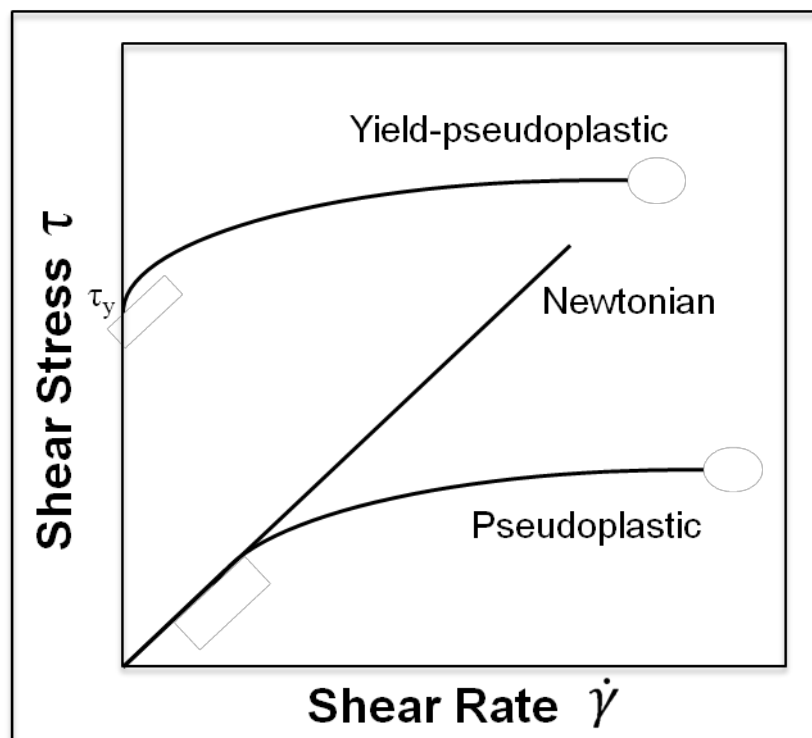


Figure 2.1 Flow curves of Newtonian, pseudoplastic and yield-pseudoplastic fluids.⁶⁸

region (i.e. above its yield point). Once the shear strain is removed, the part will retain its newly formed shape due to its yield point. Because polymer solutions that are flowable at room temperature will be used in CeraSGels, heating and cooling of the suspension do not have to be performed as in the existing ceramic injection molding process,³⁵ thus eliminating the need for heating and cooling the ceramic-polymer suspension. Additionally, CeraSGels are considered low-toxic systems compared to other colloidal processing suspensions,⁴⁴ since they are water based.

2.1.1 Alumina-PVP Suspension Preparation

Alumina suspensions used in this study were prepared using deionized (DI) water and A-16 SG alumina (Almatis, New Milford, CT) with an average particle size of $0.48 \pm$

0.13 μm determined using a Beckman Coulter LS 230 particle size analyzer (Brea, CA) and BET surface area of $7.8 \pm 0.22 \text{ m}^2/\text{g}$ found using a TriStar 3000 gas adsorption analyzer (Micromeritics Instrument Corporation, Norcross, GA). Darvan® 821A (R.T. Vanderbilt Company, Inc., Norwalk, CT) was used as an ionic dispersant. Darvan 821A (chemical structure shown in Figure 2.2a) is a low-toxic aqueous solution of 40% ammonium polyacrylate with a molecular weight of 3,500 g/mol that is highly soluble in aqueous systems.^{44, 56, 57} Like other electrolyte dispersants, Darvan 821A is a cation-exchange deflocculating agent used to obtain excellent flowability for suspensions with high solid loadings. When dissolved in water, Darvan 821A releases NH_4^+ and R-COO^- ions into the solution, which augments its ionic concentration strength, resulting in an increase in surface charge of the particles as the R-COO^- cations adsorb onto the particle surfaces. The cations modify the electrostatic double-layer of the particles, making them more negatively charged.⁵⁸ It has been observed by previous investigators that alumina suspensions containing 50-60 vol.% of the ceramic require additions of Darvan 821A of ~0.5 wt.% to be stabilized at pHs <9.⁴⁴

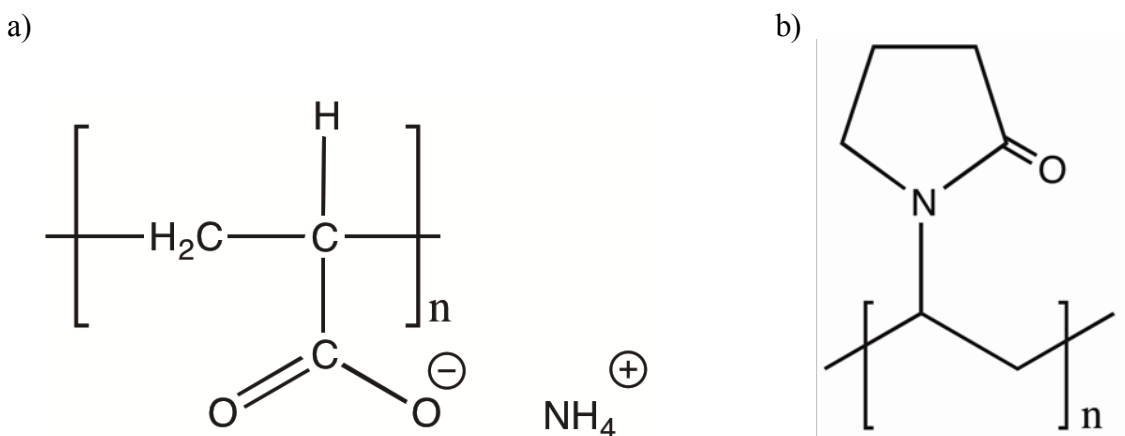


Figure 2.2 a) Chemical structure of Darvan 821A (ammonium polyacrylate) and b) polyvinylpyrrolidone (PVP).

Polyvinylpyrrolidone (PVP, 1-Ethenyl-2-pyrrolidinone homopolymer, Sigma-Aldrich, St. Louis, MO) with average molecular weights of 10,000, 55,000, 360,000 and 1,600,000 g/mol was used as a rheological modifier for the ceramic suspensions. The structure of PVP is shown in Figure 2.2b, and its content was varied from 0 to 5 vol.% in the ceramic-PVP suspensions studied. Volume percentage calculations were based on initial CeraSGel compositions, such that contents of powder, PVP, dispersant and water were considered. If water content was ignored, dry CeraSGel specimens consisted of ~85-91 vol.% alumina powder, ~1.6-8.5 vol.% PVP and ~6.5-7 vol.% dispersant. For the purposes of this study, all contents will be presented as volume percentages based on the initial CeraSGel compositions including water content.

An aqueous slurry was prepared using DI water, dispersant and alumina powder by ball milling in Nalgene bottles with alumina milling media (U.S. Stoneware, East Palestine, OH) for 24 hours. Alumina powder was incrementally added to a dispersant and DI water solution to obtain highly loaded, dispersed alumina slurries. A typical slurry contained 225 g of alumina powder in 37 mL of DI water and 5 mL dispersant. A polymer solution of PVP and DI water was mixed separately by magnetic stirring for 4-8 hours. After both the slurry and polymer solution were dispersed, the PVP-water mixture was added to the alumina slurry and ball milled over a 12-hour period. The content of PVP with molecular weight of 55,000 g/mol in suspensions evaluated were 1, 2.5, 4 and 5 vol.% to determine the optimal binder content that resulted in favorable forming and final sintered and mechanical properties. The compositions studied are highlighted in Table 2.1. Suspensions with 2.5 vol.% PVP with molecular weights of 10,000 g/mol,

Table 2.1 Compositions of alumina-PVP suspensions with corresponding curve-fit parameters using the Herschel-Bulkley equation for yield-pseudoplastic fluids, average green and sintered densities and C-ring strength values for sintered samples prepared by room-temperature injection molding of suspensions with varying content of PVP with molecular weight of 55,000 g/mol.

Al ₂ O ₃ Powder Content in vol.% (wt.%)	Polymer Content in vol.% (wt.%)	Dispersant Content in vol.% (wt.%)	σ_y (Pa)	k (Pa·s ⁿ)	n	Average Green Density in g/cm ³ (%TD)	Average Sintered Bulk Density in g/cm ³ (%TD)	Average Grain Size (μ m)	Average C-ring Strength (MPa)
57.9 (84)	0 (0.0)	4.4 (1.9)	4.57	3.94	0.408	2.56 ± 0.02 (64)	3.92 ± 0.02 (98)	-	-
56.7 (84)	1 (0.5)	4.3 (1.9)	25.1	7.47	0.391	2.52 ± 0.01 (63)	3.88 ± 0.02 (98)	3.20 ± 2.5	206 ± 36.5
54.9 (82)	2.5 (1.2)	4.2 (1.8)	30.7	26.1	0.279	2.50 ± 0.02 (63)	3.89 ± 0.01 (98)	3.66 ± 2.5	261 ± 57.6
53.0 (81)	4 (1.9)	4.0 (1.8)	35.3	17.1	0.326	2.43 ± 0.02 (61)	3.88 ± 0.02 (98)	3.18 ± 2.0	210 ± 31.8
51.7 (80)	5 (2.5)	3.9 (1.8)	59.4	12.8	0.398	2.38 ± 0.06 (60)	3.84 ± 0.06 (97)	3.40 ± 2.2	192 ± 27.2

Table 2.2 Alumina suspension compositions with corresponding Herschel-Bulkley curve-fit parameters, average green and sintered densities and C-ring strength values for sintered samples prepared by room-temperature injection molding of suspensions with 2.5 vol.% PVP of varying molecular weights.

PVP Molecular weight in g/mol	Al ₂ O ₃ Powder Content in vol.% (wt.%)	Polymer Content in vol.% (wt.%)	Dispersant Content in vol.% (wt.%)	σ_y (Pa)	k (Pa·s ⁿ)	n	Average Green Density in g/cm ³ (%TD)	Average Sintered Bulk Density in g/cm ³ (%TD)	Average C-ring Strength (MPa)
10,000	55.1 (83)	2.5 (1.2)	4.2 (1.8)	12.6	12.0	0.320	2.48 ± 0.04 (62)	3.88 ± 0.03 (98)	233 ± 73.8
55,000	54.9 (82)	2.5 (1.2)	4.2 (1.8)	30.7	26.1	0.279	2.50 ± 0.02 (63)	3.89 ± 0.01 (98)	261 ± 57.6
360,000	53.9 (82)	2.5 (1.2)	4.1 (1.8)	52.7	8.48	0.510	2.41 ± 0.02 (60)	3.86 ± 0.04 (97)	246 ± 59.8
1,300,000	52.4 (81)	2.5 (1.2)	4.0 (1.8)	56.8	4.92	0.621	2.36 ± 0.03 (59)	3.78 ± 0.05 (95)	-

360,000 g/mol and 1,300,000 g/mol (compositions listed in Table 2.2) were also prepared to evaluate the effect of molecular weight on the final properties of the samples.

Initial analysis of the flow properties of alumina CeraSGels using Darvan 821A suggested that the CeraSGels exhibited yield pseudoplasticity, which was ideal for room-temperature injection molding. Their flow properties were suitable for initial study of forming alumina ceramics by room-temperature injection molding. Further rheological analysis of alumina CeraSGels is described in Chapter 3.

2.2 Design and Approach of Room-Temperature Injection Molding

2.2.1 Room-Temperature Injection Molding Procedure

Because commercially available ceramic injection molding machines traditionally use heating and cooling processes throughout the forming procedure, a novel room-temperature injection molding apparatus was constructed. The mold cavity was specifically designed to produce a part that would be amenable to characterization, matching ASTM C1323-10 for determination of the ultimate strength of compressively loaded ceramic C-ring specimens.⁵⁹ By fabricating a ceramic ring rather than a simpler, more common geometry, like a bar, the process was developed to overcome complications that were inherent to the production of ring-shaped parts, such as convergent flow effects during filling that resulted in potential pore or defect formation in addition to the development of hoop stresses during solidification and drying that caused cracks in specimens.³³

The mold setup, shown in Figure 2.3, was designed to utilize a compression force that acts on a pushrod, which then exerts pressure on the CeraSGel and forces it into a

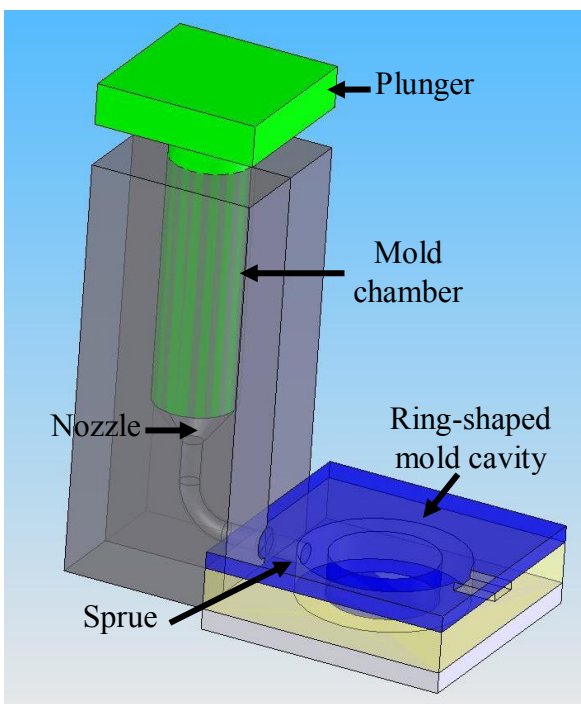


Figure 2.3 Schematic of room-temperature injection mold device.

mold. A mold was made to fabricate a ceramic ring-shaped green body with a 1-inch outer diameter, 5/8-inch inner diameter and a width of 1/4 inch, and three ports out of which extra material could flow during filling (shown in Figure 2.4a). The bottom plate and outer ring support with injection port were machined from steel. A cylindrical rod with a diameter and height of a 1/4 inch was inserted in the center of the bottom plate, and a 1/4-inch section of EPDM (ethylene propylene diene monomer) closed-cell foam rubber tube with a firmness of ~5-9 psi and outer diameter of 5/8 inch and inner diameter of 1/4 inch (McMaster-Carr, Elmhurst, IL) was placed on the rod. The top plate was machined from transparent Plexiglas. A low-friction Teflon tape (McMaster-Carr, Elmhurst, IL) and Grade 40 ashless filter paper (Whatman, U.K.) were adhered to the top and bottom steel plates of the ring-shaped die that came in contact with the ceramic-PVP suspension

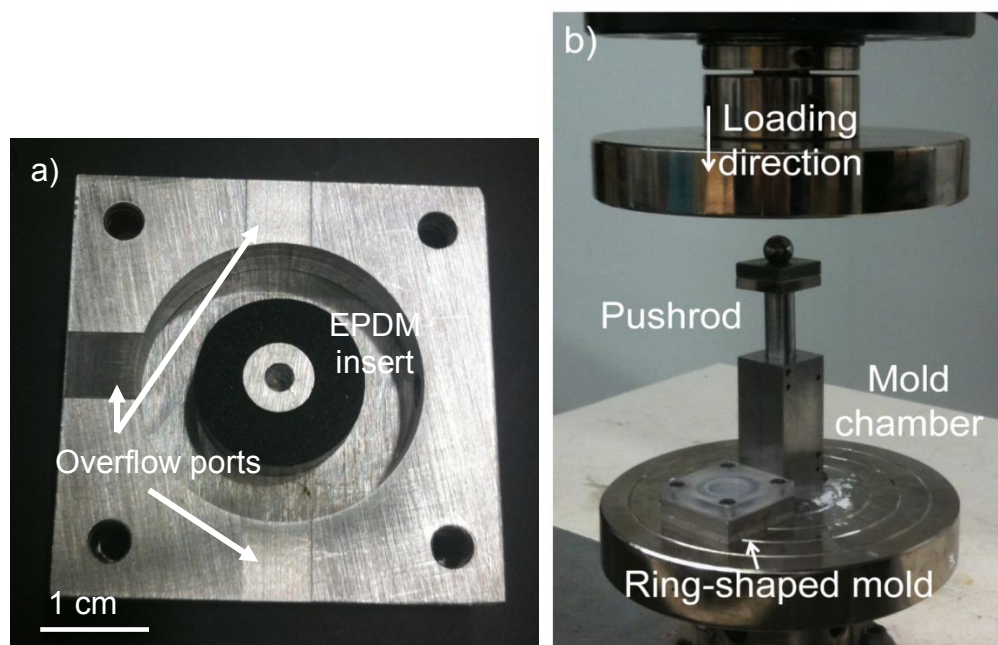


Figure 2.4 a) Ring-shaped mold with EPDM foam centerpiece and three escape ports adjacent and across from the injection port. b) The injection mold setup between two compression platens of the load frame prior to the injection molding operation. A pneumatic vibrator with dimensions of 5.5 cm \times 1.6 cm \times 2.3 cm was fixed on top of the ring-shaped mold using cable ties (not pictured) during forming.

during filling to facilitate more rapid demolding and cleaning of molds. The top and bottom plates were then fitted above and below the outer ring support, respectively, using screws to secure the plates together to create the mold cavity. The mold cavity was then attached to the suspension chamber with a 1/8-inch diameter rubber O-ring fixed between the two to ensure a tight seal, resulting in a 1/8-inch diameter sprue, through which the suspension entered the mold from the suspension chamber.

Liquid Wrench L312 Teflon spray (Indian Trail, NC) was used to lubricate the inner surfaces of the mold cavity and chamber prior to suspension loading to facilitate the removal of a formed part from the mold. The injection mold chamber was loaded with 5 mL of the alumina-PVP suspension using a 6-mL luer-slip syringe (VWR, Radnor, PA).

The cylindrical ½-inch diameter steel pushrod was inserted into the cylindrical chamber with a ½-inch diameter, and the entire mold apparatus was placed between compression platens in an electromechanical test frame (MTS Insight 100 load frame, MTS Systems Corporation, Eden Prairie, MN), as shown in Figure 2.4b.

A compression force at a crosshead speed of 100 mm/min was transferred to a 0.5-inch diameter ball bearing sitting atop the pushrod to ensure that the load was uniformly applied to the pushrod. This force, applied at a constant rate on the pushrod, exerted the pressure needed to overcome the yield point of a yield-pseudoplastic suspension, causing it to flow and fill the ring-shaped mold cavity. As a result, an alumina ring was produced. A VM-25 miniature air piston vibrator (Cleveland Vibrator Co., Cleveland, OH) was attached to the mold using cable ties. The pneumatic vibrator had a frequency of 16,000 vibrations per minute at 80 psi and was initiated immediately prior to filling for the duration of the injection molding process. When activated the vibration appeared to assist in the filling of the mold by preventing closed pore formation due to air bubbles. The injection mold setup is highlighted in Figure 2.4b. After forming, a part was allowed to dry at ambient conditions for one hour prior to removal from the mold. The resulting ceramic ring could be machined into the desired C-shape as highlighted in Figure 2.5.

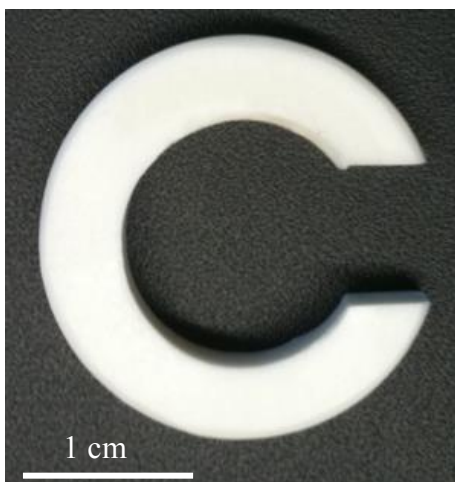


Figure 2.5 Final sintered alumina specimen after machining.

2.2.2 Previous Modifications to Room-Temperature Injection Molding Process

Preliminary study of room-temperature injection molding of CeraSGels led to a series of modifications to the injection molding process in order to optimize the design and CeraSGel loading method. Although alumina CeraSGels exhibited the appropriate flow behavior desired for injection molding even with varying polymer content (refer to *Section 2.3*), defects developed in the ring-shaped parts. Initially, cracks due to hoop stresses that arose during the drying process and closed pore formation from air bubbles that developed in alumina CeraSGels during injection molding prevented full densification of the formed alumina parts shown in Figure 2.6a and b, despite polymer content and composition of the CeraSGel.

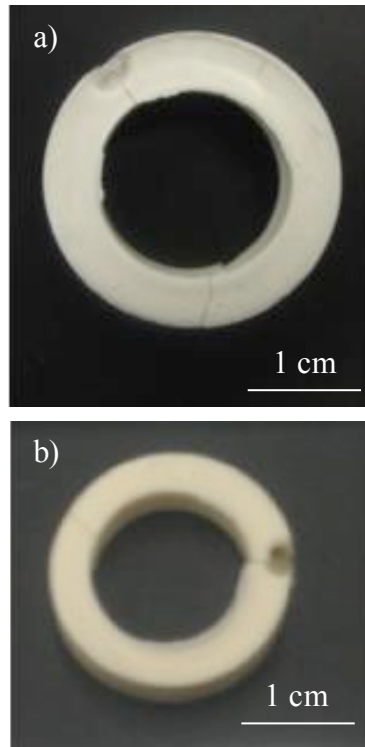


Figure 2.6 An alumina CeraSGel specimen exhibiting crack and air bubble formation a) before binder burnout and b) after binder burnout and sintering.

2.2.2.1 Eliminating Crack Formation during Drying

In order to resolve the cracking issue associated with the initial mold design that incorporated a Plexiglas centerpiece, the Plexiglas ring-shaped die from the original mold device was altered by introducing a taper to create a slightly conical centerpiece depicted in Figure 2.7, to alleviate hoop stresses that resulted due to shrinkage of the ring-shaped piece during the drying process. However, the modification did not sufficiently relieve hoop stresses, and cracks continued to develop in the part.

Consequently, an EPDM (ethylene propylene diene monomer) closed-cell foam rubber tube with a firmness of ~5-9 psi and outer diameter of 5/8 inch and inner diameter



Figure 2.7 Ring-shaped mold with tapered Plexiglas centerpiece with formed alumina part immediately after injection molding.

of $\frac{1}{4}$ inch (McMaster-Carr, Elmhurst, IL) was introduced to completely replace the Plexiglas centerpiece. This mold modification is shown in Figure 2.4a. Unlike the Plexiglas centerpiece, the flexibility of the foam allowed for adequate shrinkage of the sample during drying. Regardless of the polymer content (1-5 vol.% PVP) used in the alumina CeraSGel, cracks did not form in the injection molded part when formed with a foam centerpiece (refer to Figure 2.8). Thus, crack defects were successfully eliminated from CeraSGel specimen fabrication using an EPDM foam insert.

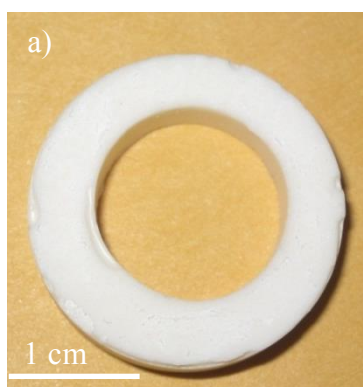


Figure 2.8 An injection molded alumina CeraSGel part that was formed using an EPDM foam insert and exhibited no cracking after binder burnout and sintering.

2.2.2.2 Preventing Closed Pore Formation

A common issue with ceramic injection molding is the entrapment of air inside the suspension during loading of the injection mold chamber and during the injection molding process causing closed pore formation. These pores in the final ceramic piece negatively impact the overall integrity of the sintered ceramic piece.³³ Several remedies were evaluated in order to resolve the air bubble issue, including a series of mold design modifications and alternate methods of loading the CeraSGel in the injection mold chamber.

a) Air escape vents Three air escape vents were machined onto the outer ring of the steel mold across and adjacent from the injection site, shown in Figure 2.4a, allowing air to escape from the mold cavity during the filling operation rather than becoming entrained in the suspension and ultimately the final part. The air escape ports were 1/8-inch wide and 0.0313 inch deep into the top portion of the steel outer ring support. Although the size and apparent number of air bubbles that formed in the part was noticeably reduced, the addition of air vents did not fully prevent air bubbles from developing.

b) Teflon tape A low-friction Teflon tape (McMaster-Carr, Elmhurst, IL) was adhered to the top and bottom stainless steel plates of the ring-shaped die that came in contact with the CeraSGel during filling in order to introduce a more uniform surface with reduced friction. This modification was intended to facilitate more consistent flow of the suspension during filling, thus, preventing air bubble formation. Although this alteration did not eliminate closed pore development, it did aid in the removal of injection

molded CeraSGel specimens by preventing the dried parts from adhering to the surface of the steel mold, resulting in more even surfaces of the ring-shaped part.

c) Vacuum Another approach that was explored to remedy air bubble development involved evacuating the suspension container using a vacuum system to remove entrained air during ball milling prior to forming. A 1-liter Nalgene bottle was fitted with a valve that was connected to a vacuum pump, as shown in Figure 2.9, in order to evacuate the bottle with CeraSGel prior to ball milling. Although air bubbles appeared to be removed from the suspension prior to loading, air bubbles still developed within the CeraSGel part during injection molding. This suggested that the primary development of air bubbles in a formed part occurred within the injection mold chamber during the filling operation rather than within the suspension during ball milling.



Figure 2.9 A valve was fitted to a ball mill bottle to evacuate using a vacuum pump.

d) Pneumatic vibrator A VM-25 miniature air piston vibrator (Cleveland Vibrator Co., Cleveland, OH) was attached to the mold in order to put the suspension in a constant state of high shear during filling to prevent air bubbles formation. The pneumatic vibrator had a frequency of 16,000 vibrations per minute at 80 psi. The injection mold setup is highlighted in Figure 2.10. It was determined that through this addition, air bubbles were removed from the suspension, resulting in dense alumina ring-shaped samples free of closed pores, as shown in Figure 2.11.



Figure 2.10 Injection mold setup with pneumatic vibrator.

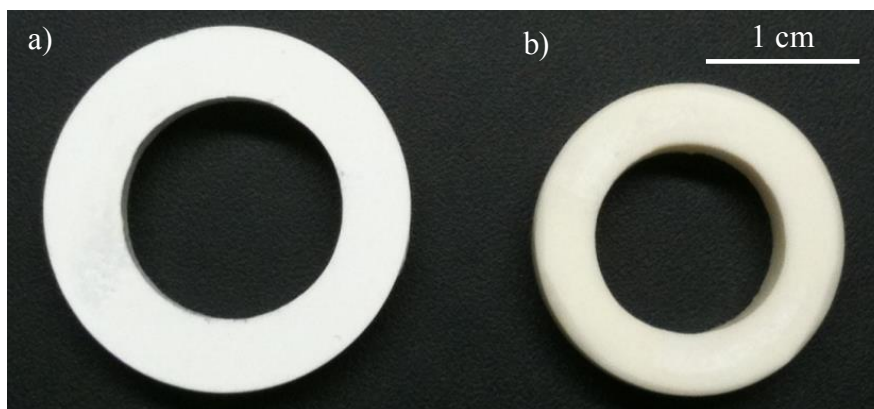


Figure 2.11 An alumina ring was formed using the pneumatic vibrator during injection molding and did not develop closed pores due to air bubble formation. Specimen a) prior to and b) after binder burnout and sintering.

2.2.3 Binder Burnout and Pressureless Sintering of Injection Molded Alumina Rings

The binder burnout process cycle for formed alumina-PVP samples was determined by thermogravimetric differential thermal analysis (SDT 2960 Simultaneous TG-DTA instrument, TA Instruments, New Castle, DE) of PVP, which indicated significant weight loss beginning at 325°C and ending at 480°C as highlighted in Figure 2.12. Removal of the binder from the formed samples was accomplished using a Sola Basic Lindberg/Blue Tube Furnace (Ashville, NC) at a heating rate of 2°C/min to 700°C with an isothermal hold of one hour followed by cooling to room temperature. The sample was then transferred to a Thermo Scientific Lindberg/Blue M 1700°C Box Furnace (Ashville, NC) for pressureless sintering, heating at a rate of 5°C/min to 1620°C with a 1.5-hour hold to densify the alumina ring.

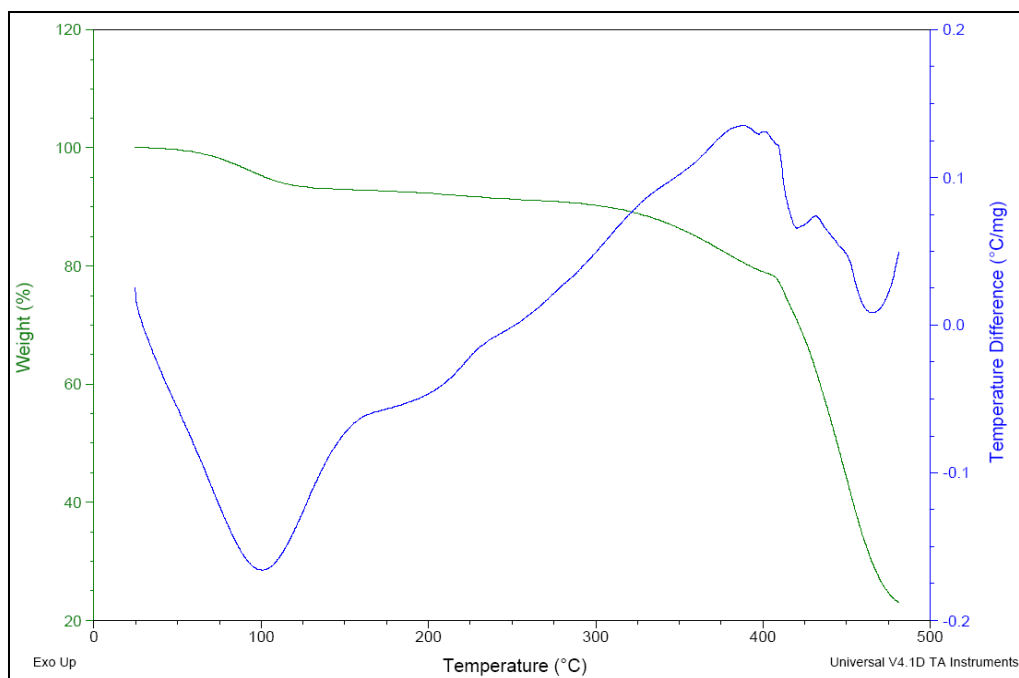


Figure 2.12 Thermogravimetric analysis revealed that PVP thermally decomposed by 500°C.

2.2.4 Preparation of Alumina Specimens for Mechanical Characterization

After a ring-shaped alumina CeraSGel part was formed via injection molding, it was then machined in its green state to chamfer the outer edges and ensure sample surfaces were sufficiently parallel in accordance with the ASTM C1323-10 C-ring test.⁵⁹ A polishing wheel with 320, 400 and 600 grit silicon carbide grinding cloth (LECO 810-265/269-PRM) was used to accomplish this green machining, as shown in Figure 2.13.

Binder burnout and sintering steps as described in *Section 2.2.3* were performed, and a slow-speed saw with a diamond blade (Leco Corporation, St. Joseph, MI) was used to cut a notch in the sample resulting in the desired C-shape. In the chance that the heat treatments resulted in warping of the ring-shaped sample, it was placed on a mandrel with adjustable diameter and then machined using a diamond-tipped blade (McMaster-Carr,



Figure 2.13 Evening out surfaces of an alumina ring in the green state using a polishing wheel.

Elmhurst, IL) on a rotating lathe to ensure outer surface were parallel. Figure 2.5 shows the final geometry of the part to be tested, which is compressively loaded until fracture in accordance with ASTM C1323-10.⁵⁹

2.3 Experimental Approach for Characterization of Alumina Rings Produced by Room-Temperature Injection Molding of Alumina CeraSGels

Room-temperature injection molding of alumina CeraSGels proved to be a viable route to produce alumina rings. In order to determine the structure-property-processing relationship of the samples produced using this method, five CeraSGel suspension compositions with varying polymer content from 0 to 5 vol.% PVP with an average molecular weight of 55,000 g/mol were evaluated according to the following characterization methods: flow properties, green machining, density and ultimate strength.

The compositions examined in this study are given in Table 2.1. Suspensions with 2.5 vol.% PVP with molecular weights of 10,000 g/mol, 360,000 g/mol and 1,300,000 g/mol (compositions listed in Table 2.2) were also prepared to evaluate the effect of molecular weight on the final properties of the samples

2.3.1 Rheology of Alumina CeraSGels with Varying PVP Content

A TA Instruments ARG2 rheometer (New Castle, DE) with a 40-mm parallel-plate geometry and a gap of 500 μm was used to characterize the rheological responses of suspensions with varying PVP contents at 25°C. A moisture trap was also employed during testing to avoid temperature differences and premature drying of the suspension while testing. Parallel plate rheometry allows for characterizing highly loaded particulate suspensions at high rates without material interrupting the flow under the gap of the geometry.^{37, 60} Similarly, other studies have previously applied parallel plate rheometry to investigate the rheological response of highly loaded alumina suspensions.^{61, 62} In this study, parallel plate rheometry was selected over cone and plate rheometry, since the gap provided by a cone and plate geometry would not allow for the instrument to run at a wide range of shear rates.^{37, 63}

By considering the sprue diameter of 1/8 inch and the applied compression rate of 100 mm/min used for room-temperature injection molding, the shear rate applied to alumina-PVP suspensions during forming was determined to be 4.20 s^{-1} . The calculated shear rate is significantly lower than that of traditional injection molding, which can be on the order of 100 s^{-1} to 1000 s^{-1} .³¹ Consequently, flow curves up to a maximum shear rate of 100 s^{-1} were obtained to quantify the low-shear rheological behavior of the

alumina-PVP suspensions utilized in this study. Flow curves were fitted using the least squares method to the Herschel-Bulkley model³⁷ typically used for yield-pseudoplastic materials that is given as:

$$\sigma = \sigma_y + k\dot{\gamma}^n \quad \text{Equation 2.1}$$

where σ was stress, σ_y represented the shear yield stress, $\dot{\gamma}$ was the shear rate applied to the material, the consistency or apparent viscosity was k and flow index of the material was n , which varied from 0 to 1. Flow behavior was considered yield pseudoplastic when a suspension demonstrated a yield stress and $n < 1$.³⁷ The yield stress of each suspension evaluated was found by extrapolating its curve fit to the axis limits, and the correlation factor, R , of fitting the curve parameters to Equation 2.1 was always ~ 0.99 . Oscillation stress sweeps were run at a frequency of 1 Hz from 0.1 to 1000 Pa to study the viscoelastic response of the suspensions. The pH of each suspension was determined using an Oakton PH5 meter (Vernon Hills, IL).

2.3.2 Machinability in Green State

A polymer binder system often imparts strength to a formed ceramic body before it is removed by thermal pyrolysis. In order to qualitatively assess the machinability of parts formed using CeraSGel, a custom steel polishing mount with micrometer shown in Figure 2.14 was machined to the exact dimensions of the alumina ring-shaped part such that every specimen polished experienced identical machining conditions. Each sample was inserted into the mount and polished using silicon carbide polishing papers of 320, 400 and 600 grit for 30 seconds on each paper in increasing order at ~ 200 rotations per minute (RPM). The effect of machining in the state prior to binder removal was

qualitatively observed by examining the final surface finish of each sample for fracture, cracking or chipping after polishing.

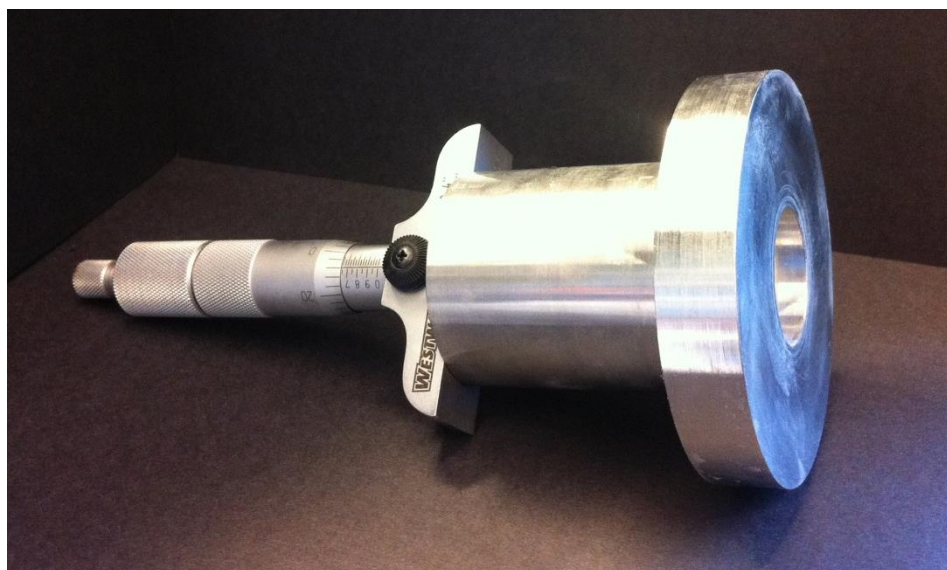


Figure 2.14 Polishing mount used to even out surfaces of CeraSGel samples in the green state using a polish wheel.

2.3.3 Density and Internal Porosity of Sintered Specimens

Density of the alumina parts before and after sintering was measured using the Archimedes technique as described by ASTM C373-88.⁶⁴ Microstructural analysis was performed using an FEI Philips XL-40 scanning electron microscope (SEM) to examine sintered, polished and thermally etched (1400°C, one-hour hold) samples. The average grain size was determined by evaluating five SEM micrographs for a particular sample composition and measuring the length of 50 arbitrary grains in each image using ImageJ image processing and analysis software. A total of 250 line segments representing 250 different grain lengths were averaged to obtain a mean grain size for each composition.

2.3.4 Ultimate Strength of Sintered Alumina C-Ring Samples

Mechanical characterization of the ring specimens was determined using the ASTM C1323-10 standard,⁵⁹ which necessitated that each C-shaped specimen fell within particular geometric tolerances. The dimensions of the sample are highlighted in the schematic in Figure 2.15. The allowable width-thickness ratio (b/t) must fall within $1 \leq b/t \leq 2$ with the ratio of the inner and outer radii of the specimen (r_i/r_o) being $0.5 \leq r_i/r_o \leq 0.95$. A slow-speed saw with a diamond blade (Leco Corporation, St. Joseph, MI) was used to cut a notch in the densified specimens resulting in the desired C-shape for mechanical testing (refer to Figure 2.5). If the heat treatments resulted in warping of the ring-shaped sample, it was placed on a mandrel with adjustable diameter and then machined using a diamond-tipped blade (McMaster-Carr, Elmhurst, IL) on a rotating lathe to ensure outer surfaces were parallel for mechanical testing. After machining samples, each specimen was measured using digital calipers to ensure that all geometrical conditions of the standard were met prior to compressive testing.

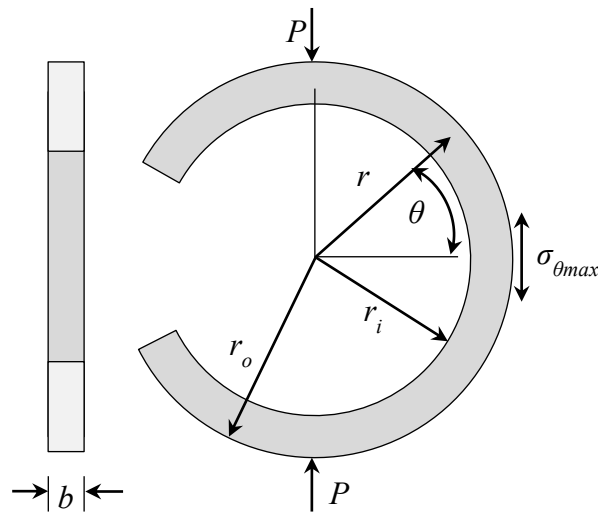


Figure 2.15 P is the compressive force, r_o is the outer radius and r_i is the inner radius, and b is the width. Thickness t is $r_o - r_i$.

In order to calculate the maximum engineering tangential (hoop) stress at fracture, $\sigma_{\theta max}$, at least six samples were tested to obtain an average C-ring strength for a given suspension composition. The alumina specimens evaluated were prepared from suspensions that contained 1, 2.5, 4 and 5 vol.% PVP of 55,000 g/mol or 2.5 vol.% PVP of 10,000 g/mol, 360,000 g/mol and 1,300,000 g/mol. C-ring specimens were positioned between two MTS platens as highlighted in Figure 2.15 and compressively loaded with a crosshead speed of 0.1 mm/s to yield a strain rate of $1 \times 10^{-4} \text{ s}^{-1}$ in accordance with the standard.⁵⁹ The top and bottom platen was covered with 2-mm thick copper plates that came in contact with the specimen during testing to protect the platen surfaces. The copper plates were changed between each test to ensure that the sample came in contact with a parallel surface. The sample dimensions and failure load, P , were used to determine the tangential (hoop) failure stress of each specimen in accordance with the equation given by the standard:⁵⁹

$$\sigma_{\theta max} = \frac{PR}{btr_o} \left[\frac{r_o - r_a}{r_a - R} \right] \quad \text{Equation 2.2}$$

where $R = \frac{(r_o - r_i)}{\ln(r_o/r_i)}$, b is the specimen width, t is its thickness and r_a is the average of r_o and r_i .

The ASTM C1323-10 mechanical characterization method is particularly sensitive to external surface flaws as it causes maximum tension at the outer surface of the specimen.⁵⁹ Because $\sigma_{\theta max}$ represents the maximum stress that occurs on the outer surface of the specimen at the midplane, defects that cause fracture that are located inside the outer sample surface or located away from the midplane will have a reduced stress value. After mechanical testing fractographic analysis was performed following the

procedure outlined in ASTM C1322-05b⁶⁶ to evaluate the angle and origin of fracture for each specimen using an Olympus SZX7 Zoom Stereo Microscope. In order to determine an average C-ring strength value, only strength values calculated using Equation 2.2 were evaluated as indicated by the standard.⁵⁹ It is important to note that the specific fracture stresses of each specimen may be corrected for subsurface origins in accordance with the standard.⁵⁹ Such rigorous analysis was not performed in this study, because the aim of this work was to determine an average C-ring strength value for each alumina-PVP suspension composition to isolate the optimal PVP concentration.

2.3.5 Statistical Analysis of Density, Grain Size and Ultimate Strength of Sintered Alumina C-Ring Samples

A two-tailed *t*-test⁶⁶ was applied to compare the means of the densities, grain sizes and mechanical strengths for varying PVP content to determine if data sets were statistically different. To infer whether a Student's *t*-test for samples with equal variance (homoscedastic) or a Cochran's *t*-test for samples with unequal variance (heteroscedastic) should be applied, an *F*-test was used to calculate the ratio, F_0 , of the two variances. Two data sets were considered homoscedastic when the value of F_0 fell between the upper- and lower-tail percentage points, $F_{0.05, u, v}$ and $F_{0.95, u, v}$, respectively, with u and v being the degrees of freedom, and heteroscedastic when $F_0 > F_{0.05, u, v}$ or $F_0 < F_{0.95, u, v}$.⁶⁶ The p -values calculated from either the Student's or Cochran's *t*-tests using the Excel function, *TTEST*, were considered to be statistically different when $p < 0.05$.⁶⁶

2.4 Results and Discussion of Alumina CeraSGels for Room-Temperature Injection

Molding

2.4.1 Rheological Behavior and Processability of Alumina Suspensions with Varying PVP Content

Flow curves of alumina-PVP suspensions prepared with ~4 vol.% Darvan 821A for polymer contents of 0, 1, 2.5, 4 and 5 vol.% PVP (MW=55,000 g/mol) with powder loadings of 57.9, 56.7, 54.9, 53.0 and 51.7 vol.% alumina, respectively, suggested that suspensions behave as yield-pseudoplastic fluids regardless of PVP or powder content with curve fit parameters to the Herschel-Bulkley model listed in *Table 1*. An increase in yield strength, which often indicates flocculation within a suspension, would be expected with an increase in overall solids content.^{60, 66} Because both PVP and powder contents were varied simultaneously in this study, the marked difference in flow properties could not be simply attributed to the amount of PVP or powder incorporated into a suspension. The 0 vol.% PVP suspension, which had the highest solids loading, had a yield point of 4.57 Pa, and laboratory observations indicated it flowed due to gravitational forces. Figure 2.16 shows the flow curves for 0, 1 and 5 vol.% PVP compositions with corresponding curve fits to the Herschel-Bulkley model (correlation factor, $R > 0.99$). With increasing PVP and decreasing powder contents, an increase in yield shear stress, σ_y , was observed. The suspension without polymer had the lowest yield point observed in this study, suggesting that PVP, even in small amounts, greatly affected the rheology of the suspensions examined for room-temperature injection molding.

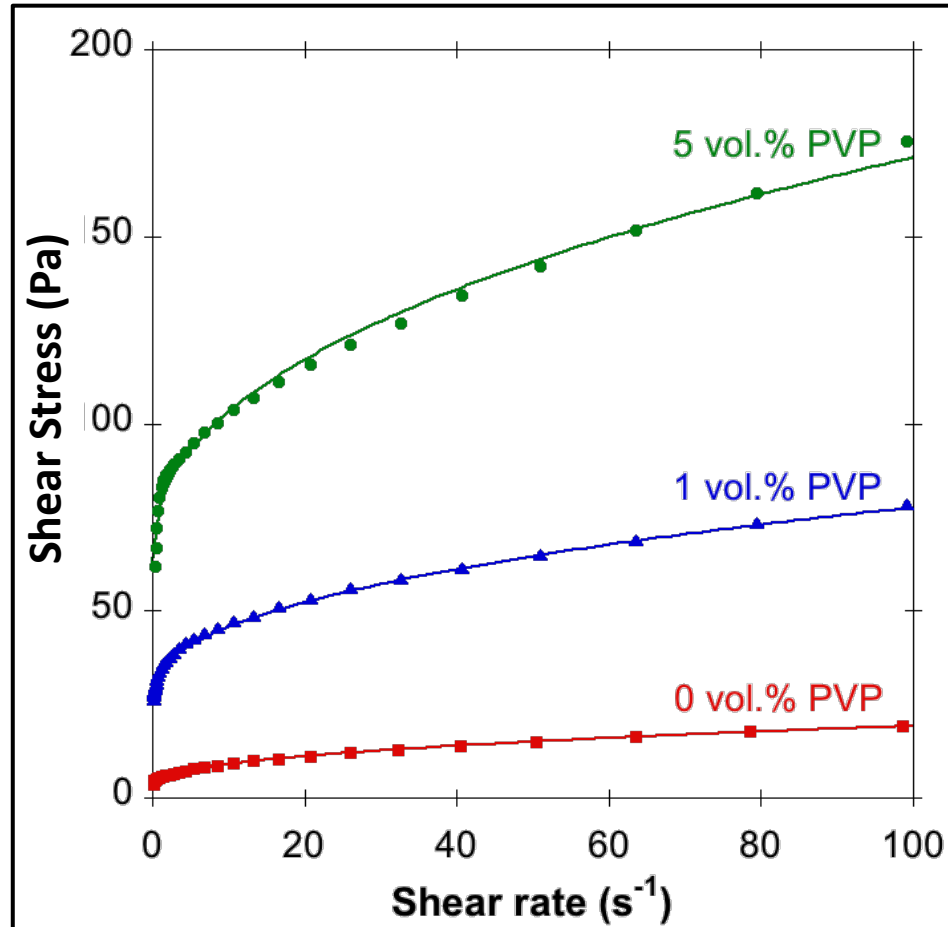


Figure 2.16 Flow curves of alumina suspensions with 0, 1 and 5 vol.% PVP (MW = 55,000 g/mol). Curve fits to the Herschel–Bulkley fluid model are shown as black continuous lines with $R > 0.99$.

During forming the yield point of suspensions without PVP was observed to be too low, as suspensions flowed into the mold before pressure was applied to the suspension via the load frame. This suggested that the rate at which the suspensions entered the mold could not be adequately controlled, resulting in unpredictable flow patterns that could cause defects in formed specimens, thus, making suspensions without PVP undesirable for room-temperature injection molding. With the introduction of a small amount of polymer, all suspensions containing PVP exhibited a yield shear stress

high enough that suspensions did not flow prematurely into the mold cavity until after pressure was initiated using the load frame. Additionally, after the suspension completely filled the mold and pressure was removed, the suspension did not flow allowing the suspension to retain its shape during drying, confirming that PVP was necessary to control the flow properties of alumina suspensions for room-temperature injection molding.

Although yield point increased with PVP content, the change in consistency, k , and flow index, n , exhibited a more complex relationship with PVP content. Consistency increased until a peak value of $26.1 \text{ Pa}\cdot\text{s}^n$ was attained at a PVP concentration of 2.5 vol.% and then began to decrease with increasing PVP content. All flow indices indicated that suspensions were highly shear thinning regardless of PVP content. A maximum flow index of 0.408 was observed for suspensions containing no polymer, and n decreased until a minimum value of 0.279 was observed for 2.5 vol.%, suggesting that this composition was the most shear thinning. The flow index then began to increase once again at PVP contents >2.5 vol.%. A highly shear-thinning response was most desirable as a relatively low viscosity aided in the complete filling of the mold and minimized pore formation by allowing entrained air bubbles to be ejected from the suspension more readily during injection molding with the pneumatic vibrator, thus enhancing processability. Figure 2.17 shows a comparison of the apparent viscosity at different shear rates of all suspensions examined in this study. It was observed that viscosity also increased with increasing polymer content, while decreasing at higher shear rates for all formulations examined due to the pseudoplastic nature of the suspensions evaluated.

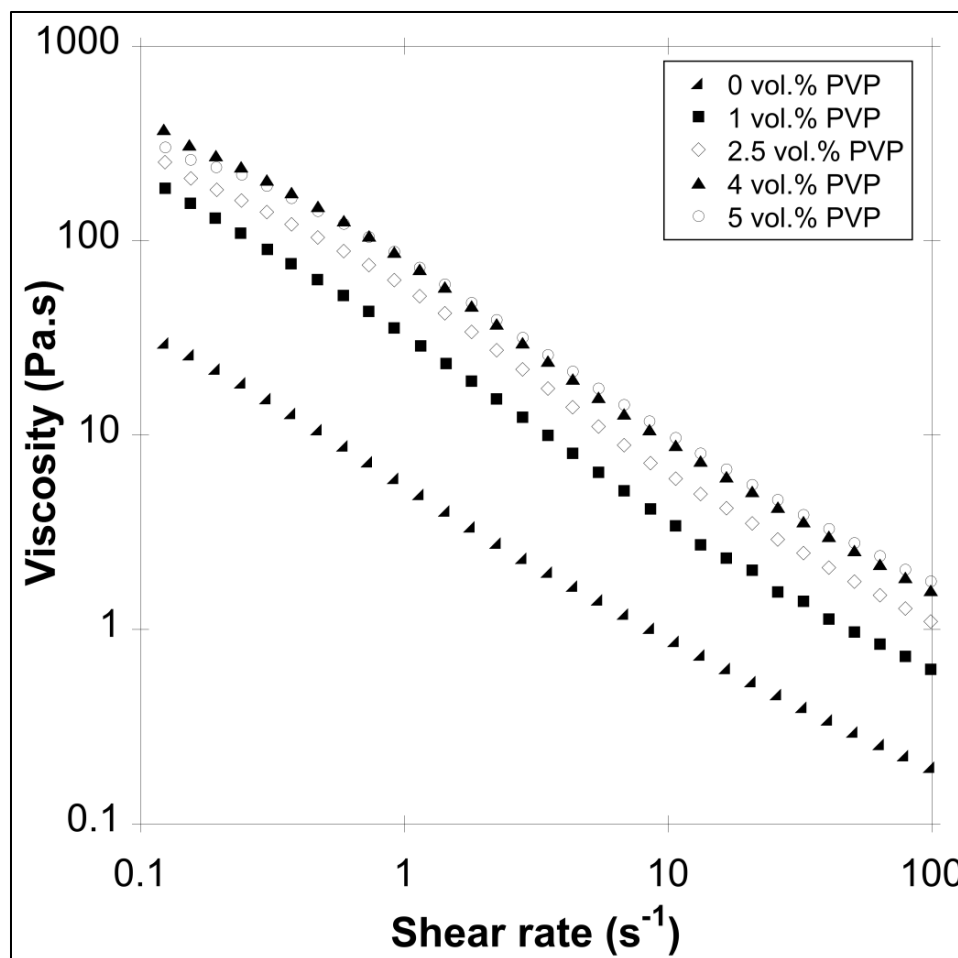


Figure 2.17 Log viscosity against log shear rate plots of alumina suspensions prepared with varying contents of PVP with molecular weight of 55,000 g/mol. Increasing PVP content resulted in higher apparent viscosities of suspensions.

The viscoelastic response of the suspensions was first evaluated in terms of an oscillatory stress. Figure 2.18 depicts the storage modulus, G' , of the CeraSGel compositions with 2 and 5 vol.% PVP at an oscillation frequency of 1 Hz. The linear viscoelastic regime exists at ranges <10 Pa for both suspensions, and as expected, G' increases as more PVP is added. In both cases at stresses >10 Pa, the storage modulus takes a precipitous drop. As shown in Figure 2.19, the storage modulus, G' , is greater than the loss modulus, G'' , suggesting the elastic properties of the CeraSGels dominate at

lower shears for both CeraSGels with 2 and 5 vol.% PVP. On the other hand, at higher shear stresses, the viscous properties dominate implying a more fluid-like behavior. This complex rheological response suggests that CeraSGels exhibit viscoelastic behavior.^{37,68}

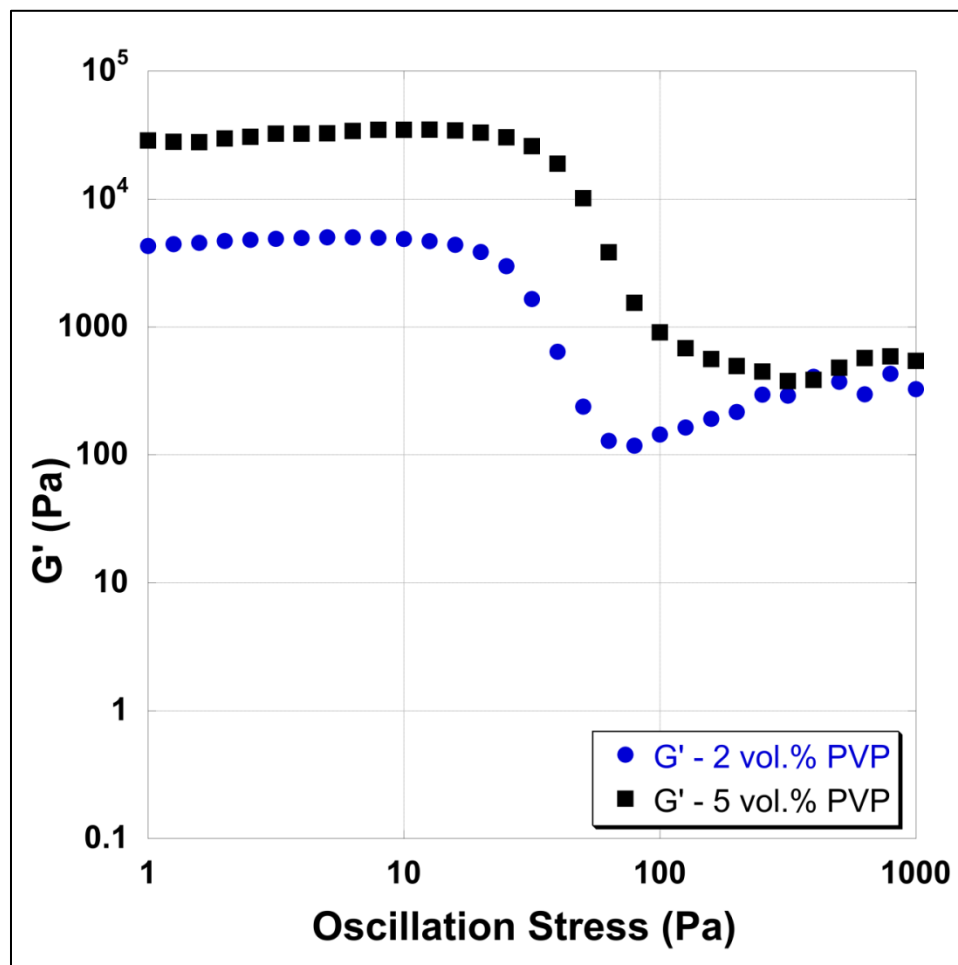


Figure 2.18 Oscillatory stress plot of alumina CeraSGels with 2 and 5 vol.% PVP. The higher polymer content corresponds to a high storage modulus, G' .

The pH of suspensions with varying PVP content changed negligibly and was 9.6 ± 0.05 , which was above the isoelectric point (IEP) of alumina in water. It has been observed that the surface charge of PVP is effectively neutral such that it does not alter the IEP of alumina-water suspensions.⁶⁹ The rheological results matched the findings of a

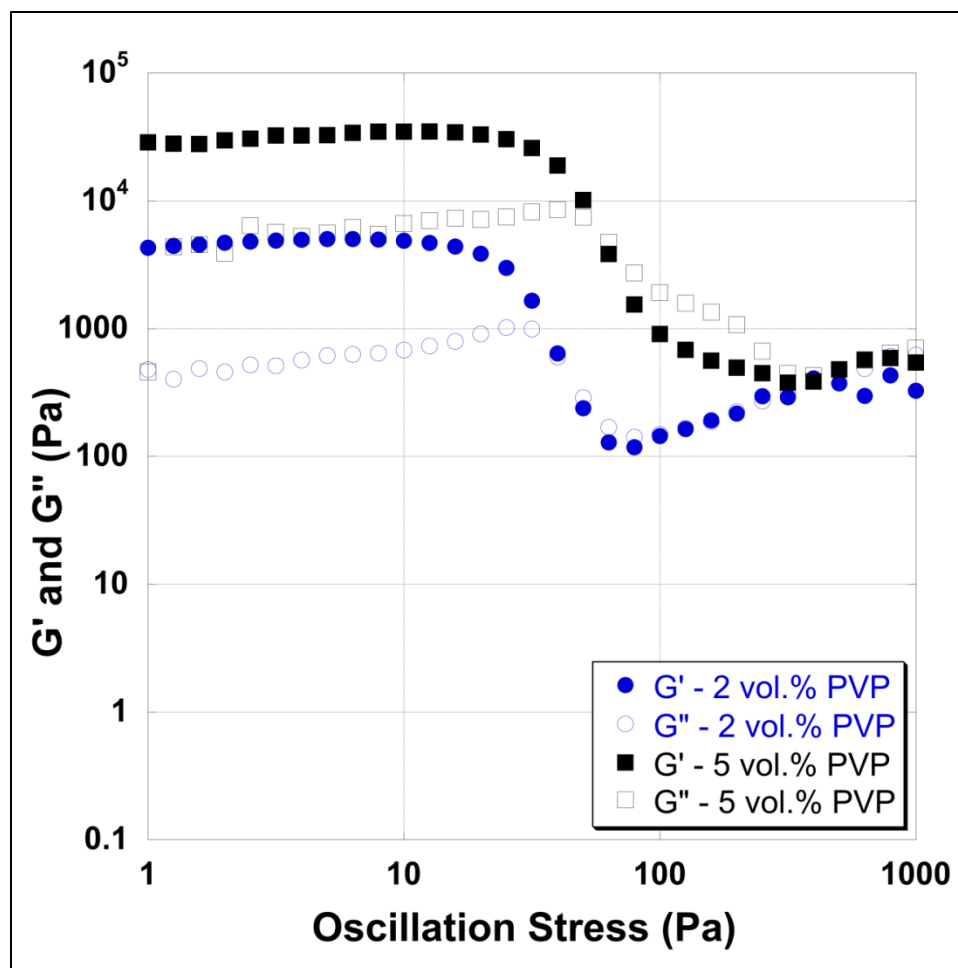


Figure 2.19 The storage modulus, G' , is greater than the loss modulus, G'' , for stress oscillations <100 Pa for CeraSGel compositions of 2 and 5 vol.% PVP.

previous study by Acosta et al.,⁵⁴ which examined alumina-PVP suspensions with a Dolapix CE64 dispersant. This past study⁵⁴ surmised that neutral PVP introduced a small amount of flocculation, because yield stress was indicative of flocculation within a suspension.⁷⁰ By increasing polymer content or molecular weight, this weak flocculation could be enhanced, manifesting itself as an increase in yield stress. This manipulability, which is discussed further in Chapter 3 along with additional rheological discussion of alumina-PVP suspensions, allows for the careful control and engineering of the flow

properties of suspensions with minimal amounts of polymer to tailor suspensions to a variety forming applications. To determine the ideal properties of suspensions for room-temperature injection molding, a variety of characterization methods were utilized to find the optimal compositions that yielded dense, strong alumina parts.

2.4.2 Green Machinability and Density of Alumina Components

Ring-shaped specimens were successfully prepared by room-temperature injection molding, suggesting that hoop stresses that developed during drying were minimized, making this a near-net shape drying process. Although sections of the specimen remained in contact with the mold during drying, no cracking due to drying gradients was observed, suggesting that capillary forces during drying did not cause defects. Prior to binder removal alumina green bodies produced by room-temperature injection molding of ceramic-PVP suspensions with varying polymer amount were deemed machinable such that the samples did not crack or shatter during the polishing procedure. It was observed that increasing binder content enhanced the machinability of the green bodies. As highlighted in Figure 2.20, green bodies formed using suspensions with ≥ 2.5 vol.% PVP exhibited little chipping or cracking compared to samples made with suspensions consisting of 1 vol.% PVP. Samples prepared with 0 vol.% PVP often did not have enough structural integrity to be removed from the mold after forming and broke either during mold removal or polishing. It was concluded that samples without PVP were too fragile to be machined in the green state using the polishing wheel and mount. Suspensions with PVP contents of 2.5, 4 and 5 vol.% were less brittle and thus less likely to chip or crack during machining using the polishing mount, suggesting that

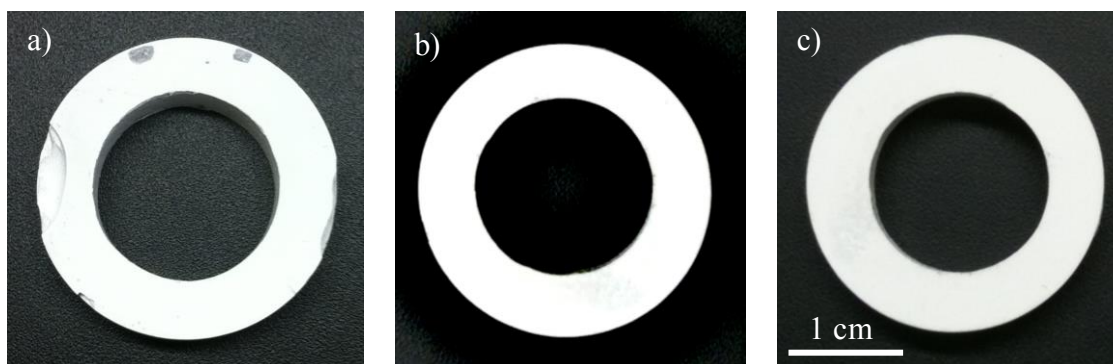


Figure 2.20 Images of alumina parts with a) 1, b) 2.5 and c) 5 vol.% PVP content after machining in the green state using a polishing mount. Samples with less than 2.5 vol.% PVP chipped during machining suggesting a lower green strength when compared with samples with higher binder content.

parts made using these compositions could be polished in an automated process. Note that while the 1 vol.% PVP suspensions could not be polished using the polishing mount without introducing defects, it could be polished by hand. This method was used to prepare 1 vol.% PVP suspensions for mechanical testing.

Table 2.1 highlights the green density values of specimens prepared with suspensions containing varying PVP contents after binder removal. Alumina samples made by room-temperature injection molding exhibited green densities $>60\%$ of the true density ($TD=3.98 \text{ g/cm}^3$) of alumina regardless of initial PVP content. Specimens prepared with 0 vol.% PVP exhibited the highest green density of 2.56 g/cm^3 (64%TD). Of the specimens prepared with polymer-containing suspensions, those consisting of 1 and 2.5 vol.% PVP were statistically the same ($p = 0.26$) with $2.52 \pm 0.01 \text{ g/cm}^3$ (63%TD) and $2.50 \pm 0.02 \text{ g/cm}^3$ (63%TD), respectively, and exhibited statistically higher green densities than 4 and 5 vol.% PVP. The p-values for specimens prepared with 1 vol.% PVP when compared with 4 and 5 vol.% PVP suspensions were $p_{1\text{vol.}\%,4\text{vol.}\%} = 7.3 \times 10^{-3}$

and $p_{1vol.\%,5vol.\%} = 0.0041$, respectively, and for specimens initially containing 2.5 vol.% PVP compared with 4 and 5 vol.% PVP suspensions were $p_{2.5vol.\%,4vol.\%} = 0.00042$ and $p_{2.5vol.\%,5vol.\%} = 0.005$, respectively. These p-values were less than 0.05 suggesting that the data sets were statistically different, whereas specimens prepared with 4 and 5 vol.% PVP suspensions were statistically similar ($p_{4vol.\%,5vol.\%} = 0.10$). Overall, parts formed by room-temperature injection molding using suspensions with PVP were successfully machined and sintered into the desired C-shaped part in accordance with the ASTM standard as highlighted in Figure 2.5.

2.4.3 Sintered Density and Microstructure of Alumina C-Ring Specimens

Archimedes density analysis confirmed that samples reached ~98%TD regardless of initial PVP content after binder burnout and pressureless sintering. Specimens prepared without PVP exhibited statistically higher sintered density values. Although the density of samples prepared with suspensions using 5 vol.% PVP appeared to decrease, the density values were determined to be statistically similar to samples using other compositions with lower PVP contents. This suggested that polymer content did not dramatically influence the final density and internal porosity of the ceramic part. Density results are highlighted in Table 2.1. Linear shrinkage for all samples after sintering was <16%.

Analysis of the internal structure using SEM revealed an overall dense microstructure with some porosity between and within grains (micrographs of samples prepared with 1, 2.5, 4 and 5 vol.% PVP are shown in Figure 2.21). By applying a *t*-test,⁶⁶ the mean grain size of specimens prepared with 2.5 vol.% PVP was determined to be

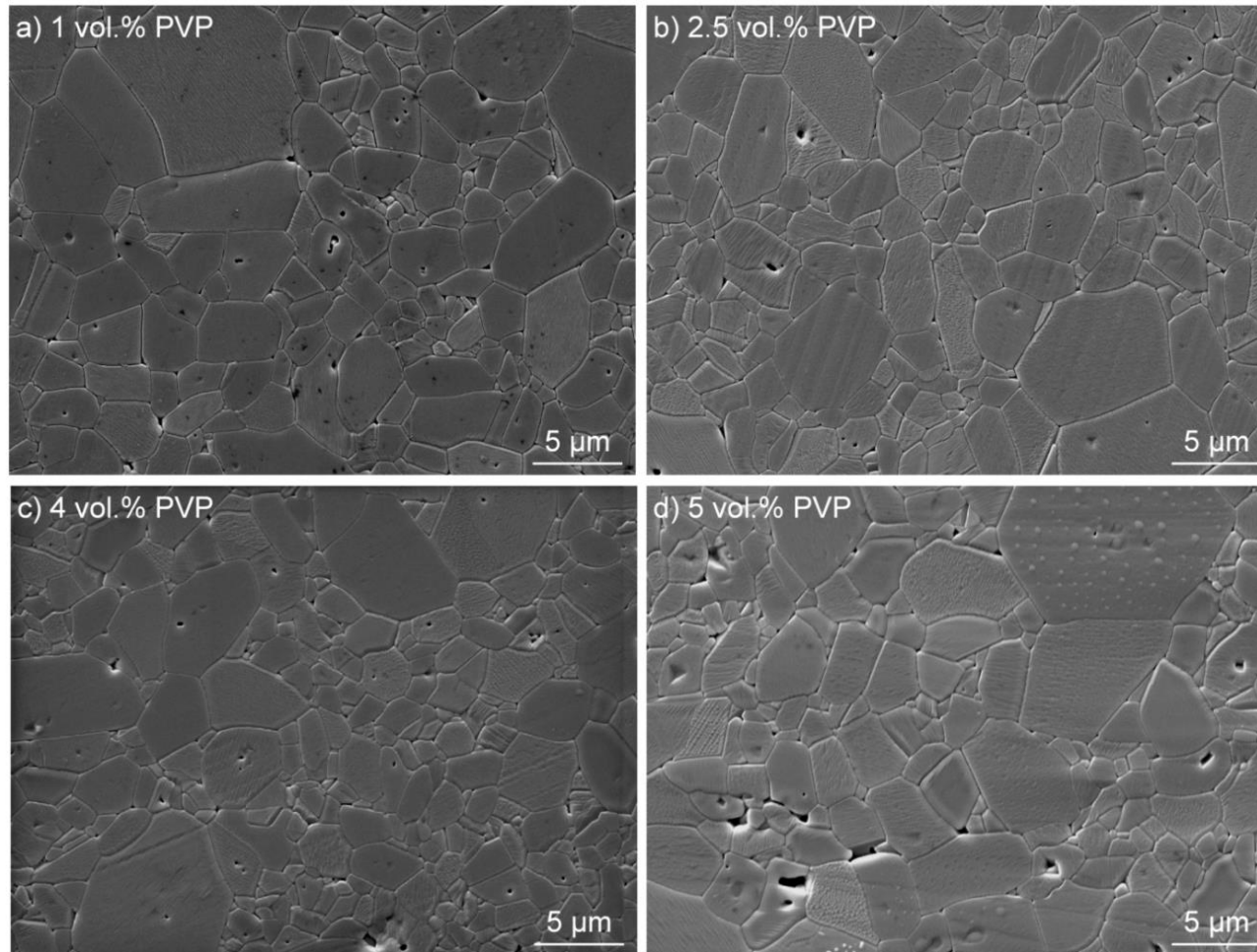


Figure 2.21 SEM micrographs of polished and thermally etched surfaces of alumina samples prepared with suspensions containing a) 1 vol.%, b) 2.5 vol.%, c) 4 vol.% and d) 5 vol.% PVP. All samples were sintered at 1620°C.

statistically larger than those containing 1 and 4 vol.% PVP as $p < 0.05$ ($p_{1\text{vol.}\%, 2.5\text{vol.}\%} = 0.043$ and $p_{2.5\text{vol.}\%, 4\text{vol.}\%} = 0.019$) yet similar to specimens using 5 vol.% PVP ($p_{1\text{vol.}\%, 5\text{vol.}\%} = 0.22$), which was similar to all compositions evaluated. Mean grain sizes of specimens manufactured using suspensions with different PVP contents are highlighted in Table 2.1. The slight discrepancies in values suggested that there was no apparent trend with PVP content that resulted in a particular grain size, although 2.5 vol.% yielded slightly higher grain sizes than 1 and 4 vol.% PVP suspensions.

2.4.4 Mechanical Properties of Sintered Alumina C-Ring Specimens

Average C-ring strength values that were determined using the ASTM C1323-10 test⁵⁹ for samples fabricated using alumina suspensions with 1, 2.5, 4 and 5 vol.% PVP are shown in Table 2.1 and plotted in Figure 2.22. Despite the fact that specimens of 2.5 vol.% PVP had a mean grain size that was statistically similar to those with 5 vol.% PVP and higher than specimens of 1 and 4 vol.%, there was a statistically significant peak of 261 ± 57.6 MPa in strength for 2.5 vol.% PVP content ($p_{1\text{vol.}\%, 2.5\text{vol.}\%} = 0.04$, $p_{2.5\text{vol.}\%, 4\text{vol.}\%} = 0.036$ and $p_{2.5\text{vol.}\%, 5\text{vol.}\%} = 0.024$). Samples with 5 vol.% PVP exhibited a significant drop in average C-ring strength, though the values were found to be statistically similar to the strengths of samples prepared with 1 and 4 vol.% PVP suspensions. When comparing the values from this study to those in literature, an average C-strength value was found to be 230 MPa for commercially available surface-finished 99.8% pure alumina tubular specimens⁷¹ and 275.3 ± 16.6 MPa for tubular gun barrel specimens prepared using 95% pure alumina AD995 by CoorsTek.⁷² The method of preparation for these tubular specimens is unknown due to proprietary information, but the density and C-strength

values obtained by room-temperature injection molding of alumina-polymer suspensions is comparable.

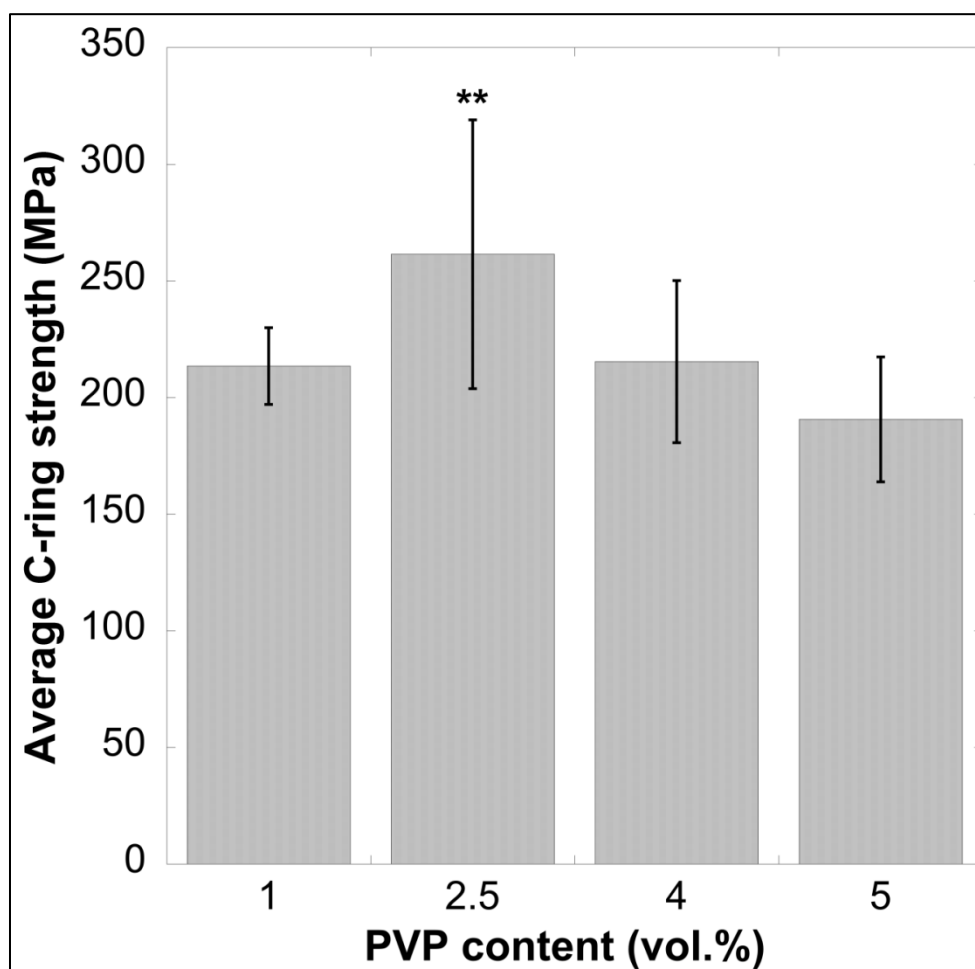


Figure 2.22 Plot of average C-ring strength data for sintered specimens prepared with suspensions containing 1, 2.5, 4 and 5 vol.% PVP (MW = 55,000 g/mol). Specimens of 2.5 vol.% PVP exhibited the highest average C-strength. ** p -Values for specimens prepared with 2.5 vol.% PVP were less than 0.05 indicating a statistically significant peak in strength for these specimens.

The ASTM C1323-10 test is prone to fracture at defects located at the outer surface of specimens.⁵⁹ The increase in strength for specimens prepared using 2.5 vol.% PVP suggested that the distribution and size of pores within these samples, not the size of grains, minimized their influence on failure resulting in higher C-strength values.

Fractographic analysis revealed that the majority of fractures originated at pores on or near the outer surface of C-rings regardless of PVP content, intimating that the amount of PVP in a suspension affected the overall arrangement and/or size of strength-limiting pores that resulted in fracture at lower loads for samples prepared with 1, 4 and 5 vol.% PVP suspensions. The favorable mechanical and microstructural properties of specimens prepared with 2.5 vol.% PVP implied that the flow behavior of such suspensions, including the relatively low viscosity and flow index, which allowed the suspension to fill the mold and minimize strength-limiting defect development, was ideal for processing by room-temperature injection molding. In spite of this conclusion, the large standard deviation in all samples, particularly samples prepared with 2.5 vol.% PVP, suggest that further processing improvements are needed to tighten this distribution and improve the reproducibility of dense, high-strength alumina parts with uniform microstructures.

2.4.5 Varying Molecular Weight at Optimal PVP Concentration

The desirable flow properties and apparent peak in strength along with relatively high green and sintered densities suggested that 2.5 vol.% PVP was the optimal concentration of polymer to use in the alumina suspensions for room-temperature injection molding. Three additional suspensions using PVP with molecular weights of 10,000, 360,000 and 1,300,000 g/mol with alumina contents of 55.1 vol.%, 53.9 vol.% and 52.4 vol.%, respectively, were evaluated to determine the effect of molecular weight on the rheological behavior of the suspensions as well as on microstructural and mechanical properties of samples fabricated by room-temperature injection molding.

The formulations of the alumina-PVP suspensions prepared using 2.5 vol.% PVP with molecular weights of 10,000, 55,000, 360,000 and 1,300,000 g/mol are given in Table 2.2. Each composition exhibited yield-pseudoplastic behavior (refer to Table 2.2 for the Herschel-Bulkley model curve fit parameters) similar to that of suspensions prepared with varying contents of 55,000 g/mol PVP. It was observed that the yield points in suspensions increased with increasing molecular weight and decreasing powder content, while consistency values and flow indices varied with increasing molecular weight. Suspensions with 10,000 g/mol PVP exhibited the lowest yield stress of suspensions containing polymer, whereas the yield stress of formulations having PVP molecular weights $\geq 360,000$ g/mol jumped significantly to >50 Pa, only surpassed in magnitude by suspensions with 5 vol.% PVP of 55,000 g/mol, which had $\sigma_y = 59.4$ Pa. Although consistency increased from $12.0 \text{ Pa}\cdot\text{s}^n$ at 10,000 g/mol to $26.1 \text{ Pa}\cdot\text{s}^n$ for 55,000 g/mol, it then decreased in value from $8.48 \text{ Pa}\cdot\text{s}^n$ to $4.92 \text{ Pa}\cdot\text{s}^n$ for 360,000 g/mol and 1,300,000 g/mol, respectively. Shear-thinning behavior was reflected by all flow indices, and n decreased in value from 0.320 for 10,000 g/mol until reaching a minimum value of 0.279 at a molecular weight of 55,000 g/mol. Above 55,000 g/mol n increased significantly, and the maximum value was observed in suspensions containing 1,300,000 g/mol. Most notably, compositions including PVP with a molecular weight of 1,300,000 g/mol exhibited the lowest consistency value and the highest flow index of 0.621, which implied that they were the least shear thinning of all PVP-containing suspensions studied. Furthermore, the suspensions with 2.5 vol.% PVP of 55,000 g/mol had the highest consistency and lowest flow index, making it the most shear thinning of the suspensions.

Figure 2.23 shows a comparison of the apparent viscosity at different shear rates of all suspensions containing 2.5 vol.% PVP with varying molecular weights examined in this study. Although suspensions with 10,000 g/mol PVP exhibited the lowest apparent viscosity, the overall apparent viscosities for suspensions with PVP of 55,000 g/mol, 360,000 g/mol and 1,300,000 g/mol were comparable, as highlighted in Figure 2.23. Due to the order of magnitude increase in molecular weight, suspensions with 1,300,000 g/mol were expected to have a significantly higher viscosity, but they were observed to have only a slightly higher viscosity than suspensions prepared with 55,000 g/mol and

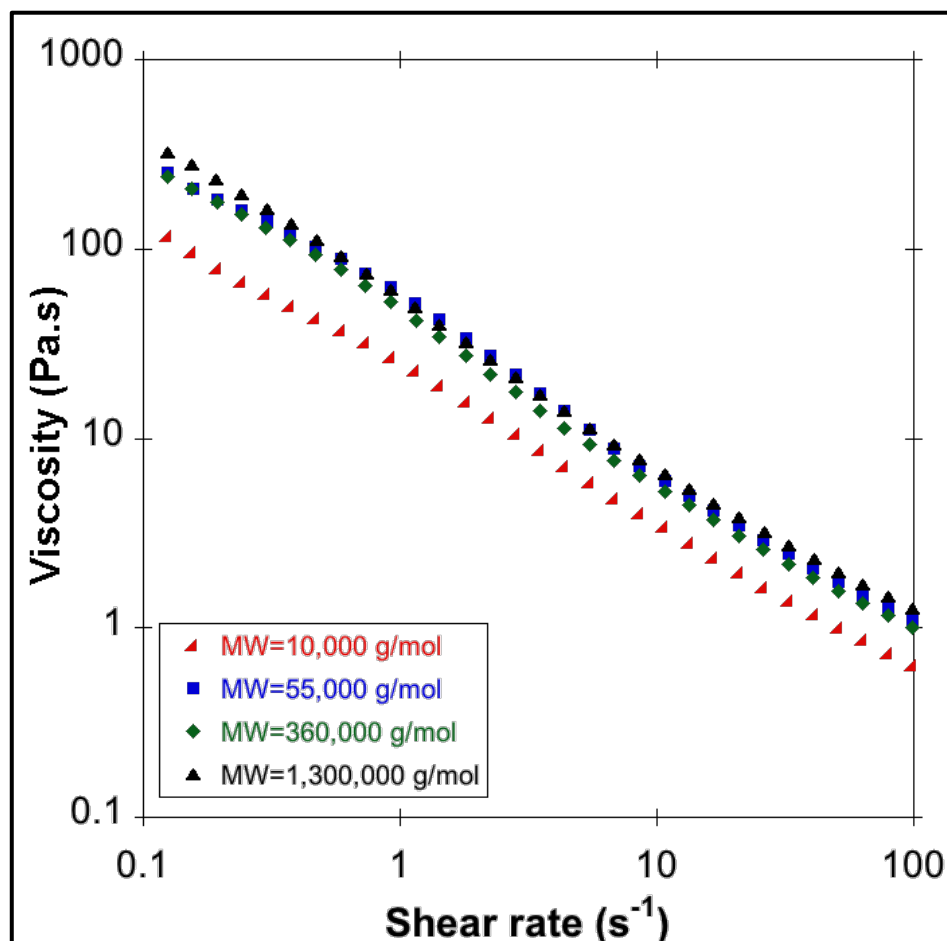


Figure 2.23 Plots of log viscosity vs. log shear rate of alumina suspensions prepared with 2.5 vol.% PVP of varying molecular weights.

360,000 g/mol over the shear rates evaluated. This slight increase in viscosity could potentially be attributed to the decrease in alumina content in suspensions prepared with PVP of higher molecular weights, but further analysis of suspensions at constant powder loadings would be needed to isolate the main factor.

The low yield point and apparent viscosity made suspensions containing 10,000 g/mol PVP more difficult to control during injection molding, though samples were successfully fabricated for testing. On the other hand, the slightly higher viscosity of suspensions with 1,300,000 g/mol PVP impacted processability by preventing fabrication of alumina samples without large macroscopic defects. These defects likely resulted from air bubbles developing and becoming trapped within suspensions during forming due to the lower degree of pseudoplasticity and the slightly higher apparent viscosity of suspensions with 1,300,000 g/mol PVP. Consequently, parts for mechanical characterization could not be prepared with this high of a molecular weight. Additionally, the specimens exhibited low green and sintered densities when compared with specimens prepared using PVP with lower molecular weights. The inferior microstructural properties that plagued specimens prepared with 1,300,000 g/mol PVP were likely the result of the improper flow characteristics of these suspensions, suggesting that this molecular weight was not suitable for room-temperature processing.

Alumina parts prepared using 10,000 g/mol and 360,000 g/mol PVPs were machinable prior to binder removal. These samples exhibited green densities comparable to those made using 55,000 g/mol PVP, even though the lower molecular weight yielded the highest green densities (refer to Table 2.2). Green bodies with 10,000 g/mol and 55,000 g/mol were statistically similar ($p = 0.26$) and statistically higher than samples

with 360,000 g/mol and 1,300,000 g/mol ($p < 0.05$). After binder removal and pressureless sintering, densities of ~98%TD were attained for specimens prepared with 10,000 g/mol, 55,000 g/mol and 360,000 g/mol (density values highlighted in Table 2.2). Specimens using 1,300,000 g/mol had a statistically lower density of 3.78 g/cm³ (95%TD).

There appeared to be a notable difference in C-ring strengths of samples with 10,000 g/mol having lower values than those produced with 360,000 g/mol (values shown in Table 2.2), but statistical analysis revealed that mechanical properties were comparable (all $p > 0.05$). The C-strength values were statistically similar to all samples prepared with varying amounts of 55,000 g/mol PVP. Despite the similar mechanical properties, the highly shear-thinning flow behavior needed for room-temperature processing as well as high green and sintered densities distinguished suspensions containing 2.5 vol.% PVP with a molecular weight of 55,000 g/mol from all other suspensions examined in this study as the optimal PVP molecular weight and concentration to be incorporated into alumina suspensions for room-temperature injection molding.

2.5 Summary and Conclusions of Room-Temperature Injection Molding of Alumina-PVP Suspensions

A novel, environmentally benign room-temperature injection molding method has been developed and successfully applied to an alumina-PVP system. Through careful control of high ceramic powder loadings and a minimal amount of polymer additives, the viscosity of an alumina-PVP suspension was optimized to afford room-temperature

injection molding of dense, near-net shaped alumina ring-shaped parts. Analysis of the flow properties suggested that the suspensions exhibited yield pseudoplasticity, which was ideal for room-temperature injection molding. Consistent with a previous investigation,⁵⁴ PVP was a neutral species at the pHs of suspensions studied here, and it likely induced a controlled degree of weak flocculation with varying PVP content, making these suspensions tailorable to the room-temperature processing method examined in this study. Because powder content was varied simultaneously with PVP content and molecular weight, further study of the rheological behavior of suspensions with constant powder loadings is needed to fully ascertain whether the amount and/or molecular weight of PVP is the main factor in obtaining specimens with desirable properties as well as suspensions with suitable rheology for room-temperature injection molding.

After preparing an alumina part by room-temperature injection molding, specimens were dried for roughly an hour in air and then removed from the mold. In traditional ceramic injection molding, parts are typically ejected from a mold within the first minute of forming.³⁰ To reduce drying times of specimens prepared by room-temperature injection molding, modifying the current process, for example by utilizing a more porous mold material to facilitate evaporation, will be required to promote more rapid demolding times. The polymer binder in dried specimens, which were machinable in the green state, was effectively removed by thermal pyrolysis, resulting in parts with high green densities (>60%TD). High sintered densities (98%TD) were achieved by pressureless sintering, and SEM micrographs confirmed that sintered samples had an overall dense microstructure. Minimal shrinkage (<16% linear) of samples was observed.

Alumina specimens with mechanical properties comparable to literature were successfully fabricated by this unique room-temperature processing method.

Suspensions containing 2.5 vol.% PVP (MW=55,000 g/mol) resulted in the most favorable combination of properties in formed alumina specimens. The suspensions exhibited a yield shear stress such that suspensions did not flow under gravitational stresses, thus preventing premature filling of the mold and providing for a higher degree of control of the flow during forming. Additionally, suspensions with 2.5 vol.% PVP (MW=55,000 g/mol) had the lowest flow index observed in this study, suggesting that the rheology was most suitable for the production of alumina samples with relatively high green and sintered densities along with high C-strengths via room-temperature injection molding. As a result, 2.5 vol.% PVP with molecular weight of 55,000 g/mol was considered the optimal concentration and type of polymer in the suspensions prepared and processed in this study. Further development of injection molding alumina-PVP suspensions at room temperature will ultimately allow for faster and less expensive fabrication of near-net shape ceramic parts with complex geometries through this unique green injection molding process.

2.6 Perspectives on Improving and Optimizing Room-Temperature Injection Molding for Manufacturing Alumina Ring-Shaped Specimens

2.6.1 Reducing Drying Time of Formed CeraSGel Samples

Industrial level high-throughput ceramic injection mold processing requires near instantaneous solidification and/or drying of samples after injection molding to allow for immediate demolding.³⁰ The drying and solidification times of CeraSGels for the current

room-temperature injection molding process are approximately an hour varying slightly with binder content. In order to reduce the time required for a sample to reach a high enough green strength for faster or immediate demolding, a more porous mold material should be investigated. A more breathable mold material will likely facilitate quicker evaporation of water from the specimen allowing for more rapid demolding.

2.6.2 Improving Sintered Mechanical Properties of Alumina Rings

Flexural strength of conventionally processed alumina is typically 200-700 MPa.⁷⁴ Studies by Krell et al.⁷⁴ evaluated the mechanical properties of alumina bars prepared with submicron powder particles prepared by cold isostatic pressing and gelcasting in order to evaluate the strength dependence on grain size. Krell successfully attained >99% true density in gelcast alumina specimens by pressureless sintering at 1350°C for 2 h in air. In these particular samples, flexural strength values were 800-900 MPa with final grain sizes were ~1-1.3 μm . It was believed that the binder content allowed high uniform dispersion in feedstocks that consequently reduced the frequency of flaws in the final ceramic parts. In another study, alumina samples that reached >99% true density prepared by gelcasting were successfully pressureless sintered at 1280°C with similarly high flexural strengths.⁷⁵ In lines with the Krell study,⁷⁴ alternate pressureless sintering procedures of alumina CeraSGel samples should be evaluated to reduce the final grain size so as to increase ultimate strength of the alumina samples.

CHAPTER 3. EXPERIMENTAL AND ANALYTICAL INVESTIGATION OF THE RHEOLOGY AND STABILITY OF ALUMINA-PVP SUSPENSIONS

The highly loaded aqueous alumina suspensions that were utilized for room-temperature injection molding described in Chapter 2 were observed to exhibit a similar rheological behavior as suspensions prepared with Dolapix® CE64, an anionic dispersant. The study of alumina-PVP suspensions was needed to determine the optimal flow properties best suited for room-temperature injection molding. Through parallel plate rheometry, the effect of ceramic powder content and varying polymer average molecular weight and concentration on the rheological response of the suspensions was evaluated. The interparticle interactions governing the suspensions' stability were also approximated through application of Derjaguin-Landau-Verwey-Overbeek (DLVO), steric and depletion models. The potential estimations were then matched with experimental observations. This chapter elucidates current understanding of how the rheological response of stable alumina suspensions with polymers, in this case polyvinylpyrrolidone (PVP), that are nonadsorbed to the inorganic powders can be manipulated using colloidal stabilization and/or destabilization methods.

3.1 Understanding Dispersion and Stability in Colloidal Systems

Understanding the rheological response, which is often a reflection of the colloidal stability or instability,⁷⁰ of highly loaded ceramic suspensions is vital to enable fabrication of ceramic components into useful geometries and near-net shapes. By carefully crafting the flow properties, it is possible to adapt colloidal suspensions to a variety of processing methods including tape casting, casting, injection molding, and extrusion for a variety of applications in electronics, aerospace, energy and other sectors of industry.^{37, 76} Colloidal formulations that have been designed for typical ceramic casting methods are usually complex.⁷⁷⁻⁷⁹ Depending on the adsorption behavior of a polymer added to a dispersant/ceramic slurry, suspensions can be further stabilized by either electrostatic, steric and/or depletion interactions.⁷⁷ In order to prepare CeraSGels based on zirconium diboride for injection molding, a deep understanding of the room-temperature colloidal stability of alumina-based CeraSGels was needed to mature and adapt the novel process to alternate material systems.

3.1.1 Colloidal Stability

Colloidal suspensions are typically comprised of particles ranging from 10 nm up to 1 μm dispersed in a solvent. The particles themselves can be either *lyophilic* or *lyophobic* depending on the system. Lyophilic particles tend to stay dispersed, whereas lyophobic particles tend to spontaneously aggregate in an external phase often due to the weak attractive van der Waals forces associated with the dipoles of each colloid. Brownian motion, which is the random motion of particles due to collisions with other particles in solution, will cause lyophobic particles to interact and flocculate, resulting in

a clump of particles. In order to prevent particles from coagulating, or forming aggregates, mechanisms of stability can be employed.⁸⁰

Electrostatic stability may be imparted to a system of particles by altering or maintaining a particular surface charge, whether positive or negative, to promote repulsion. If all of the particles have a similar charge, they will repel each other as the distance between the particles is decreased, thus inhibiting agglomeration. A surfactant or electrolyte can be incorporated into a colloidal system to enhance the surface charge of the particles, resulting in the development of the electrical double layer. The electrical double layer thickness dictates the repulsion between particles, which ultimately governs the stability of a colloidal system (refer to Figure 3.1).

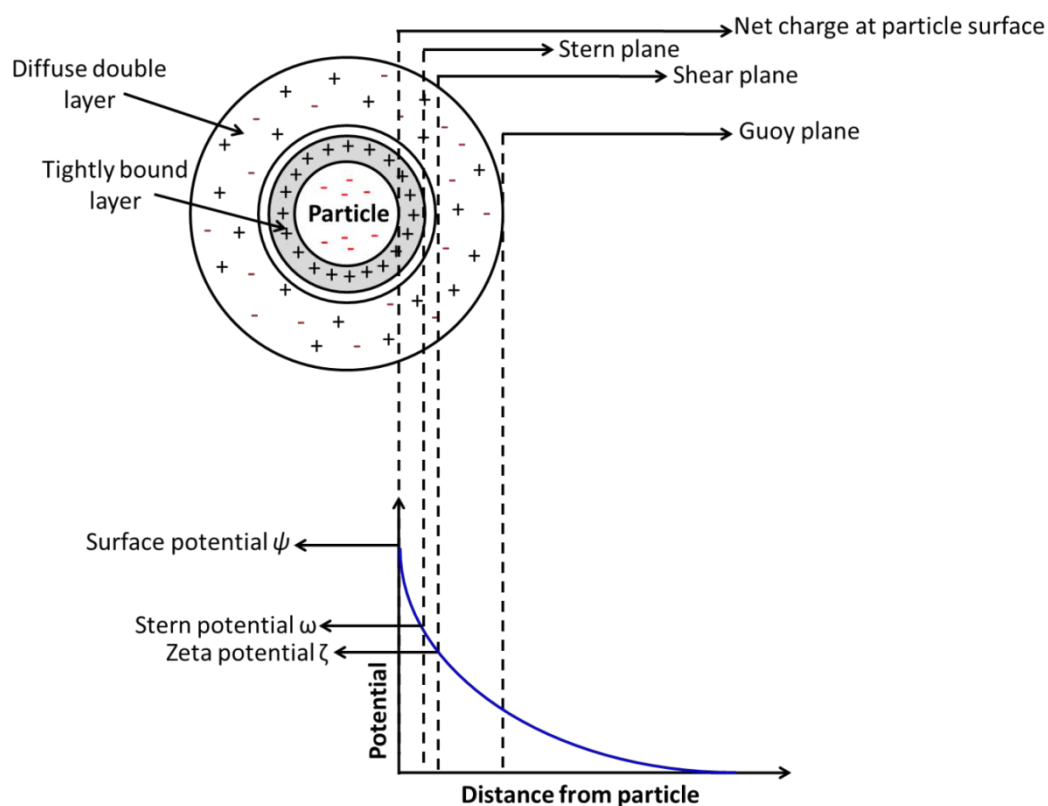


Figure 3.1 Schematic of a charged ceramic particle in solution with associated charge distribution for its diffuse double layer.⁸⁰

Alternately, particles can be coated with a layer of lyophilic molecules, often a polymer phase, to promote *steric stability* (shown in Figure 3.2). In steric stabilization, the adsorbed polymer, often introduced by a surfactant, chemically or physically attaches to the colloid surface, and its tail acts as a barrier to prohibit adjacent particles from approaching and agglomerating. Careful selection of a surfactant is imperative in order to engineer a stable colloidal system, and moderate polymer concentrations are needed to achieve effective steric stabilization. Should improper selection of a surfactant take place, the adsorbing polymer species, particularly of a higher molecular weight, can connect or bridge individual colloids by attractive electrostatic interactions, resulting in bridging flocculation (highlighted in Figure 3.2). Bridging flocculation may occur in colloidal suspensions with low polymer content (~p.p.m.).⁸⁰

In colloidal systems with nonadsorbing polymer at moderate to high concentrations, the interparticle distance may become small enough that polymer molecules are unable to fill all of the space between particles. As a result, depletion zones consisting of only solvent develop, causing *depletion flocculation* via osmotic gradients.⁸¹ This colloidal mechanism may transition to another regime depending on the achievable conformations of the nonadsorbed polymers. In a similar case in which polymers do not bond to the powder surface, and the dispersant does not promote their adsorption, the polymers can be located in the volume between particle surfaces, thus re-stabilizing the suspension. This phenomenon is referred to as *depletion stabilization*.⁸²⁻⁸⁴ There the polymers can constitute a barrier for contact between particles depending on their concentration and molecular weight with respect to the surface area and size of the

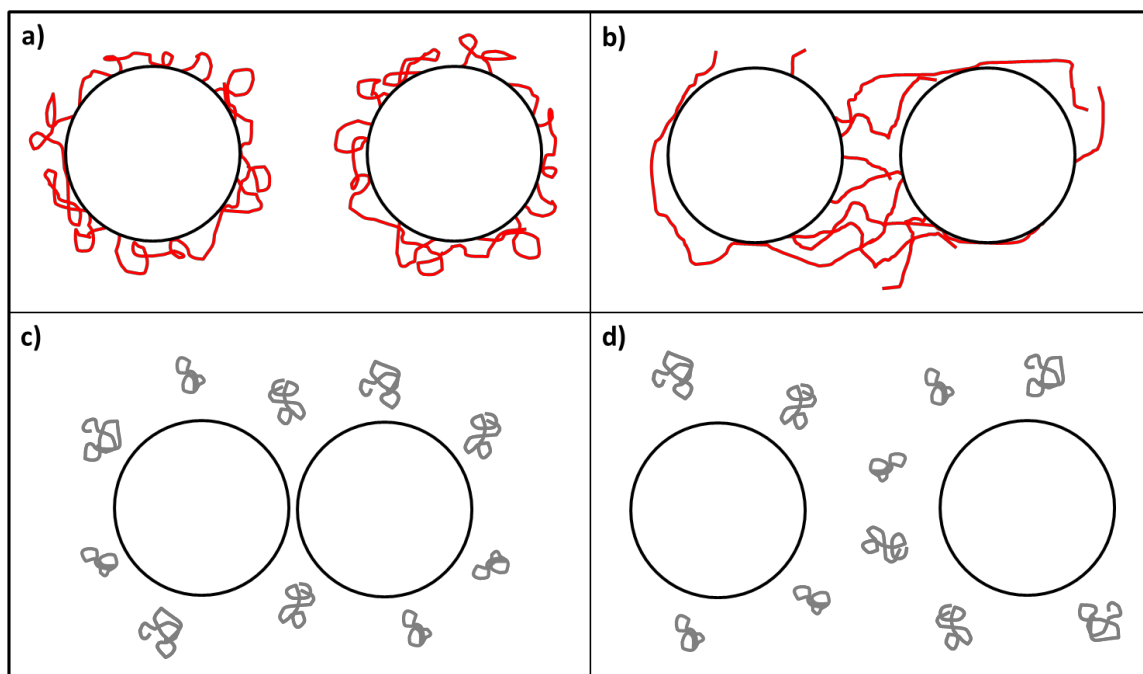


Figure 3.2 Schematic of a) steric stabilization, b) bridging flocculation, c) depletion flocculation and d) depletion stabilization.⁸⁰

powders.^{83, 85} A schematic of depletion flocculation and stabilization mechanisms are shown in Figure 3.2.

Stability may be transferred to a colloidal system by a single mechanism or combination of mechanisms described above in order to promote the repulsion or slight flocculation of the particles depending on the colloidal application.⁸⁰ In order to develop alumina-PVP suspensions with suitable flow properties for a variety of ceramic processing methods, their unique rheology was explored and then matched with current mathematical predictions of the underlying stability mechanisms to understand and predict their rheological behavior.

3.2 Experimental Investigation of Room-Temperature Rheology of Alumina-PVP Suspensions

3.2.1 Formulating Alumina-PVP Suspensions

Alumina-PVP suspensions were prepared in a manner identical to the procedure described in *Section 2.1.1*; however, suspensions utilized Dolapix® CE64 (Zschimmer & Schwarz, Milledgeville, GA) as a dispersant rather than Darvan 821A. As previously investigated by Dakskobler et al.,⁸⁶⁻⁸⁸ Dolapix CE64, a commercially available anionic dispersant, is a poly(methacrylic acid) ammonium salt (PMAA-NH₄, chemical structure shown in Figure 3.3), which is a cation-exchange deflocculating agent used to obtain excellent flowability for suspensions with high solid loadings.⁸⁹ It modifies the electrical double-layer and enhances the negative charge of particle surfaces. Spectroscopy studies performed by Dakskobler and Kosmač revealed that Dolapix CE64 typically had an average molecular weight of 320 g/mol,⁸⁷ which was an order of magnitude smaller than that of Darvan 821A.⁵⁷ However, Dolapix CE64 possesses the same starting pH value of 7 and a solids loading comparable to Darvan 821A. It has been observed by previous

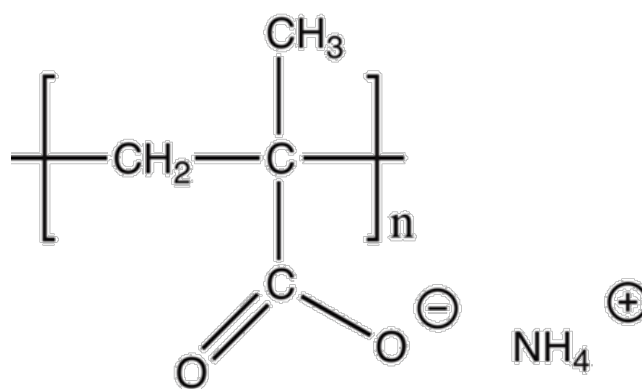


Figure 3.3 Structure of Dolapix CE64 poly(methacrylic acid) used in fabrication of alumina suspensions.

investigators that alumina suspensions containing 30-50 vol.% ceramic powder require additions of Dolapix CE64 of ~0.6 vol.% to be stabilized at pHs <9.⁹⁰⁻⁹² Approximately 4 vol.% of Dolapix CE64 was incorporated into the suspensions as was used in suspensions evaluated in *Section 2.1.1* with Darvan 821A. For the type of compositions in this investigation the dispersant did not considerably affect the effective particle size while maintaining a stable configuration of the powders.^{37, 60, 90-93} The amount of alumina varied from 53.4 to 55.7 vol.% depending on the concentration of PVP, which varied from 0 to 5.1 vol.% with molecular weights of 55,000 g/mol and 1,300,000 g/mol (compositions shown in Table 3.1), for Dolapix CE64-containing suspensions. All compositions are presented as volume percentages based on initial CeraSGel compositions, including powder, PVP, dispersant and water contents.

Table 3.1 Compositions of A16 SG alumina suspensions fabricated without PVP and with increasing inorganic content (30-54.7 vol.% alumina).

Suspension	Al ₂ O ₃ vol. %	H ₂ O vol. %	Dolapix® CE64 vol. %
1	54.7	41.3	4.0
2	50.0	45.5	4.5
3	40.0	54.7	5.3
4	30.0	63.7	6.3

To isolate the effect of PVP alone on the flow properties of the alumina-PVP suspensions, a series of four polymer solutions comprised of 12.1 vol.% PVP with average molecular weights of 10,000 g/mol, 55,000 g/mol, 360,000 g/mol and 1,300,000 g/mol, respectively, in water were also prepared by magnetic stirring. The PVP content in these four solutions was selected to correspond to 5.1 vol.% PVP in an alumina-PVP

suspension. Additionally, the pH of a solution of PVP with molecular weight of 360,000 g/mol and Dolapix CE64 in water at concentrations identical to the alumina suspension with 5.1 vol.% PVP was modified to 9.5, the pH observed in alumina-PVP suspensions dispersed with Dolapix CE64, using ammonium hydroxide to determine if PVP and PMAA could together cause an alternate adsorption effect.

Additionally, the influence that PVP additions had on the pH of the system was studied in selected suspensions (3A, 6A, 8A, 10A, and 13A) from Table 3.2. An Oakton PH5 meter (Vernon Hills, IL) previously calibrated with electrolytic buffer solutions at pHs of 4, 7, and 10 was used to obtain pH values of polymer-water solutions and ceramic slurries before and after adding the PVP-DI water solution to the suspensions. The electrokinetic potential (ζ in mV) of alumina powder surfaces was measured in dilute solutions of alumina and DI water with Dolapix CE64 using a Malvern Nano ZS Zetasizer (Westborough, MA). The pH of the solution was adjusted using ammonium hydroxide additions and monitored using the previously mentioned Oakton PH5 meter.

Table 3.2 Compositions and calculated curve fit parameters from the Herschel-Bulkley model used in flow curves ($R=0.99$) of A16 SG alumina suspensions fabricated with PVP contents of 1, 2.6 and 5.1 vol.% PVP as well as PVP solutions without alumina or dispersant. P_r represents the ratio of the lowest molecular weight PVP to the total amount of PVP in the formulation.

Suspension	Al ₂ O ₃ vol.%	Dolapix® CE-64 vol.%	1.3x10 ⁶ g/mol PVP vol.%	55x10 ³ g/mol PVP vol.%	Total polymer vol.%	P_r	σ_y (Pa)	k (Pa·s ⁿ)	n
1	54.7	4.0	-	-	-	-	18.5±4.1	2.5±1.5	0.59±0.11
1A	55.7	3.9	-	1.00	1.0	1	74.9±3.2	12.2±1.5	0.51±0.02
2A	55.7	3.9	0.25	0.75	1.0	0.75	81.3±2.0	9.9±0.9	0.55±0.02
3A	55.7	3.9	0.50	0.50	1.0	0.5	54.8±3.1	7.8±0.8	0.52±0.01
4A	55.7	3.9	0.75	0.25	1.0	0.25	80.6±1.2	6.9±0.5	0.58±0.01
5A	55.7	3.9	1.00	-	1.0	0	58.4±0.6	5.3±0.2	0.59±0.01
6A	54.8	3.8	-	2.60	2.6	1	81.1±2.1	8.2±0.8	0.60±0.02
7A	54.8	3.8	0.65	1.95	2.6	0.75	114.7±2.5	9.6±0.9	0.62±0.02
8A	54.8	3.8	1.30	1.30	2.6	0.5	93.6±1.6	7.5±0.5	0.66±0.01
9A	54.8	3.8	1.95	0.65	2.6	0.25	174.1±2.8	7.6±0.5	0.84±0.01
10A	54.8	3.8	2.60	-	2.6	0	165.7±2.9	7.8±0.5	0.87±0.01
11A	53.4	3.7	-	5.10	5.1	1	177.5±6.1	17.8±2.1	0.65±0.02
12A	53.4	3.7	1.30	3.80	5.1	0.75	163.8±3.3	14.6±0.8	0.76±0.01
13A	53.4	3.7	2.55	2.55	5.1	0.5	150.0±1.0	11.6±0.5	0.77±0.01
14A	53.4	3.7	3.80	1.30	5.1	0.25	169.3±35.8	93.6±13.8	0.60±0.03
15A	53.4	3.7	5.10	-	5.1	0	161.0±84.1	127.8±35.9	0.56±0.05
16A [†]	53.4	3.7	-	-	5.1	-	54.1±1.3	8.7±0.6	0.52±0.01
17A [‡]	53.4	3.7	-	-	5.1	-	149.1±18.5	13.8±4.3	0.78±0.06

Table 3.2 Continued.

1P [†]	-	-	-	-	12.1	-	0.067±0.15	8.9×10^{-4} $\pm 4.5 \times 10^{-3}$	1.1±0.81
2P	-	-	-	12.1	12.1	1	0.14±0.4	3×10^{-3} $\pm 1.4 \times 10^{-2}$	1.1±0.74
3P [‡]	-	-	-	-	12.1	-	0±0.27	3.3×10^{-1} $\pm 2.3 \times 10^{-2}$	0.95±0.01
4P	-	-	12.1	-	12.1	0	1.3±0.33	1.2±0.04	0.84 ±5.3× 10 ⁻³

3.2.2 Rheological Characterization of Dispersed Alumina-PVP Suspensions

The rheological response of the suspensions dispersed using Darvan 821A or Dolapix CE64 as well as of aqueous polymer solutions were analyzed using a TA Instruments ARG2 rheometer (New Castle, DE) with a 40-mm parallel plate geometry and a gap of 500 μm at 25°C and a moisture trap to avoid temperature gradients and drying of the material during testing. The alumina-PVP suspensions and PVP solutions were pre-sheared at the maximum shear rate (100 s^{-1}) for 5 minutes and stabilized for one minute before ramping continuously to 100 s^{-1} and back to 0 s^{-1} to obtain flow curves, which were fitted to Equation 2.1 described in *Section 2.3.1*. Oscillation stress sweeps were run at a frequency of 1 Hz from 0.1 to 1000 Pa, and frequency sweeps were performed at an oscillation stress of 1 Pa (in the linear viscoelastic region) from 0.01 to 100Hz. To evaluate the thixotropy of the alumina-PVP suspensions with Dolapix CE64, three consecutive hysteresis loops were measured up to three different maximum shear rates in decreasing order (600 s^{-1} , 100 s^{-1} and 10 s^{-1}).

3.3 Results and Discussion of the Experimental Characterization of Alumina-PVP Suspensions

3.3.1 Polymer-Dispersant Interactions with Alumina

The pH of the alumina-PVP suspensions with Darvan 821A was 9.6 ± 0.05 , and in slurries of alumina and DI water with Dolapix CE64 the pH changed negligibly from 9.50 ± 0.01 to 9.50 ± 0.05 after adding PVP. Thus, the inherent pH of the suspension was always greater than the pH at the IEP of ~ 8.8 for suspensions containing Darvan 821A⁴⁴ and ~ 8.7 for suspensions utilizing Dolapix CE64⁸⁶⁻⁸⁸ as reported previously, implying a

negatively charged surface on the alumina particles. The zeta potential was determined to be -72 mV at a pH of 9.44 ± 0.06 , which was comparable to the pH of the suspensions investigated that were dispersed with Dolapix CE64.

The pH of the alumina/DI water/Dolapix CE64 system was such that the ceramic surfaces experienced highly repulsive interactions allowing for high solid loadings.^{87, 94} The pH of the suspensions remained nearly constant with the addition of PVP suggesting that PVP chains could act as a neutral agent in the alumina/DI water/Dolapix CE64 system yet dramatically alter the rheological response by situating themselves between the powder particles, suggesting that depletion interactions may have been occurring.^{95, 96} Due to PVP additions with neutral surface charge, a significantly higher powder loading (>50 vol.% solids) was attainable in the ceramic suspension gels. In order to ascertain the colloidal mechanism(s) underlying the unique apparent stability of the alumina-PVP suspensions, rheological analysis, which is often a reflection of the colloidal stability or instability of a suspension, was performed.

3.3.2 Effect of PVP Concentration and Average Molecular Weight

Analysis of flow curves of alumina-PVP suspensions prepared with ~4 vol.% Darvan 821A for polymer contents of 1, 2.5 and 5 vol.% PVP with powder loadings of 56.7, 54.9 and 51.7 vol.% alumina, respectively, shown in Figure 2.16 suggested that the suspensions behaved as yield-pseudoplastic fluids regardless of PVP content as discussed in *Section 2.4.1*. With increasing PVP content, gradual rises in flow index, n , and a significant jump in yield shear stress, σ_y , were observed.

Further study of suspensions prepared with Dolapix CE64 with varying molecular weight was performed to evaluate the effect of molecular weight on rheological properties. Suspensions were fabricated with the same amount of PVP (5.1 vol.%) but with four different average molecular weights (10,000, 55,000, 360,000 and 1,300,000 g/mol) corresponding to compositions 16A, 1A, 17A and 15A, respectively, as listed in Table 3.2. The flow responses of these compositions are plotted in Figure 3.4. An increase in consistency and yield stress was observed for the suspensions with molecular weights of 55,000 g/mol and 360,000 g/mol with respect to the suspension containing the lowest molecular weight PVP, but this increment was noticeably higher for the suspension containing the 1,300,000 g/mol PVP.

The flow behavior in Figure 3.4 suggests that consistency rises slowly (or is relatively constant) at low to moderate molecular weights, but that above some critical molecular weight, it increases dramatically as observed in suspensions 14A and 15A. At this point, the flow index decreased for the two suspensions. The increase in consistency noted in Table 3.2 and Figure 3.4 and simultaneous decrease in flow index as indicated in Table 2.2 for suspensions with high average molecular weights could be attributed to the following: the effect of bridging between particles and PVP chains or PVP and PMAA chains, entanglements between adjacent polymer chains, and/or an increase in the radius of gyration of the polymer.

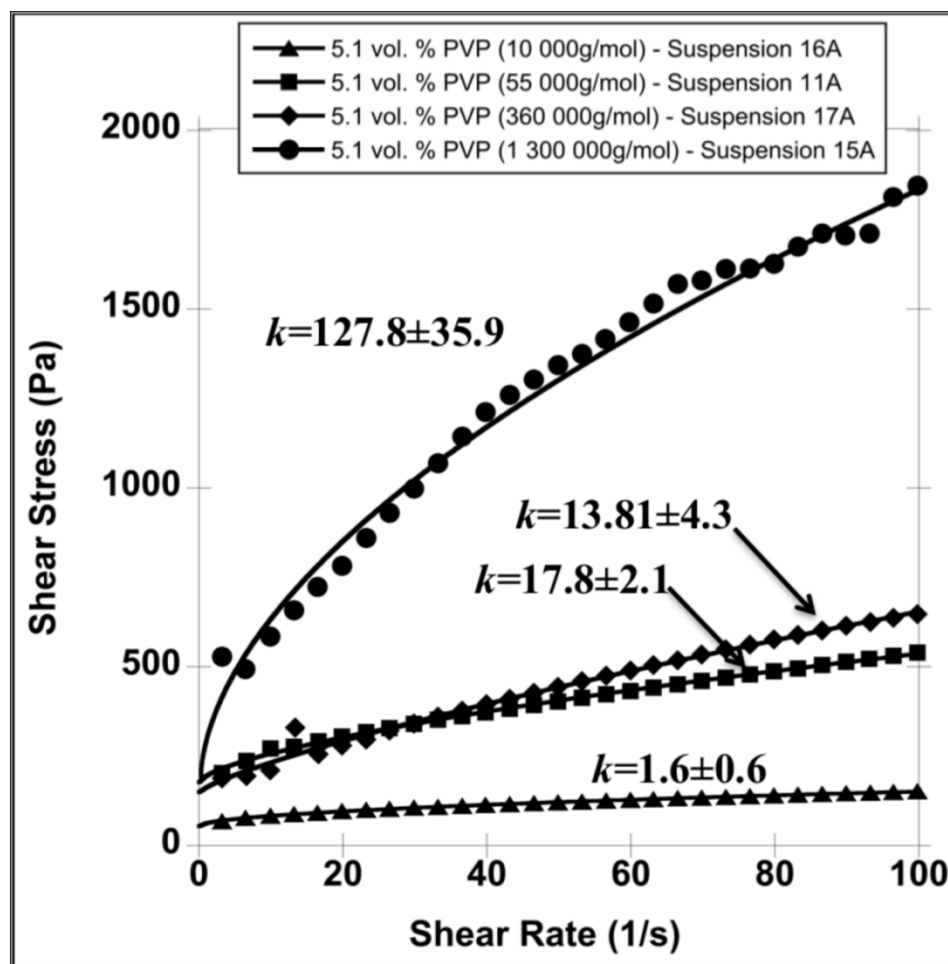


Figure 3.4 Flow behavior of alumina suspensions containing 5.1 vol.% PVP of 10,000 g/mol, 55,000 g/mol, 360,000 g/mol, and 1,300,000 g/mol average molecular weights (suspensions listed in Table 2). The black continuous lines are curve fits to the Herschel-Bulkley fluid model ($R \sim 0.99$). Increasing average molecular weight directly affects the consistency (k) and yield stress (σ_y) of the suspensions. Parameters calculated using the Herschel-Bulkley model are listed in Table 2.2.

3.3.3 Stress and Frequency Response of Alumina-PVP Suspensions

The viscoelastic response of the suspensions was first evaluated in terms of an oscillatory stress. Figure 2.18 depicts the storage modulus, G' , of the alumina-PVP suspensions dispersed with Darvan 821A compositions with 2 and 5 vol.% PVP at an oscillation frequency of 1 Hz. The linear viscoelastic regime exists at ranges <10 Pa for

both suspensions, and as expected, G' increases as more PVP is added. In both cases at stresses >10 Pa, the storage modulus takes a precipitous drop. As shown in Figure 2.19, the storage modulus, G' , is greater than the loss modulus, G'' , suggesting the elastic properties dominate at lower shears for both suspensions containing 2 and 5 vol.% PVP. On the other hand, at higher shear stresses, the viscous properties dominate implying a more fluid-like behavior. This complex rheological behavior suggested that the aqueous alumina-PVP suspensions containing Darvan 821A exhibited viscoelastic behavior.^{37, 68}

Similarly, alumina-PVP suspensions containing Dolapix CE64 as the dispersant exhibited a viscoelastic response. Figures 3.5a and b depict the storage modulus, G' , of four of the compositions in Table 3.2 at an oscillation frequency of 1 Hz. These compositions were chosen to show the effects of PVP loading and average molecular weight. In both Figures 3.5a and b the linear viscoelastic regime exists at ranges <10 Pa. As expected G' increased as more PVP was added or as the average molecular weight of the PVP was increased. In all cases at stresses >10 Pa, the storage modulus decreased.

Based on the results highlighted in Figures 3.5a and b, frequency sweeps at 10^{-1} Hz through 10^2 Hz were performed at an oscillation stress inside the linear viscoelastic region (1 Pa) to simplify the complex modulus response of suspensions dispersed with Dolapix CE64. Figure 3.6a shows the storage (G') and loss (G'') modulus for suspensions with constant average molecular weight ($P_r=0.5$) and polymer contents of 1 and 5.1 vol.% PVP, typical of all formulations studied. As shown in Figure 3.6a, a small increase in both G' and G'' was observed for both suspension formulations as test frequency was increased. For some suspensions tested near 100 Hz there was a decline in G' that might have indicated the onset of crossover into a more liquid-like regime. However, further

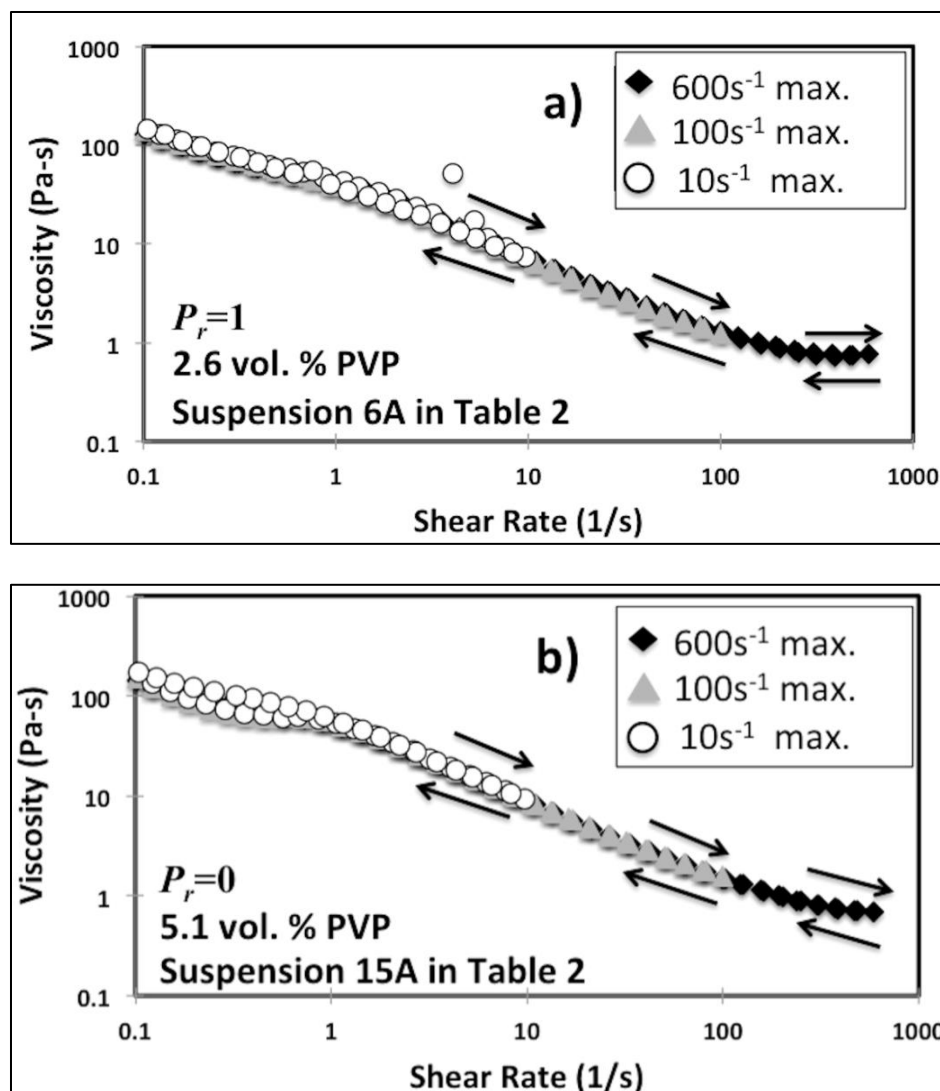


Figure 3.5 Multiple experimental hysteresis loops performed on a) suspension 6A and b) suspension 15A from Table 3.2. The resultant loops are very narrow since the response of the suspensions is not thixotropic (i.e. no time dependence).

testing at rates greater than 100 Hz would be needed to verify this. Additionally, over the frequency ranges measured, G' was always greater than G'' , indicating that the solid properties of the suspension dominate over these frequency ranges. The G' and G'' response of suspensions with the same PVP content but different molecular weight are presented in Figure 3.6b. G' and G'' increased with increasing average molecular weight, and G' was greater than G'' for all frequencies.

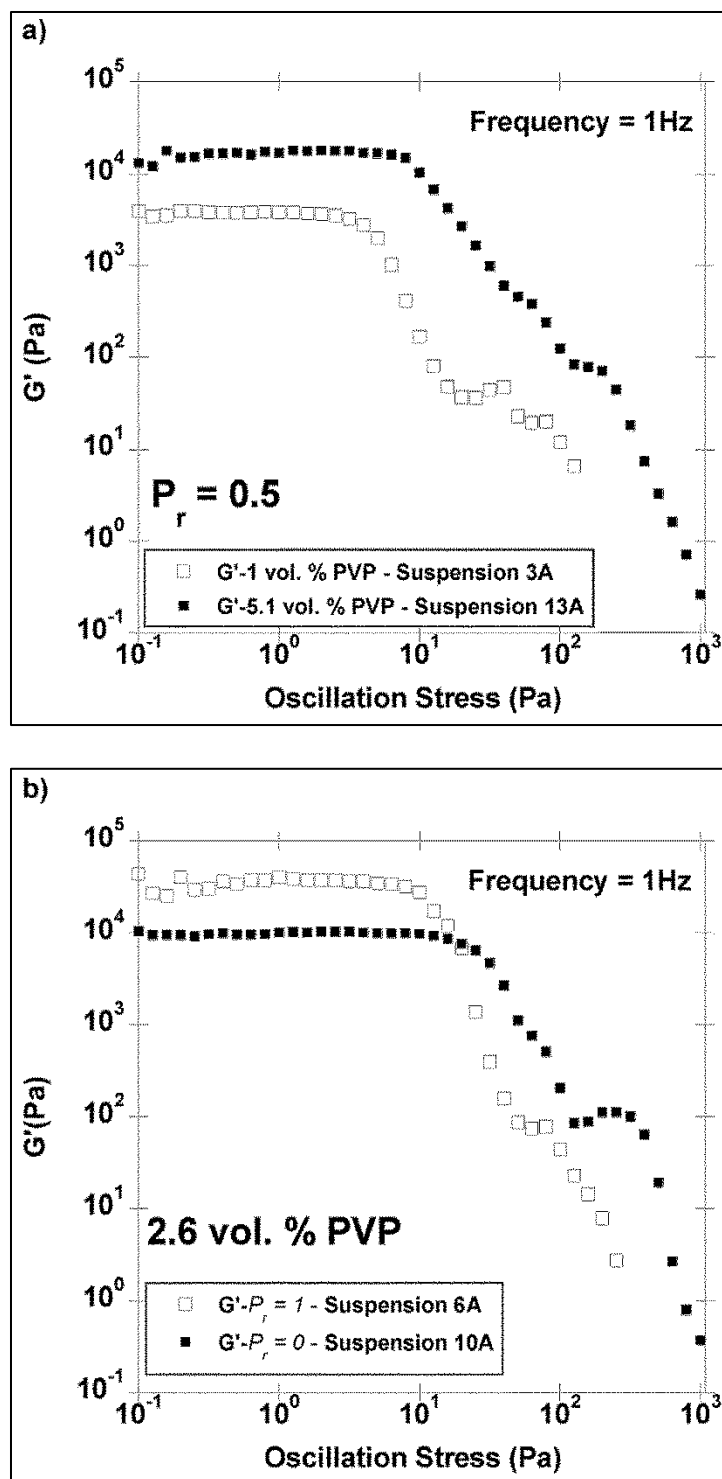


Figure 3.6 Oscillation stress sweep on alumina a) suspensions 3A and 13A (Table 3.2) and b) suspensions 6A and 10A (Table 3.2) showing a linear viscoelastic region <10 Pa.

In both cases, the range of the linear viscoelastic region is independent of polymer concentration and molecular weight.

The behavior described above corresponds to a nearly frequency independent solid-like response from the alumina-PVP suspensions, which is typical of an elastic material that can recover stored energy. In this case, the weak interaction of the polymer with the dispersant and the alumina generate a colloidal structure with a response that is mostly dependent on the polymer configuration, but not on the adsorption to the ceramic powder or the dispersant.^{62, 67, 79, 97-99} These types of yield-pseudoplastic suspensions with frequency independent responses can be manipulated by selecting the type, molecular weight and concentration of polymer to obtain the desired rheological response, which can be tailored to different ceramic fabrication processes. Additionally, the frequency independent response of the suspensions affords a robust processing window over a large forming speed range.

3.3.4 Thixotropy Investigations of Alumina/Dolapix CE64/PVP Aqueous Suspensions

Suspensions that are thixotropic exhibit a time-dependent response, requiring a finite time period to achieve an equilibrium viscosity. For instance, a thixotropic fluid may demonstrate a decrease in viscosity over several seconds or longer at a constant shear rate and then may take a finite amount of time to achieve its final viscosity after shear is removed.³⁷ Thixotropic suspensions are generally undesirable for ceramic processing as a steady-state viscosity is difficult to maintain over time after stress is removed. The time interval required for a thixotropic suspension to return to equilibrium viscosity and stabilize the yield point could cause a formed part to self-flow or slump, affecting its final dimensions, or restrict the range of forming speeds, resulting in limited control of the suspensions during processing.⁹⁰

The time-dependent characteristics, if any, of the current suspensions were evaluated by sequentially ramping and unraming the suspension using shear rates from 0 s^{-1} to 600 s^{-1} , from 0 s^{-1} to 100 s^{-1} , and finally from 0 s^{-1} to 10 s^{-1} and back to 0 s^{-1} . Thixotropy will be apparent if a different viscosity is measured between the ramped and unramped portion of the data at the same shear rate. This difference could arise due to several reasons, including the active break up of a network of colloidal particles or particles bridged by dispersant or polymer.^{37, 60, 100, 101} Furthermore, viscosity hysteresis will be observed if there is a finite time frame for reforming the original network that has been disturbed by shear.

Figures 3.5a and b for specimens 6A and 15A, respectively, show the viscosity versus shear rate for the tests conducted. After each maximum shear rate was reached, the path of the ramp upon reduction of the shear rate followed was the same as the positive ramp regardless of the average molecular weight and the PVP concentration. Although thixotropic behavior would be intuitively expected from the sharp increase in consistency data for samples 14A and 15A shown in Table 3.2, the data highlighted graphically in Figures 3.5a and b indicated that the viscosity of the suspensions was not time-dependent. Thus, thixotropy was not apparent in Figures 3.5a and b, nor was thixotropy observed in suspensions 1A through 15A. Thus, there is likely little to no bridging across powders to form network structures. Additionally, with depletion interactions the neutral polymer, by virtue of its manifestation in the interstitial volume, may interrupt the inherent network formation of a colloidal powder. For either reason described above, the lack of network formation prevented thixotropy from being observed experimentally suggesting depletion interactions were at play.^{85, 100}

3.3.5 Rheological Influence of Polymer Solutions

The effect of the polymer solutions on the suspension were further examined, where Table 3.2 shows the parameters obtained from fitting the Herschel-Bulkley model to solutions comprised of water and PVP with varying average molecular weights without alumina or dispersant. These PVP solutions acted more Newtonian than yield pseudoplastic, although the PVP solution with molecular weight of 1,300,000 g/mol was more shear thinning than the other three solutions of lower molecular weights. The lack of yield point and more Newtonian flow pattern of the PVP solutions do not wholly explain the more complicated flow properties exhibited by the alumina suspensions with PVP additions as described above. This suggests that a solute effect cannot entirely explain the rheology of the suspension and that another interaction mechanism is dominating. Additionally, the PVP-Dolapix CE64 solution at a pH of 9.5 in water exhibited no qualitative change in viscosity compared with the PVP-water solution suggesting that PVP and PMAA did not synergistically cause adsorption. The combination of the two polymers alone did not directly affect the flow properties of the highly loaded alumina suspensions.

3.3.6 Implications of Experimental Evaluation of the Rheological Properties of Aqueous Alumina-PVP Suspensions

Although further rheological analysis is required of alumina-PVP suspensions with Darvan 821A, it is believed that they behave similarly to those prepared with Dolapix CE64.⁵⁴ Study of alumina-PVP suspensions using both Darvan 821A and Dolapix CE64 as dispersing agents suggested that the rheological behavior of these

suspensions can be manipulated by simply adjusting content of PVP, a polymer species that was neutral at the pHs of the suspensions.^{95,96}

Although bridging flocculation cannot be fully ruled out, it is not likely to be the sole culprit behind the dramatic increase in yield stress and consistency that has been observed in the alumina-PVP suspensions. This conclusion was based on discussion in *Section 3.2.1* in which adsorption of PVP to the particle surface for a pH of ~9.5 was negligible. Additionally, the solution of PVP with Dolapix CE64 did not exhibit a high viscosity to suggest that the two polymers interacted to cause an absorption effect that would result in bridging. Entanglement does occur between adjacent polymer molecules up to some critical molecular weight. Above this value, an increase in molecular weight does not significantly affect the number of entanglements between adjacent chains. It is possible that the order-of-magnitude increase in consistency between the 10,000 g/mol PVP suspension and the 55,000 g/mol PVP suspension represents this transition between polymer chains moving independently and dependently with respect to one another. However, entanglement of polymer chains does not wholly explain the dramatic increase in consistency for polymers with molecular weights above 55,000 g/mol. In other words, because entanglement would be expected for the suspensions containing 55,000 g/mol, 360,000 g/mol, and 1,300,000 g/mol polymer, differences in flow behavior cannot be attributed solely to this phenomenon.

In depletion interactions, the polymer chains are segregated to the interstitial volume between powders, because they do not adsorb on their surface. It has been established that the radius of gyration (R_g) of a polymer scales with molecular weight.¹⁰² Furthermore, for a good solvent as is the case for water dissolving PVP, the volume that

the polymer occupies can be described as a sphere with an R_g that increases as the number of repeats (or molecular weight) to the 0.6 power ($N^{0.6}$).^{102, 103} There is a limit to the interstitial volume that is available between the particles, and it is reduced as powder volume is increased.¹⁰⁴ This becomes important in highly loaded suspensions such as those studied currently. Alternatively, as molecular weight increases, a single polymer chain eventually occupies a large enough volume such that it approaches the interstitial volume available between the particles.^{105, 106} Thus, the coiled polymer molecules will be forced into interaction with the particles. However, at higher molecular weights, interactions between particle and polymer can distort the spherical random coil representing the thermodynamic ground state of the polymer and affect flow of the polymer around the powders. Such chain distortions, interparticle forces, and/or resistance to easy flow between particles will be visible in rheological data.^{85, 100, 107} To correlate the underlying interparticle interactions with the rheological observations presented in previous sections, a qualitative assessment of the colloidal interactions in the alumina-PVP system was performed.

3.4 Analytical Study of Alumina/DI Water/Dolapix CE64/PVP Suspensions through

Modeling of Potential Interactions

3.4.1 Modeling Potential Interactions of Alumina/DI Water/Dolapix CE64/PVP

Suspensions

In order to understand the unique observed rheological behavior of alumina-PVP suspensions dispersed using Dolapix CE64, potential interactions of the suspensions were qualitatively modeled using current theoretical predictions to elucidate the underlying

dispersion mechanisms.⁷⁷ The total potential energy of a colloidal system can reveal the interparticle interactions that determine the overall stability of such a system. To qualitatively ascertain the interparticle potentials of the alumina-PVP suspension evaluated in this study, the total interaction potential energy, V_{tot} , was calculated such that

$$V_{tot} = V_{vdw} + V_{steric} + V_{elect} + V_{dep} \quad \text{Equation 3.1}$$

where V_{vdw} was the long-range van der Waals attractive potential energy, V_{steric} represented the repulsive steric potential energy term that resulted from the adsorbed PMAA from the dispersant interacting with particle surfaces, V_{elect} was the repulsive electrostatic potential energy originating from interactions among particles with similar surface charges and V_{dep} was the depletion potential energy arising due to the nonadsorbing PVP in solution. This approach has been previously applied to complex, dilute systems containing free polymer, and the model has been observed to qualitatively match experimental observations.^{108, 109}

The V_{vdw} interaction potential for equal-sized spherical particles is given by the Hamaker expression:

$$V_{vdw} = -\frac{A}{6} \left(\frac{2}{s^2-4} + \frac{2}{s^2} + \ln \left(\frac{s^2-4}{s^2} \right) \right) \quad \text{Equation 3.2}$$

where A is the non-retarded Hamaker constant, $s = \frac{2a+h}{a}$, h is the spacing between the surfaces of the alumina particles and a is the radius of the alumina particles.⁸⁰ For this study, the Hamaker constant, $A = 3.67 \times 10^{-20} J$, for alumina interacting across water at 298K was used.¹¹⁰

The V_{steric} potential energy term was determined using the approach developed by Vincent et al.¹¹¹ for adsorbed polymer layers on spherical particles. The steric potential

contribution is dependent on particle spacing with respect to the adlayer thickness, δ , and can be subdivided into three domains of interaction: the noninteractional domain, the interpenetration domain and the interpenetration-plus-compressional domain.¹¹² In the first domain, the adsorbed polymer layers do not interact at separation distances $h \geq 2\delta$, and $V_{steric} = 0$. The interpenetration domain applies when steric layers begin to interact at $\delta \geq h \geq 2\delta$. This steric mixing component assuming that the adsorbed polymers behave as a pseudo-homopolymer is given by $V_{s,mix}$:

$$V_{s,mix} = \frac{32\pi a k_B T (\phi_2^a)^2}{5v_1 \delta^4} \left(\frac{1}{2} - \chi\right) \left(\delta - \frac{h}{2}\right)^6 \quad \text{Equation 3.3}$$

where k_B is the Boltzmann constant, T is temperature, v_1 is the molar volume of the solvent, χ is the Flory-Huggins polymer/solvent interaction parameter, and ϕ_2^a is the average volume fraction of segments in an adsorbed layer determined to be 0.28 for this system using equations set forth by van den Boomgaard et al.¹¹³ The interpenetration-plus-compressional domain occurs at very low interparticle spacings of $0 \geq h \geq \delta$. Assuming that the adsorbed polymer segment density is homogeneous, the steric potential, V_{steric} , is comprised of the sum of two terms accounting for a mixing component, $V_{s,mix}$, and elastic compression of the polymer chains, $V_{s,el}$.

$$V_{s,mix} = \frac{4\pi a \delta^2 k_B T}{v_1} (\phi_2^a)^2 \left(\frac{1}{2} - \chi\right) \left[\frac{h}{2\delta} - \frac{1}{4} - \ln \frac{h}{\delta}\right] \quad \text{Equation 3.4}$$

$$V_{s,el} = \frac{2\pi a \delta^2 k_B T \rho_2 \phi_2^a}{M_2^a} \left\{ \frac{h}{\delta} \ln \left[\frac{h}{\delta} \left(\frac{3-h/\delta}{2} \right)^2 \right] - 6 \ln \left[\frac{3-h/\delta}{2} \right] + 3 \left(1 - \frac{h}{\delta} \right) \right\} \quad \text{Equation 3.5}$$

where ρ_2 is the density and M_2^a is the molecular weight of the adsorbed polymer.¹¹¹

The electrostatic component, V_{elect} , was calculated using an approximation for a 1:1 electrolyte to determine the electrostatic potential between two spheres of equal size,

$$V_{elect} = 4.61 \times 10^{-11} a \tanh^2(ze\psi_0/4k_B T) e^{-\kappa h} \quad \text{Equation 3.6}$$

with valency $z = 1$, elementary charge e , ψ_0 approximated by the zeta potential and $1/\kappa$ being the Debye length.¹⁰² This numerical approximation was selected over the more frequently applied Debye-Huckel approximation for low surface potentials¹¹⁴ due to the high surface potential ($ze\psi_0/2k_B T > 1$)¹⁰⁸ observed in the suspensions of alumina particles with adsorbed PMAA-NH₄ in water as determined by zeta potential analysis (Section 3.1). The Debye length was found to be 0.743 nm assuming PMAA-NH₄ to be a 1:1 electrolyte¹¹⁵ and that complete dissociation of PMAA-NH₄ occurred at the pH of the suspension, pH~9.5, as previously observed for basic alumina-Dolapix CE64 solutions.⁸⁶

This study adopted the approach taken by Ogden and Lewis¹⁰⁹ to approximate depletion interactions by applying the model set forth by Mao et al.¹¹⁶ The model calculates the depletion potential between large spheres in dilute solutions of small, equally sized spheres with radius a_{dep} of volume fraction, ϕ_{dep} , as

$$\frac{V_{dep}(\lambda)}{k_B T} = 0, \quad h \geq 2a_{dep} \quad \text{Equation 3.7}$$

$$\frac{V_{dep}(\lambda)}{k_B T} = \frac{a(\phi_{dep})^2}{10a_{dep}} (12 - 45\lambda + 60\lambda^2 - 30\lambda^3 + 3\lambda^5), \quad 4a_{dep} > h \geq 2a_{dep} \quad \text{Equation 3.8}$$

$$\frac{V_{dep}(\lambda)}{k_B T} = -\frac{3a\phi_{dep}}{2a_{dep}} \lambda^2 + \frac{a(\phi_{dep})^2}{10a_{dep}} (12 - 45\lambda - 60\lambda^2), \quad h < 2a_{dep} \quad \text{Equation 3.9}$$

where $\lambda = \frac{h-2a_{dep}}{2a_{dep}}$. The caveat of applying this set of equations is that it is only valid

when particles are considered hard spheres (i.e. the steric effect of the adsorbing polymer on the particle surfaces is neglected) with the adsorbed polymer species modeled as monodispersed spheres. These assumptions can only be represented by a dilute solution, that is when ϕ_{dep} is given by the excluded volume fraction, $\phi_{dep} = n_b \pi (2a_{dep})^3 / 6$

with n_b corresponding to the bulk density of the free polymer in the suspension, and ϕ_{dep} is less than the critical concentration for the dilute-semidilute transition, ϕ^* .^{109, 116} Above ϕ^* the nonadsorbing polymer coils begin to overlap resulting in more complex interactions with the particles and surrounding coils affecting the overall achievable polymer conformations as well as the free volume they may occupy.¹¹⁷ Furthermore, the high solid loadings (>50 vol.%) used in the alumina-PVP suspensions further complicated the behavior of the neutral polymer when compared with previous studies at much lower solid contents (< 20 vol.%).¹⁰⁹ Conformations of neutral polymer chains in solution were likely further restricted by the small interparticle spacings making it difficult to isolate the precise effect of the nonadsorbing phase on the stability of the system. These factors greatly influenced the overall value of ϕ_{dep} and thus the magnitude of the depletion potential calculated using Equations 3.7-3.9. As a result, the magnitudes at different PVP contents described below serve merely as a basic qualitative assessment of the depletion interactions occurring in the suspension.

The total potential energy curve for the suspension without neutral PVP is shown in Figure 3.7. At close interparticle spacings, the V_{steric} and V_{elect} terms dominated causing an overall repulsive interaction until the particle spacing was greater than four nanometers resulting in the formation of a potential minimum. Although the minimum of attraction was somewhat shallow, its presence suggested that the dispersed alumina system was weakly flocculated.⁷⁰ However, in accordance with stability criteria described by Russel,¹⁰⁷ where stable colloidal suspensions exhibited $\epsilon_0 \psi_0^2 a / k_B T \gg 1$, with ϵ_0

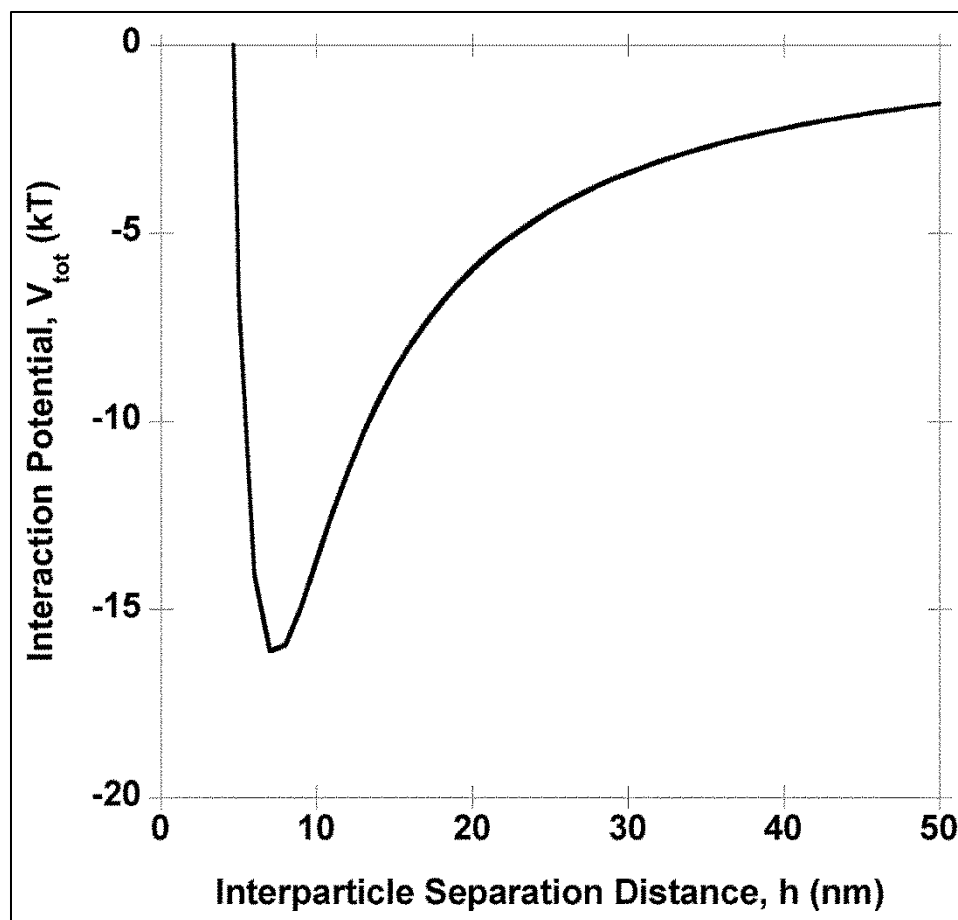


Figure 3.7 Total interaction potential curve for alumina-Dolapix CE64 suspensions without PVP additions exhibits a shallow potential minimum indicating weak flocculation of the suspension.

being the dielectric constant, or $\frac{1}{2}\chi > 0$, the suspensions without PVP were considered to be stable. It was important to include both V_{steric} and V_{elect} in the determination of the total potential curve as Dolapix CE64 was a low molecular weight dispersant that caused a thin adsorbed layer (calculated to be <1 nm) to form, which modified the surface charge of the particles thus enhancing stability.⁸⁶⁻⁸⁸ Without consideration of both terms, the attractive van der Waals potential would have inaccurately dominated potential interactions suggesting instability of the suspension.

By accounting for the repulsive steric, electrostatic and attractive van der Waals terms, the depletion component was calculated by treating the neutral PVP as the depletant in solution. The total potential minimum including V_{dep} with depletant volume fractions approximated as 0.01, 0.026 and 0.051 qualitatively decreased with increasing PVP content for each of the four molecular weights investigated. However, it was observed that with increasing molecular weight the magnitude of both the depth and height of the depletion potential curves decreased, which contradicted current theoretical predictions that depletion interactions would be enhanced with increasing molecular

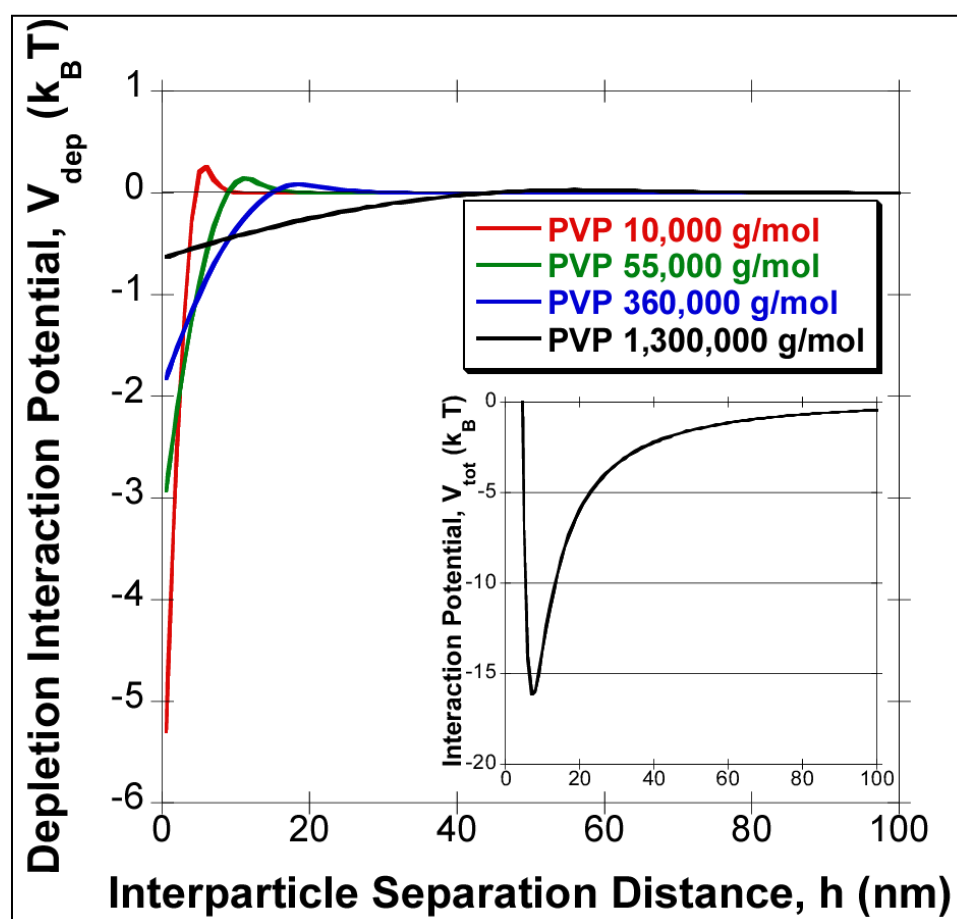


Figure 3.8 Depletion interaction potential curves for alumina-Dolapix® CE64 suspensions with 5.1 vol.% PVP of varying molecular weights. (Inset depicts total interaction potential curve.)

weight.^{83, 118} The increase in the depth of the total potential energy minimum with increasing volume fraction implied that PVP slightly enhanced the attractive potential interactions. This qualitative observation corresponded to the rheological behavior of the alumina-PVP suspensions where yield stress increased with increasing PVP content as highlighted in Figure 3.4. Since increasing yield stress is indicative of stronger attractive interactions in a colloidal system,³⁷ this enhanced flocculation may possibly be attributed to a depletion flocculation mechanism with the introduction of PVP. Although secondary minima were present, the magnitudes of the depletion forces that were estimated, as shown in Figure 3.8, were too small to justify the marked difference in flow stresses observed in the rheological data of Figure 3.4. It is clear that the calculated depletion interactions considered here have a minimal effect on the overall stability or instability of the system suggesting that other interparticle interactions, like polymer chain overlap, free volume restrictions or interpenetration of the adlayer on particle surfaces, are influencing the system.

Although the qualitative estimation of interparticle interactions without depletion considerations reflected the rheological behavior exhibited by the suspensions without PVP, depletion interactions calculated using current predictions did not account for the discrepancies observed in yield stress values with increasing PVP content. This can likely be ascribed to the fact that the current model does not fully reconcile the subtleties of conformation effects and free volume restrictions on depletion interactions in more complex concentrated suspensions of high molecular weight free polymer and with high solids loading.¹¹⁹ Further analysis is required to identify the exact interparticle

interactions of these highly loaded alumina suspensions in which a minimal amount of neutral polymer is necessary to dramatically alter the rheological response.

3.5 Summary and Conclusions of Ascertaining the Rheology and Potential Interactions of Aqueous, Highly Loaded Alumina-Polyvinylpyrrolidone Suspensions

The rheological behavior of highly loaded alumina (>50 vol.%) aqueous suspensions was studied for formulations in which Darvan 821A or Dolapix CE64 was used as a dispersant, and PVP with different average molecular weights was added as response modifiers. Stable suspensions were fabricated with $\text{pH} \approx 9.5$, and PVP additions of 1, 2.5 and 5 vol.% with different average molecular weights allowing for a yield-pseudoplastic flow behavior. Parallel plate rheometry was used to examine the effect of alumina loading, polymer amount, and average molecular weight of the polymer on the flow, stress, and oscillatory response of the suspensions fabricated.

In suspensions with inorganic content higher than 50 vol.%, adding PVP had a strong effect on the flow behavior. PVP greatly increased the yield stress of the formulations at low shear rates as well as increased the shear stress for the range studied. The flow curves measured from the specimens were fit to the Herschel-Bulkley fluid model with good agreement for all cases. At alumina concentrations between 45 and 50 vol.%, a general increase in shear stress was observed as a result of the reduction of interaction volume between particles suggesting weak flocculation. It was found that for suspensions containing PVP, it was possible to increase the yield stress by increasing polymer content and average molecular weight. The consistency, k , of the formulations

showed a drastic increase for higher polymer contents (5.1 vol.% PVP) and higher average molecular weights ($P_r > 0.25$). This was proposed to be due to the PVP gyration volume being greater than the interstitial volume between powders.

The aqueous alumina/Dolapix CE64/PVP suspensions fabricated in this study demonstrated very narrow viscosity versus shear rate hysteresis loops, which is an indication of non-thixotropic behavior. Oscillatory response measurements performed in the linear viscoelastic region of the suspensions (<10 Pa) showed that the formulations were frequency independent and had a highly elastic and solid-like behavior ($G' \gg G''$ for all frequencies tested). This was attributed to the high alumina concentration and the weak interaction of PVP with the dispersant and the alumina. Both non-thixotropic and frequency independent behavior along with the neutral character of PVP at the pH of the suspensions suggested that depletion interactions might have affected the overall interparticle interactions, since PVP minimally interacted with the dispersant (Dolapix CE64) and the surface of the alumina.

Through qualitative consideration of interparticle forces, the potential interaction plot captured overall experimental observations. By incorporating the depletion interaction model presented by Mao et al.,¹¹⁶ it was determined that the depletion component negligibly affected the colloidal stability of the suspensions examined suggesting that other interactions were at play, such as PVP chain overlap, polymer conformation restrictions or interpenetration of the adsorbed PMAA layer on the alumina particle surfaces. Current depletion calculation methods cannot yet capture such fine polymer dynamic details particularly in suspensions with high depletant concentrations and solid loadings. Although simple suspensions with lower solid loadings lend

themselves to the study and direct observation of depletion interactions, high loadings are more suitable for practical applications in ceramics processing in which high loadings are most desirable. In order to better understand highly loaded suspensions with a neutral polymer species, a model that accounts for such system conditions is needed. Depletion interactions may offer a simple approach to manipulate the response of ceramic colloids that can be adapted to a number of ceramic fabrication methods that require near-net morphologies.

In conclusion, the exact mechanism dictating the unique rheological response of these highly loaded alumina suspensions with minimal polymer carrier cannot be resolved without additional study. However, the minimal addition of polymer in a highly loaded suspension allowed for the introduction of a slight, controlled degree of weak flocculation indicated by the increase in yield stress. This ability to tailor rheological properties with a minimal amount of a neutral polymer carrier will no doubt prove useful in the development of novel ceramic processing methods.

CHAPTER 4. ADAPTING ROOM-TEMPERATURE INJECTION MOLDING TO ZIRCONIUM DIBORIDE-POLYVINYLPIRROLIDONE SUSPENSIONS

Suspensions comprised of alumina (Al_2O_3) and polyvinylpyrrolidone (PVP) were successfully prepared by room-temperature injection molding. In order to prove the viability of this novel process, a more complex system of zirconium diboride (ZrB_2), boron carbide (B_4C) and tungsten carbide (WC) was selected to produce dense ZrB_2 rings by room-temperature injection molding. The design and development of room-temperature injection molding of ZrB_2 -based suspensions with PVP additions are presented in this section.

4.1 Producing Dense Zirconium Diboride Rings by Room-Temperature Injection

Molding

4.1.1 Formulation of ZrB_2 -PVP Suspension Gels

As discussed in *Chapter 1*, studies that utilized boron carbide and tungsten carbide as sintering aids successfully pressureless sintered ZrB_2 compacts to near full density at temperatures below 2000°C .^{20, 21} Consequently, boron carbide and tungsten carbide were also incorporated into ZrB_2 CeraSGels. The powders used in this study were Grade B ZrB_2 and Grade HS B_4C with an average particle size of 2-4 microns and 0.8 microns, respectively, as provided by H. C. Starck (Newton, MA). 4 wt.% B_4C was combined with the as received ZrB_2 powders, and the powder mixture was then attrition milled at 600 RPM in 200-proof ethanol using 1/8"-diameter Co-bonded WC media.

satellites (Union Process, Akron, OH) for 2 h. The mass of the milling media was weighed before and after attrition milling to estimate the amount of WC introduced to the system. The powders were then dried at 70°C on a hot stir plate. To break up any agglomerates that potentially formed during the drying process, the dried powders were then ball milled for 24 h using 1/2"-diameter WC satellite media. A final drying step in a box furnace for 12 h at 100°C was performed to remove any moisture. SEM images confirmed that attrition milling effectively reduced the size of ZrB₂ and B₄C particles. The average particle size was calculated by averaging particle size measurements in five SEM images. It was determined to be ~0.5 μm, which was comparable in size to that of the alumina initially applied to develop the CeraSGels process.¹²⁰

Previous dispersion studies performed by Acosta¹²⁰ evaluated a series of dispersants for use in ZrB₂ CeraSGels in order to maximize powder loadings. As with alumina samples, higher powder loadings are desirable to enhance densification during pressureless sintering.¹²¹ ~7 vol.% Darvan 821A was observed to facilitate powder loading of ~50 vol.% ZrB₂-B₄C in DI water. A study performed by Huang et al.¹²² observed that Darvan 821A maximized the zeta potential of aqueous solutions of ~30 wt.% ZrB₂ and <2 wt.% Darvan 821A from 50 mV to 110 mV at pH=9 as well as shifted the IEP to pH=1.8 from 4.7 as observed for aqueous ZrB₂ solutions without dispersant.

As with alumina CeraSGels, content of PVP (1-Ethenyl-2-pyrrolidinone homopolymer, Sigma-Aldrich, St. Louis, MO) with average molecular weight of 10,000 g/mol was varied to evaluate the rheological behavior and processability of ZrB₂-based CeraSGels and the resulting ZrB₂ specimens prepared by room-temperature injection molding. The ZrB₂/B₄C/WC powder loading was kept fixed at 48.6 vol.% in all

suspensions, while the PVP content was evaluated at 1, 2 and 3 vol.%. All volume percentages were calculated by considering CeraSGel compositions containing powder, PVP, dispersant and water. Dry ZrB₂-based CeraSGel specimens consisted of ~83-86 vol.% ZrB₂/B₄C/WC powder, ~1.8-5.1 vol.% PVP and ~12 vol.% dispersant. Volume percentages based on the initial CeraSGel compositions including water content will be used in this study. The methods by which ZrB₂-based suspensions containing PVP and specimens were evaluated are described in subsequent sections.

Preparation of ZrB₂ CeraSGels was carried out in a fashion similar to that applied to alumina CeraSGels as described in *Chapter 2*. A slurry of DI water, Darvan 821A and attrition milled ZrB₂/B₄C/WC powder were combined and ball milled in 8 oz. Nalgene bottles with 1/4"-diameter WC satellite media milling media. ZrB₂/B₄C/WC powders were incrementally added to the dispersant and DI water solution to obtain highly loaded, dispersed slurries. A typical slurry contained 330 g of ZrB₂/B₄C/WC powder in 47 mL of DI water and 9 mL dispersant. A polymer solution of PVP with average molecular weight of 10,000 g/mol and DI water was mixed separately by magnetic stirring for 4-8 hours. After both the slurry and polymer solution were dispersed, the PVP-water mixture was added to the ZrB₂-based slurry and ball milled over a 12-hour period. The content of PVP with molecular weight of 10,000 g/mol in suspensions evaluated were 1, 2 and 3 vol.% to determine the optimal binder content that resulted in favorable forming and final sintered and mechanical properties. The compositions studied are highlighted in Table 4.1.

Table 4.1 Compositions of zirconium diboride-based CeraSGels with effective yield stress and pH values for suspensions with varying amounts of PVP with molecular weight of 10,000 g/mol as well as average grain size and C-ring strengths for specimens prepared by room-temperature injection molding.

ZrB ₂ /B ₄ C/WC Powder Content in vol.% (wt.%)	PVP Content in vol.% (wt.%)	Dispersant Content in vol.% (wt.%)	Effective σ_y (Pa)	pH	Average Sintered Bulk Density in g/cm ³ (%TD)	Average Grain size (μm)	Average C-ring Strength (MPa)
48.6 (84)	1 (0.5)	7.0 (2.3)	567	8.85 \pm 0.1	6.13 \pm 0.02 (99)	9.82 \pm 6.2	30.7 \pm 12.0
48.6 (82)	2 (1.2)	7.0 (2.3)	405	8.91 \pm 0.1	6.2 \pm 0.02 (100)	10.6 \pm 5.3	73.0 \pm 15.2
48.6 (81)	3 (1.9)	7.0 (2.3)	235	8.89 \pm 0.1	6.06 \pm 0.05 (98)	7.71 \pm 3.7	75.1 \pm 26.7

4.1.2 Modifications of Room-Temperature Injection Molding for ZrB₂-Based Suspensions

The injection mold apparatus and procedure that was described in *Chapter 2* to prepare alumina rings was utilized in an identical manner for processing of the ZrB₂/B₄C/WC-PVP suspensions. The only mold modification to the mold design that was made involved replacing the EPDM closed-cell foam rubber centerpiece with an inner ring of super soft black latex rubber tubing (1/4" inner diameter, 1/2" outer diameter) and outer ring of super soft yellow latex rubber tubing (1/2" inner diameter and 5/8" outer diameter) from McMaster-Carr (Elmhurst, IL) as highlighted in Figure 4.1. The EPDM foam was found to be too inflexible, causing rings to crack after forming during drying. The yellow outer "super soft" latex and inner black polyurethane foams had firmness of 10 psi and 30 psi at 25% deflection (shore A35), respectively. Additionally, the crosshead speed was reduced from 100 mm/min to 75 mm/min, which was applied by the MTS to the pushrod during the injection molding procedure of ZrB₂-based CeraSGels.

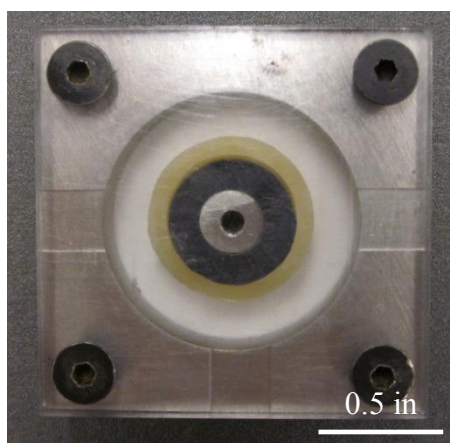


Figure 4.1 Ring-shaped mold with foam centerpiece and three overflow ports.

4.1.3 Binder Burnout and Pressureless Sintering of Injection Molded ZrB₂ Rings

The binder burnout and pressureless sintering procedures were combined into one heat treatment, which was accomplished in a Centorr Vacuum Industries high-temperature controlled environment furnace (Nashua, NH). Three specimens were placed in a graphite crucible for each run. Removal of the binder from the formed samples occurred in an initial step at a heating rate of 4°C/min to 600°C with an isothermal hold of one hour in medium vacuum ($\sim 10^{-5}$ Torr). Heating continued at a rate of 10°C/min to 1650°C for a 1-h hold at which point argon was flowed into the system. A final 10°C/min ramp to 1850°C for an isothermal hold of 1.5 h was performed in an inert argon environment to densify the ZrB₂ ring followed by cooling to room temperature at 25°C/min.

4.1.4 Preparation of ZrB₂ Specimens for Mechanical Characterization

After a ring-shaped ZrB₂ CeraSGel part was formed by room-temperature injection molding, it was then machined in its green state to chamfer the outer edges and ensure sample surfaces were sufficiently parallel in accordance with the ASTM C1323-10 C-ring test.⁵⁹ A polishing wheel with 320, 400 and 600 grit silicon carbide grinding cloth (LECO 810-265/269-PRM) was used to accomplish this green machining, as shown in Figure 4.2.

After binder burnout and pressureless sintering as described in the above *Section 4.1.3* were accomplished, a slow-speed saw with a diamond blade (Leco Corporation, St. Joseph, MI) was used to cut a notch in the ring specimen resulting in the desired C-shape. In the chance that heat treatments resulted in warping of the sample, it was placed on a

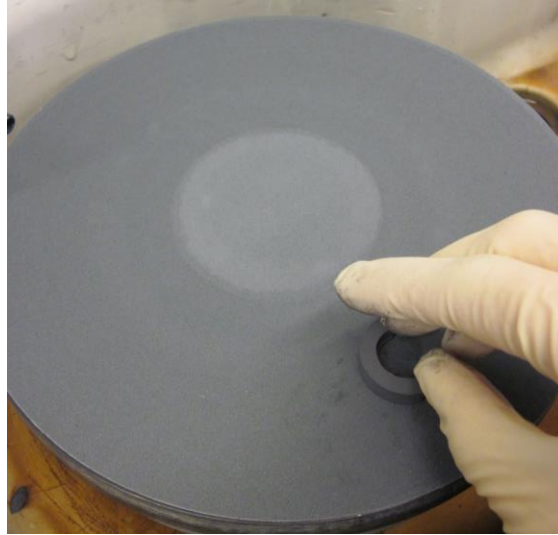


Figure 4.2 Preparing ZrB_2 -based green body for mechanical testing.

mandrel with adjustable diameter and then machined using a diamond-tipped blade (McMaster-Carr, Elmhurst, IL) on a rotating lathe to ensure outer surfaces were parallel. Figure 4.3 shows the final geometry of the part to be tested, which is compressively loaded until fracture in accordance with ASTM C1323-10.⁵⁹

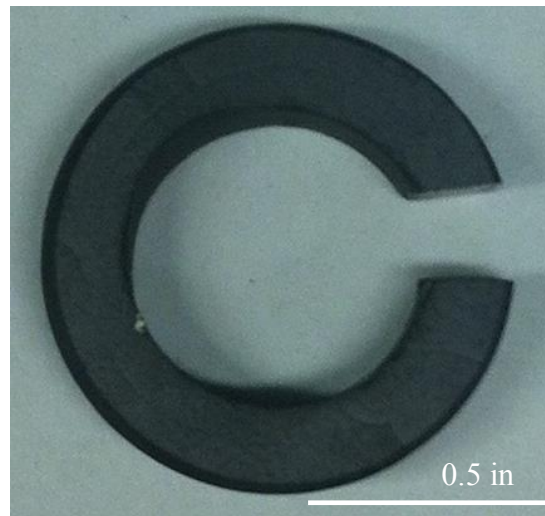


Figure 4.3 Final sintered C-shaped ZrB_2 sample.

4.2 Characterizing ZrB₂/B₄C/WC-PVP Suspensions for Room-Temperature Injection

Molding

4.2.1 Characterization of ZrB₂/B₄C/WC-PVP Suspensions Rheology and pH

An Anton Paar Modular Compact Rheometer (MCR) 302 (Ashland, VA) with a 25-mm profiled plate geometry and a gap of 1 mm was used to evaluate the rheological responses of ZrB₂/B₄C/WC suspensions with varying PVP contents at 25°C. Because the viscosity of the ZrB₂-based suspensions was qualitatively paste-like, the profiled plate allowed for better contact between the suspension and the plate during testing.

The ZrB₂-PVP suspensions were ramped continuously to 100 s⁻¹ and back to 0 s⁻¹ to obtain preliminary flow curves. Flow startups in which a constant shear rate ranging from 0.01 s⁻¹ to 100 s⁻¹ was applied were performed to reveal the transient (i.e. time-dependent) response of the suspensions. Creep tests were ultimately utilized to evaluate the flow behavior by approximating the yield stress of the suspensions. Creep tests involve applying a constant shear stress to a suspension and then measuring the shear rate response. Applied stress values ranged from 0.01 Pa up to 600 Pa for 100s to 300 s to determine the stress needed to initiate flow of the suspensions. pH was characterized using an Oakton PH5 meter (Vernon Hills, IL) calibrated with electrolytic buffer solutions at pHs of 4, 7, and 10.

4.2.2 Density and Material Composition of Sintered Specimens

Density of the ZrB₂ parts after sintering was determined using the Archimedes technique.⁶⁴ The theoretical density of the specimens containing ZrB₂, B₄C and WC was calculated using a rule-of-mixtures approach based on the total amount of powder

incorporated into the suspensions.²¹ The calculated theoretical density was used as a comparison to determine how dense the ceramic specimens became after binder burnout and pressureless sintering.

Microstructural analysis was performed using an FEI Philips XL-40 scanning electron microscope (SEM) to examine sintered, polished and chemically etched (NaOH-water solution, 7 min) samples. The average grain size was calculated by evaluating five SEM micrographs for a particular sample composition and measuring the length of 50 arbitrary grains in each image using ImageJ image processing and analysis software. A total of 250 line segments representing 250 different grain lengths were averaged to obtain a mean grain size for each composition. To determine if grain sizes were significantly different for the compositions evaluated, statistical analysis was performed as described in *Section 2.3.5*.

Energy dispersive spectroscopy (EDS) was utilized to evaluate the composition of ZrB₂ specimens after sintering to determine if any undesired oxide phases were present. The microstructure of the specimens was also evaluated to determine the composition of grains with different contrast. X-ray diffraction (XRD) using a Bruker D8 Focus X-Ray Diffractometer (Madison, WI) was performed for qualitative phase analysis. By determining the phase and composition of the resulting specimens, the effects, if any, on the resulting material from using a PVP as a binder could be detected.

4.2.3 Ultimate Strength of Sintered ZrB₂ C-Ring Samples

Mechanical characterization of the ZrB₂ rings prepared by room-temperature injection molding was accomplished using the ASTM C1323-10 standard⁵⁹ in a manner

identical to that presented in *Section 2.3.5* for alumina specimens. Fractographic analysis was performed following the procedure outlined in ASTM C1322-05b⁶⁵ to determine the fracture origin for each specimen using an Olympus SZX7 Zoom Stereo Microscope. Statistical analysis was performed as described in *Section 2.3.5*.

4.3 Determining the Optimal ZrB₂/B₄C/WC-PVP Suspension for Room-Temperature

Injection Molding

4.3.1 Rheological Behavior and Processability of ZrB₂/B₄C/WC Suspensions with Varying PVP Content

Flow curves of ZrB₂/B₄C/WC CeraSGels with 48.6 vol.% and 1, 2 or 3 vol.% PVP with average molecular weight of 10,000 g/mol without significant scatter could not be obtained. As a result, flow startups were performed at constant shear rates of 0.01 s⁻¹ up to 100 s⁻¹ as shown in Figure 4.4 for a ZrB₂ CeraSGel containing 3 vol.% PVP. These tests revealed that all of the ZrB₂-based suspensions evaluated behaved very differently over the time scales investigated, suggesting that the suspensions regardless of PVP content had a transient, or time-dependent, response unlike the alumina CeraSGels, which exhibited time-independent yield pseudoplasticity. This transient, multifaceted flow behavior was likely the consequence of having three different powder phases at high concentrations in the suspension.

Creep tests were utilized to approximate the shear stress required to initiate flow of the ZrB₂/B₄C/WC CeraSGels. Figure 4.5 highlights creep test results for a ZrB₂-based CeraSGel containing 2 vol.% PVP. At low applied shear stresses, the suspension did not readily flow and exhibited a shear thickening response. However, the flow response

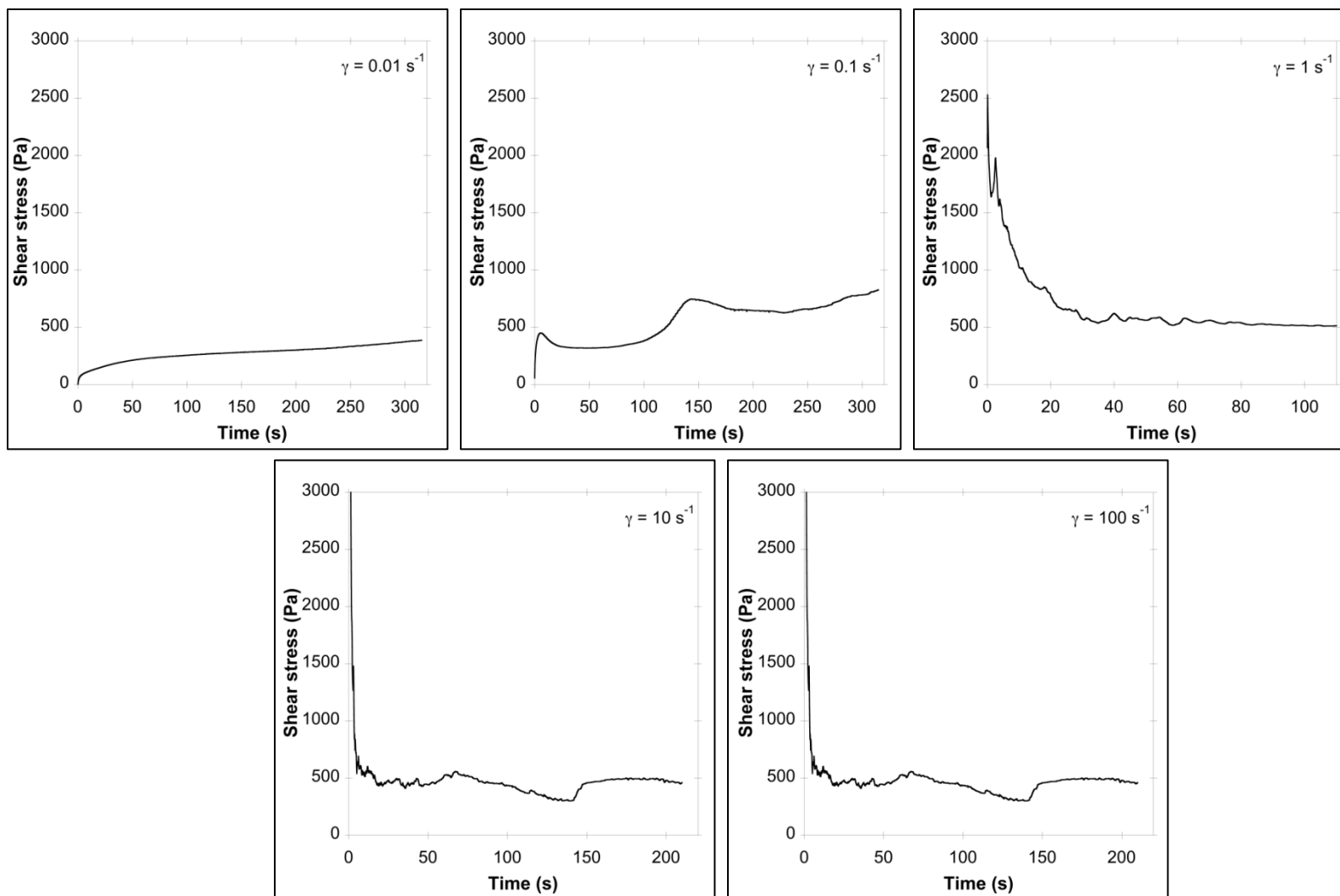


Figure 4.4 Flow startups (constant shear rate) revealed transient (time-dependent) response of ZrB₂-based CeraSGels containing 3 vol.% PVP.

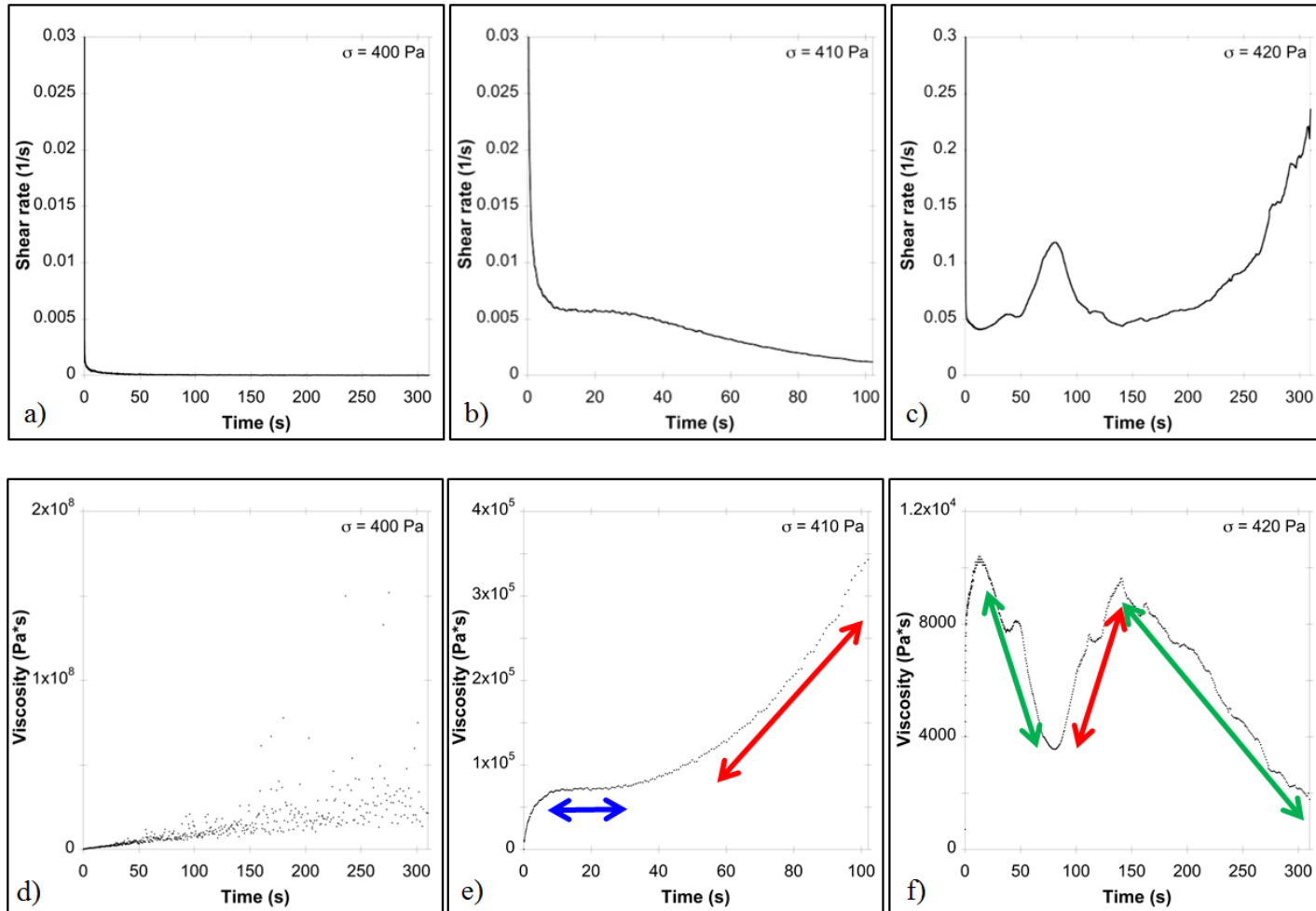


Figure 4.5 Creep plots of shear rate vs. time at stresses of a) 400 Pa, b) 410 Pa and c) 420 Pa. Identical creep data plotted in terms of viscosity vs. time for d) 400 Pa, e) 410 Pa and f) 420 Pa. Blue arrows, green arrows and red arrows indicate Newtonian, shear-thinning shear-thickening behaviors, respectively.

transitioned to Newtonian-like flow and eventually to a shear-thinning response near a critical shear stress, above which suspensions exhibited a time-dependent shear-thinning and thickening behavior. As shown in Table 4.1, $\text{ZrB}_2/\text{B}_4\text{C}/\text{WC}$ -PVP suspensions required significantly higher applied shear stresses to initiate flow in comparison with alumina-PVP suspensions. It was also observed that with increasing PVP content, the stress required to cause flow decreased from approximately 567 Pa for $\text{ZrB}_2/\text{B}_4\text{C}/\text{WC}$ suspensions containing 1 vol.% PVP to 235 Pa for suspensions of 3 vol.% PVP. Furthermore, suspensions tended to exhibit shear-thickening behavior at lower stresses immediately after flow was initiated. However, at higher stresses, suspensions appeared to have both shear-thickening and shear-thinning properties depending on the time scale evaluated. Although a shear-thickening response is not desirable for ceramic processing, it is believed that the time scale of processing as well as the shear stress applied with aid from the pneumatic vibrator put the ZrB_2 CeraSGels into a flowable, more pseudoplastic state allowing for the adequate filling of the ring-shaped mold. As a result, ring-shaped zirconium diboride specimens were effectively fabricated. Further analysis of suspensions containing higher contents of PVP as well as PVP of varying molecular weight is needed to fully understand the complex flow behavior of suspensions of $\text{ZrB}_2/\text{B}_4\text{C}/\text{WC}$.

The pH of $\text{ZrB}_2/\text{B}_4\text{C}/\text{WC}$ suspensions with different PVP contents were all roughly 8.9, as shown in Table 4.1, suggesting that different amounts of PVP did not dramatically change the pH of the suspensions. It is believed that PVP is effectively neutral at the pHs of the $\text{ZrB}_2/\text{B}_4\text{C}/\text{WC}$ suspensions evaluated here as has been previously observed for alumina-containing suspensions at comparable pHs,⁵⁴ as

described in *Chapter 3*. A study by Huang et al.¹²² observed a maximum zeta potential value of 110 mV occurring at pH~9 using Darvan 821A. Although this previous study¹²² evaluated aqueous solutions containing only ZrB₂ powders, a similar maximization of the zeta potential at the pH of the multi-component ZrB₂/B₄C/WC suspensions was likely contributing to dispersion. Further analysis of the pH and zeta potential of aqueous ZrB₂ slurries is needed in order to understand the character of PVP in these complex suspensions and determine their colloidal stability.

4.3.2 Green Machinability of Room-Temperature Injection Molded ZrB₂ Specimens

Ring-shaped specimens were successfully produced by room-temperature injection molding using ZrB₂-based CeraSGels of varying PVP content. By utilizing the super soft latex rubber centerpieces in the mold, hoop stresses that developed during drying were mitigated to produce ring-shaped specimens without cracks. Prior to binder burnout and sintering, specimens were polished by hand to even out the planar surfaces of the rings without cracking or chipping during the procedure, suggesting that the minimal amount of PVP used in suspensions imparted sufficient strength to the ZrB₂/B₄C/WC green bodies.

4.3.3 Sintered Density, Microstructure and Composition of Room-Temperature

Injection Molded ZrB₂ Specimens

After polishing specimens underwent the heat treatment described in *Section 4.1.3* to remove the binder and densify the part. The theoretical density was calculated to be 6.17 g/cm³ based on a composition of 86 wt.% ZrB₂, 3.5 wt.% B₄C and 10.5 wt.% WC,

as approximately 22 g of WC was introduced into the 200 g of $\text{ZrB}_2\text{-B}_4\text{C}$ powders during attrition milling. Initially, only ~8 wt.% WC was expected to be incorporated into the powder mixture; however, Archimedes test revealed that specimens reached near full density as shown in Table 4.1 despite the higher WC content. The average densities for specimens prepared with different CeraSGel compositions were found to be statistically different. Specimens produced using 2 vol.% PVP compositions exhibited the highest average density. Specimens prepared with suspensions containing 3 vol.% PVP had the lowest density as well as the highest standard deviation. This large scatter in densities could have been an artifact of mechanical error of the sintering furnace that resulted in improper sintering of a sample batch. Because specimens prepared with the same compositions were sintered simultaneously, it was unclear if a trend linking density with PVP content existed. Further analysis is required to resolve the dependence, or independence, of density on PVP content in starting $\text{ZrB}_2/\text{B}_4\text{C}/\text{WC}$ suspensions.

SEM micrographs of polished, chemically etched cross-sections of $\text{ZrB}_2/\text{B}_4\text{C}/\text{WC}$ rings indicated a mostly dense microstructure with minor porosity between and within grains as highlighted in Figure. 4.6. The average grain sizes of specimens prepared with 1 and 2 vol.% PVP CeraSGels were statistically similar at about 10 μm in length. The average grain size for specimens produced using 3 vol.% PVP CeraSGels was somewhat lower at 7.7 μm as shown in Table 4.1. The smaller grain size could be attributed to less significant grain growth occurring during sintering, as the specimens with high PVP content did not reach full density in comparison with specimens prepared using suspensions containing lower PVP contents. Linear shrinkage was ~21% for all specimens evaluated.

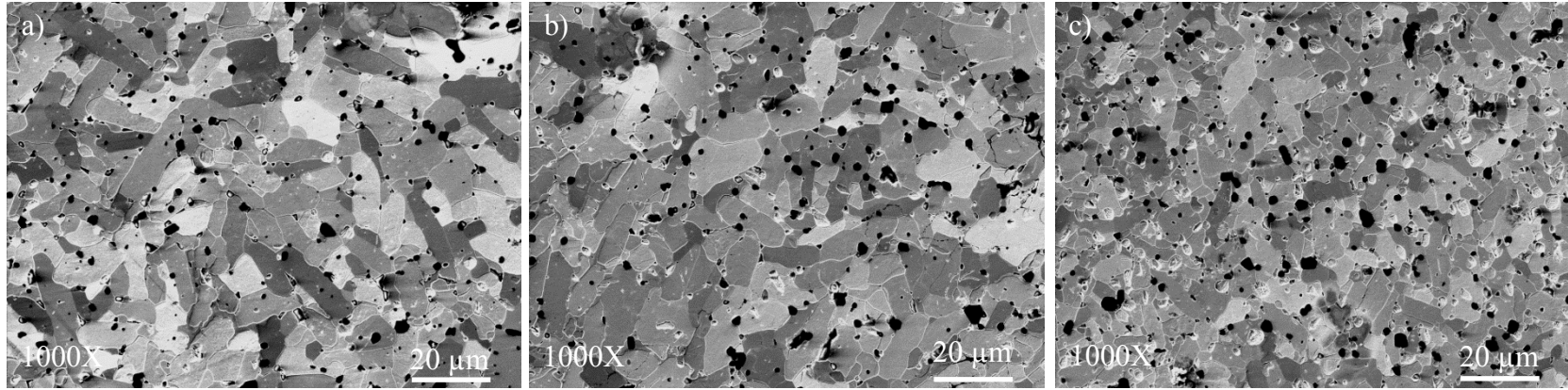


Figure 4.6 SEM micrographs of ZrB₂ cross-sections of ZrB₂ specimens prepared by room-temperature injection molding of suspensions with a) 1 vol.%, b) 2 vol.% and c) 3 vol.% PVP contents.

EDS revealed the presence of zirconium, boron and tungsten in sintered specimens as highlighted in Figure 4.7. Utilizing EDS quantitative analysis, the compositions of the specimens roughly corroborated the estimated material composition as ~86 wt.% ZrB_2 , 3.5 wt.% B_4C and 10.5 wt.% WC. EDS point analysis suggested that the black grains were likely boron carbide, whereas the lighter gray grains were zirconium diboride with varying tungsten content as highlighted in Figure 4.7. It has been observed that tungsten tends to dissolve into the ZrB_2 matrix at the elevated temperatures encountered during sintering, resulting in a solid solution of a tungsten-containing ZrB_2 phase.^{123, 124} Consequently, no pure tungsten or tungsten carbide phases were detected using EDS point analysis in lines with previous investigations.¹²⁴

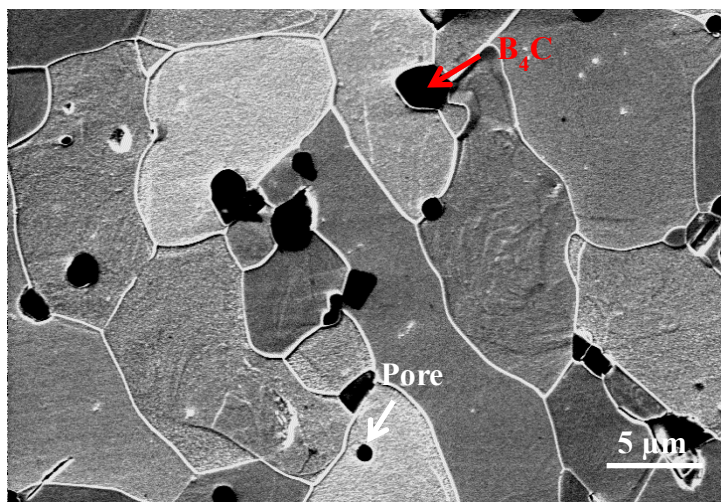


Figure 4.7 Cross section of specimen prepared with 1 vol.% PVP CeraSGel evaluated by EDS showed B_4C grains surrounded by ZrB_2 grains.

Peaks corresponding to ZrB_2 , B_4C and WC powders were observed in XRD spectra of attrition milled powders as seen in Figure 4.8(a). XRD also confirmed that the phases present in each specimen regardless of starting PVP content were ZrB_2 and B_4C after densification as shown in Figure 4.8(b-d). However, little to no signal from tungsten

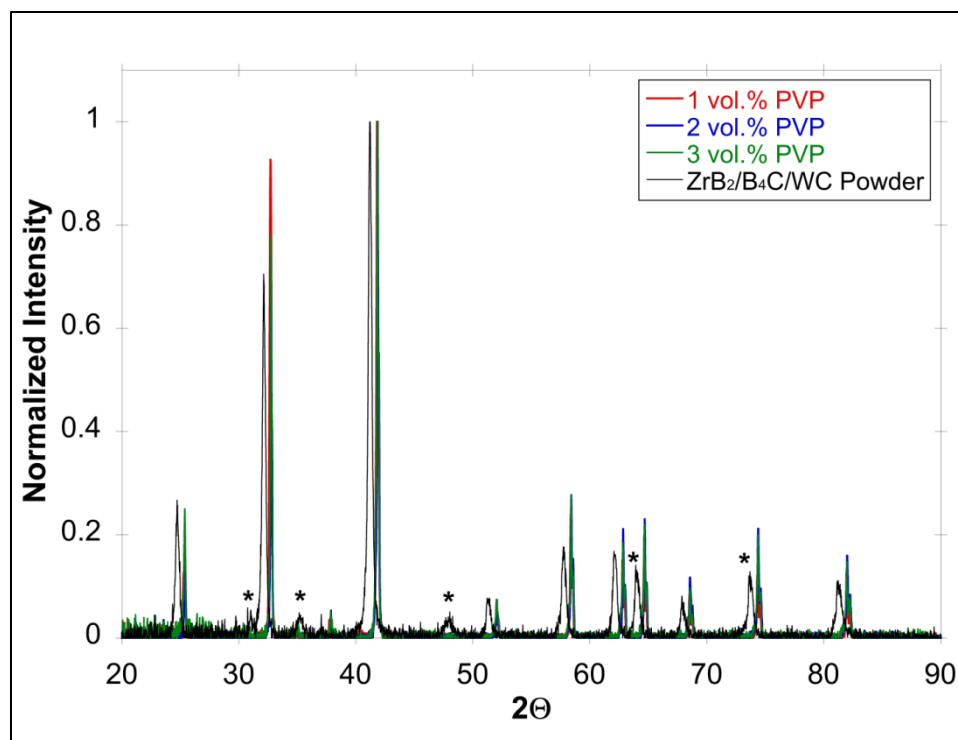


Figure 4.8 XRD spectra of sintered ZrB_2 specimens prepared with 1, 2 and 3 vol.% PVP CeraSGels along with spectrum from starting attrition milled $ZrB_2/B_4C/WC$ powders. * indicates WC peak, which was only detected in the attrition milled powders. After sintering, tungsten signals were not observed in the spectra due to tungsten forming a solid solution with ZrB_2 , resulting in the apparent ZrB_2 peak shift to higher angles.

or tungsten carbide was detected by XRD in sintered specimens, despite the detection of tungsten's presence by EDS. The absence of tungsten as identified by XRD in sintered samples was likely a result of tungsten being incorporated into the ZrB_2 lattice. Previous studies have shown that tungsten tends to form a solid solution with ZrB_2 at high temperatures.^{19, 123} Consequently, XRD peaks of ZrB_2 are typically shifted to slightly higher angles after W is incorporated into the ZrB_2 lattice. This is because tungsten has a covalent radius of 1.4 Angstrom (\AA), whereas zirconium has one of 1.6 \AA .¹²⁴ When tungsten substitutes a zirconium atom in the ZrB_2 lattice, the unit cell slightly decreases in size. This decrease in lattice spacing results in an increase in 2θ in accordance with

Bragg's law of diffraction.¹²⁵ Similarly, the XRD spectra in Figure 4.8 illustrate the shift to higher 2θ values suggesting that tungsten is forming a solid solution with zirconium diboride. Additionally, it is important to note that no oxide phases, like zirconia, were detected, suggesting that PVP, Darvan 821A and water did not negatively impact processing, pressureless sintering or the resulting composition of the ZrB₂ rings.

4.3.4 Mechanical Properties of Sintered ZrB₂ C-Ring Specimens

Preliminary average C-ring strength values were obtained for 1, 2 and 3 vol.% PVP as shown in Table 4.1. No C-ring strengths for ZrB₂ have been reported in literature, but ZrB₂ C-ring strength values comparable to those obtained for alumina as described in *Section 2.4.4* were anticipated as alumina and zirconium diboride have comparable flexure strengths.^{73, 126} The actual C-ring values were much lower than expected. Although the C-ring strength values obtained by ASTM C1323-10⁵⁹ are not directly comparable to flexure strengths obtained by conventional bending tests, ZrB₂ has been shown to exhibit room-temperature flexure strength between 275 to 480 MPa.¹²⁶ A strength of 370 MPa obtained by four-point bending of pressureless sintered dense pellets of attrition milled ZrB₂ powder with 4 wt.% B₄C and 8 wt.% WC with average grain size of 8 μm has been reported.²¹ Despite the grain size of specimens prepared with 1 and 2 vol.% PVP suspensions being slightly larger at ~10 μm, C-ring strengths <100 MPa were not anticipated.

Preliminary fractographic analysis suggested that most of the fractures originated at a pore that was likely introduced during forming or at a surface defect that resulted from machining using the diamond-tipped blade on the outer edge of the sintered ring.

Further analysis is needed to reconcile the exact cause of the lower-than-expected strength values; however, improvements to the room-temperature injection molding process and rheological development of current ZrB₂-based CeraSGels will likely help to reduce or even eliminate the strength-limiting flaws that have been observed in ZrB₂ rings.

4.4 Summary and Conclusions of Room-Temperature Injection Molding of ZrB₂-Based CeraSGels

Room-temperature injection molding was effectively adapted to ZrB₂/B₄C/WC-PVP suspensions to produce dense, ring-shaped parts. Although the rheological behavior was time dependent and not yield pseudoplastic like alumina-PVP suspensions, ZrB₂-based CeraSGels with 1, 2 and 3 vol.% PVP of (MW = 10,000 g/mol) exhibited an effective yield shear stress such that they were flowable under the conditions of the process. Initial findings show that the shear stress required to initiate flow decreased with increasing PVP content. Evaluating compositions with higher PVP content is needed to determine if the trend holds to adapt flow properties of suspensions for injection molding. Because the pH of ZrB₂/B₄C/WC suspensions with varying PVP content was constant at ~8.9, increasing the amount of PVP did not appear to alter the pH of the suspensions.

The ring-shaped ZrB₂ parts that resulted from room-temperature forming of ZrB₂-based CeraSGels were polished prior to binder removal and densification, suggesting that the minimal PVP additions imparted sufficient green strength. After binder burnout and pressureless sintering, EDS and XRD confirmed that no undesirable oxide phases developed within the ZrB₂ parts yielding compositions of ZrB₂ grains with tungsten in a

solid solution, as observed in previous studies^{21, 124} and B₄C grains. Archimedes results showed that specimens reached near full density (>98%TD) regardless of content. Specimens prepared with 1 and 2 vol.% PVP had the highest relative densities (99%TD and 100%TD, respectively), whereas parts that initially contained 3 vol.% PVP only reached ~98%TD. It was unclear if the statistically lower relative densities were an artifact of improper sintering due to mechanical error or a result of PVP content. Further analysis is required to isolate the main factor.

Despite the variance in densities, rings prepared with 3 vol.% PVP demonstrated the highest C-strength values, while rings prepared using 1 vol.% PVP had the lowest values as determined using ASTM C1323-10.⁵⁹ It is believed that the decrease in shear stress required to flow the CeraSGels containing 3 vol.% PVP assisted in reducing the number of strength-limiting flaws introduced during processing. However, because all of the C-strength values obtained for each composition were lower than anticipated, processing improvements, like reducing the crosshead speed during filling or evaluating more contents or molecular weights of PVP in ZrB₂-based CeraSGels, could reduce the number of defects and thus increase mechanical properties of the ZrB₂ rings. Although further analysis of suspensions is needed to perfect the process, room-temperature injection molding of aqueous ZrB₂-based CeraSGels has proven to be a feasible method to obtain dense, ZrB₂ rings in an environmentally friendly way.

4.5 Recommendations for Future Work

4.5.1 High-Temperature Mechanical Testing of ZrB₂-Based C-Rings

One of the primary advantages of employing zirconium diboride ceramics in high-temperature applications is that ZrB₂ maintains its robust mechanical properties even at elevated temperatures.¹²⁷ Hot-pressed ZrB₂ without additives at 87% theoretical density have exhibited four-point flexural strength upwards of 300 MPa even at 1200°C.¹²⁸ After room-temperature strength properties are obtained for ZrB₂ C-ring specimens prepared by room-temperature injection molding, the high-temperature (~1500°C) mechanical properties will be investigated for the specimens prepared by room-temperature injection molding. Although ASTM C1323-10 is intended to determine the ultimate strength of samples at room temperature,⁵⁹ the procedure, described in *Section 2.3.4*, can be adapted to calculate C-ring strength at elevated temperatures. Sintered ZrB₂ bar specimens with dimensions of 25 × 2.5 × 2 mm³ will be prepared by injection molding in order to attain flexure strengths by four-point bend testing at room and high temperature. The strength values obtained by four-point bending will be compared with the values found in literature.

4.5.2 Silicon Carbide Particulate Reinforcing Phase for ZrB₂ Prepared by Room-Temperature Injection Molding

Although zirconium diboride has lower room-temperature flexural strengths compared to other advanced ceramics, silicon carbide (SiC) particulates used as a reinforcing phase have been found to greatly improve the strength of monolithic ZrB₂. Flexural strength of pure ZrB₂ is roughly 275-490 MPa with a maximum strength of 565

MPa observed in samples hot-pressed at 1900°C.¹²⁹ Chamberlain et al.¹²⁶ found that with 10, 20 and 30 vol.% SiC additions (starting size of ~0.7 μm) to ZrB₂ powders that were attrition milled using WC media, room-temperature flexural strength increased to 713, 1003, and 1089 MPa, respectively, in samples hot-pressed at 1900°C. This dramatic increase is attributed to a reduction in grain size due to SiC particulate additions along with the WC phase introduced during attrition milling. Toughness also increased with SiC additions to 4.1 to 5.3 MPa√m compared to 3.5 MPa√m for pure ZrB₂.¹²⁶

Pressureless sintering of ZrB₂-SiC composites has been accomplished at temperatures above 2000°C in the past,¹³⁰ although it is significantly more challenging due to the formation of a borosilicate glass phase at 1000°C that inhibits sintering. A recent study²⁷ prepared ZrB₂-SiC specimens, which contained ZrB₂ powder (d₅₀=2 μm), SiC powder (d₅₀=0.5 μm), 2 vol.% B₄C (d₅₀=0.5 μm) and 2 vol.% carbon black powder (d₅₀=0.5 μm), by aqueous gelcasting. >98% theoretical density was obtained for specimens at 2100°C for 2 h. Another study successfully pressureless sintered ZrB₂-SiC composites at temperatures <2000°C with the addition of B₄C (~4 wt.%) and carbon (~5-7.3 wt.%).²² In the study,²² ZrB₂ with starting particle size of 2 μm was combined with SiC of varying particle sizes ranging from 0.45 μm to 1.45 μm without attrition milling. Carbon varying from 2.8 to 7.3 wt.% in conjunction with 4 wt.% B₄C additions was observed to help remove the borosilicate glass phase at 1000°C in vacuum during pressureless sintering as well as mitigate liquid phase development prior to coarsening or densification of ZrB₂-SiC. The resulting mechanical properties of the pressureless sintered ZrB₂-SiC composites corresponded to those obtained in samples that were hot pressed.

In order to improve the mechanical properties of ZrB_2 parts formed by room-temperature injection molding CeraSGels, SiC particulates will be introduced as a reinforcing phase. SiC will be added to ZrB_2 powders to attain powder loadings of 10, 20 and 30 vol.% and then attrition milled as described in *Section 4.1* to attain a more uniform particle size. These powders will then be combined with Darvan 821A dispersant and polyvinylpyrrolidone (PVP) as the polymer binder to produce a ZrB_2 /SiC-based CeraSGel as described in *Section 4.1*. Initial study will be performed using PVP; however, an additional carbon-forming phase in the form of carbon black powder will be explored to increase carbon content if full densification is not achieved with pressureless sintering at 2100°C as in previous studies.²⁷

Processing and characterization to determine if room-temperature injection molding is a viable production method of ZrB_2 -SiC composites will follow a similar procedure as described previously in *Sections 4.2* and *4.3* for ZrB_2 with B_4C sintering aids.

CHAPTER 5. CONCLUSIONS AND FUTURE WORK

A novel, green room-temperature injection molding process was developed and successfully applied to an alumina (Al_2O_3) system and tailored to a multi-component material system of zirconium diboride (ZrB_2), boron carbide (B_4C) and tungsten carbide (WC). Through careful control of high ceramic powder loadings and a minimal amount of polymer additives, the viscosity of the ceramic-PVP suspension was optimized to afford room-temperature injection molding of dense, near-net shaped alumina and ZrB_2 -based ring-shaped parts.

Rheological study using parallel-plate rheometry suggested that the alumina-PVP suspensions dispersed with Darvan 821A exhibited yield pseudoplasticity, which was ideal for room-temperature injection molding. Consistent with past study,⁵⁴ PVP was effectively neutral at the pHs of the suspensions studied, consequently inducing a controlled degree of weak flocculation with varying PVP content, making these suspensions tailorable to the room-temperature processing method presented in this work. Similar alumina-PVP suspensions prepared with Dolapix CE64 instead of Darvan 821A revealed that PVP had a pronounced influence on the flow properties as an increase in yield stress was observed with increasing PVP content or molecular weight. Flow curves of the alumina-PVP suspensions were matched with the Herschel-Bulkley model for yield-pseudoplastic suspensions with high precision. All alumina-based CeraSGels

investigated had a frequency independent, highly elastic and solid-like response ($G' \gg G''$ for all frequencies tested). Furthermore, alumina suspensions exhibited no thixotropy or time-dependent flow.

The unique flow properties were analytically evaluated by qualitative consideration of the interparticle forces at play in the suspensions in order to uncover the possible source(s) dictating the alumina CeraSGels' rheological behavior. Plots showcasing the potential interactions based on DLVO theory echoed experimental rheological observations. However, by including depletion interactions to account for neutral PVP at varying molecular weights in suspension, the depletion component negligibly affected the colloidal stability of the suspensions. This result suggested that other interactions, including PVP chain overlap, polymer conformation restrictions or interpenetration of the adsorbed poly(methacrylic acid) layer on the alumina particle surfaces, were likely dominating the unique rheology of the alumina-PVP suspensions.

Further experimental study of the rheological behavior of suspensions with constant powder loadings of Al_2O_3 is needed to fully isolate the main factor in obtaining suspensions with suitable flow properties for this process, because powder content was varied simultaneously with PVP content. In spite of this, it is important to note that current depletion calculation approaches are only effective at resolving interactions in dilute or semi-dilute suspensions and not in the highly concentrated suspensions, like CeraSGels, evaluated here. Current depletant theory cannot yet reconcile subtle polymer dynamic phenomena in suspensions with such high powder loadings or depletant concentrations. Highly loaded suspensions are more practical for application in ceramic forming methods in which high ceramic content is most desirable to yield parts with high

relative densities and consistent microstructures. A more complete model that resolves the effect of a neutral polymer depletant in highly loaded systems is needed to fully understand depletion interactions, which may offer a simple approach to manipulate the response of ceramic colloids that can be adapted to a number of ceramic fabrication methods that require near-net morphologies.

Alumina CeraSGels that were injection molded at room-temperature produced ring-shaped samples that were machinable in the green state after drying. The PVP-based binder was removed by thermal pyrolysis, resulting in alumina rings with high green densities (>60%TD). In conventional ceramic injection molding, parts are typically ejected from a mold within the first minute of forming.¹³¹ To reduce the time required to dry and remove an injection molded CeraSGel part, utilizing a more porous mold material to facilitate evaporation will promote more rapid demolding in future studies. High sintered densities (98%TD) were achieved by pressureless sintering, and SEM micrographs confirmed that sintered specimens had a dense microstructure with minimal pore formation and grain sizes of $\sim 3.4 \mu\text{m}$. Linear shrinkage of <16% was observed in samples. Alumina specimens with mechanical properties comparable to literature were successfully fabricated by this unique room-temperature processing method.

It was determined that alumina CeraSGels containing 2.5 vol.% PVP (MW=55,000 g/mol) resulted in the most favorable combination of properties in formed alumina specimens. These suspensions exhibited a suitable yield point such that suspensions readily flowed in the regimes needed to allow for complete filling of the mold without the suspension prematurely entering the mold. Rheometry revealed that suspensions with 2.5 vol.% PVP (MW=55,000 g/mol) had the lowest flow index found in

this study, implying that the flow behavior was best suited for the fabrication of alumina rings with high green and sintered densities along with high C-strengths via room-temperature injection molding. As a result, 2.5 vol.% PVP with molecular weight of 55,000 g/mol was considered the optimal concentration and type of polymer in the CeraSGels evaluated for room-temperature processing in this study.

PVP with a molecular weight of 10,000 g/mol was varied at contents of 1, 2 and 3 vol.% in ZrB₂/B₄C/WC suspensions to adapt the process to ZrB₂-based CeraSGels for obtaining dense ultra-high temperature ceramic rings. CeraSGels comprised of ZrB₂/B₄C/WC with different PVP contents were found to have a transient flow response that fluctuated from shear thinning to shear thickening at high applied shear stresses. However, the critical shear stresses, which decreased with increasing PVP content, required to initiate flow allowed suspensions to readily fill the mold during the injection molding operation resulting in a ring-shaped part.

The subsequent ZrB₂ rings exhibited robust green strengths such that they could be polished to even out surfaces. A heat treatment to remove the binder and pressureless sinter fully densified the parts, as determined using the Archimedes technique, without impurities negatively affecting the final composition as found by elemental analysis. SEM revealed minimal pore formation within the microstructure and B₄C grains dispersed among ZrB₂ grains containing tungsten, a result of tungsten forming a solid solution with ZrB₂. Although mechanical properties were lower than anticipated, reducing the crosshead speed during filling, increasing PVP content in ZrB₂-based CeraSGels along with other procedural modifications would likely reduce the number of strength-limiting flaws introduced during processing in turn improving the resultant

mechanical properties. Further study of ZrB_2 -based suspensions with increasing PVP contents and varying molecular weight will assist in determining the optimal ZrB_2 CeraSGel composition for room-temperature injection molding.

Future work includes performing high-temperature mechanical testing in addition to room-temperature testing of ZrB_2 rings for compression testing and bars for flexure testing prepared by CeraSGels to compare results with samples made by other processing methods, like hot pressing or gelcasting. Furthermore, a silicon-carbide particulate reinforcing phase will be introduced into ZrB_2 -based suspensions to produce ZrB_2 -SiC composites. Rheological, microstructural and mechanical evaluation will be performed to determine the efficacy of room-temperature injection molding as a processing alternative for advanced ceramic composite material systems.

Initial work has focused on cultivating the process for alumina and ZrB_2 ceramics with promising results. The ultimate goal will be to optimize CeraSGel preparation and room-temperature injection molding for use with any powder-based material system, including but not limited to other advanced ceramics and metals, making room-temperature injection molding a truly universal route for fabricating complex-shaped components in a cost-effective, environmentally safe way. Advancing the understanding of the colloidal stability and instability mechanisms of CeraSGels based on a variety of materials will be crucial to predicting the flow properties of new material systems and their processability. CeraSGels can ultimately be incorporated into other traditional processing methods, like tape casting or extrusion, by careful control and understanding of CeraSGels under different conditions. Through further study and development, the simplicity and adaptability of CeraSGels to a variety of material systems and processing

methods will revolutionize ceramic processing by progressing towards more economical and eco-friendly fabrication of complex-shaped components of advanced ceramic materials.

LIST OF REFERENCES

LIST OF REFERENCES

- ¹E. Wuchina, E. J. Opila, M. Opeka, W. Fahrenholtz, and I. Talmy, "UHTCs: Ultra-High Temperature Ceramic Materials for Extreme Environment Applications," *The Electrochemical Society Interface* (2007).
- ²D. M. Van Wie, D. G. Drewry, Jr., D. E. King, and C. M. Hudson, "The hypersonic environment: Required operating conditions and design challenges," *Journal of Materials Science*, 39[19] 5915-24 (2004).
- ³E. L. Corral and R. E. Loehman, "Ultra-High-Temperature Ceramic Coatings for Oxidation Protection of Carbon-Carbon Composites," *Journal of the American Ceramic Society*, 91[5] 1495-502 (2008).
- ⁴S. R. Levine, E. J. Opila, M. C. Halbig, J. D. Kiser, M. Singh, and J. A. Salem, "Evaluation of ultra-high temperature ceramics for aer propulsion use," *Journal of the European Ceramic Society*, 22[14-15] 2757-67 (2002).
- ⁵L. Scatteia, F. Monteverde, D. Alfano, G. Marino, and S. Cantoni, "Advances in Ultra High Temperature Ceramics For Hot Structures," *Transactions of Space Technology Japan*, 7[26] 73-78 (2009).
- ⁶F. Monteverde, A. Bellosi, and L. Scatteia, "Processing and properties of ultra-high temperature ceramics for space applications," *Materials Science and Engineering: A*, 485[1-2] 415-21 (2008).
- ⁷R. Licheri, R. Orrù, C. Musa, and G. Cao, "Combination of SHS and SPS Techniques for fabrication of fully dense ZrB₂-ZrC-SiC composites," *Materials Letters*, 62[3] 432-35 (2008).
- ⁸W. G. Fahrenholtz, G. E. Hilmas, A. L. Chamberlain, and J. W. Zimmermann, "Processing and characterization of ZrB₂-based ultra-high temperature monolithic and fibrous monolithic ceramics," *Journal of Materials Science*, 39[19] 5951-57 (2004).
- ⁹M. Gasch, S. Johnson, and J. Marschall, "Thermal Conductivity Characterization of Hafnium Diboride-Based Ultra-High-Temperature Ceramics," *Journal of the American Ceramic Society*, 91[5] 1423-32 (2008).
- ¹⁰J. W. Zimmermann, G. E. Hilmas, W. G. Fahrenholtz, R. B. Dinwiddie, W. D. Porter, and H. Wang, "Thermophysical Properties of ZrB₂ and ZrB₂-SiC Ceramics," *Journal of the American Ceramic Society*, 91[5] 1405-11 (2008).

- ¹¹R. Telle, L. S. Sigl, and K. Takagi, "Boride-Based Hard Materials," pp. 802-945. in Handbook of Ceramic Hard Materials. Wiley-VCH Verlag GmbH, 2008.
- ¹²S.-Q. Guo, "Densification of ZrB₂-based composites and their mechanical and physical properties: A review," *Journal of the European Ceramic Society*, 29[6] 995-1011 (2009).
- ¹³Y. M. Chiang, D. P. Birnie, and W. D. Kingery, "Physical Ceramics: Principles for Ceramic Science and Engineering." Wiley, (1996).
- ¹⁴A. Bellosi, F. Monteverde, and D. Sciti, "Fast Densification of Ultra-High-Temperature Ceramics by Spark Plasma Sintering," *International Journal of Applied Ceramic Technology*, 3[1] 32-40 (2006).
- ¹⁵H. Wang, C.-A. Wang, X. Yao, and D. Fang, "Processing and Mechanical Properties of Zirconium Diboride-Based Ceramics Prepared by Spark Plasma Sintering," *Journal of the American Ceramic Society*, 90[7] 1992-97 (2007).
- ¹⁶Z. A. Munir, U. Anselmi-Tamburini, and M. Ohyanagi, "The effect of electric field and pressure on the synthesis and consolidation of materials: A review of the spark plasma sintering method," *Journal of Materials Science*, 41[3] 763-77 (2006).
- ¹⁷V. Medri, F. Monteverde, A. Balbo, and A. Bellosi, "Comparison of ZrB₂-ZrC-SiC Composites Fabricated by Spark Plasma Sintering and Hot-Pressing," *Advanced Engineering Materials*, 7[3] 159-63 (2005).
- ¹⁸M. Omori, "Sintering, consolidation, reaction and crystal growth by the spark plasma system (SPS)," *Materials Science and Engineering: A*, 287[2] 183-88 (2000).
- ¹⁹A. L. Chamberlain, W. G. Fahrenholtz, and G. E. Hilmas, "Pressureless Sintering of Zirconium Diboride," *Journal of the American Ceramic Society*, 89[2] 450-56 (2006).
- ²⁰S. C. Zhang, G. E. Hilmas, and W. G. Fahrenholtz, "Pressureless Densification of Zirconium Diboride with Boron Carbide Additions," *Journal of the American Ceramic Society*, 89[5] 1544-50 (2006).
- ²¹W. G. Fahrenholtz, G. E. Hilmas, S. C. Zhang, and S. Zhu, "Pressureless Sintering of Zirconium Diboride: Particle Size and Additive Effects," *Journal of the American Ceramic Society*, 91[5] 1398-404 (2008).
- ²²S. C. Zhang, G. E. Hilmas, and W. G. Fahrenholtz, "Pressureless Sintering of ZrB₂-SiC Ceramics," *Journal of the American Ceramic Society*, 91[1] 26-32 (2008).
- ²³S. Zhu, W. G. Fahrenholtz, G. E. Hilmas, and S. C. Zhang, "Pressureless sintering of carbon-coated zirconium diboride powders," *Materials Science and Engineering: A*, 459[1-2] 167-71 (2007).
- ²⁴Z. Lü, D. Jiang, J. Zhang, and Q. Lin, "Microstructure and Mechanical Properties of Zirconium Diboride Obtained by Aqueous Tape Casting Process and Hot Pressing," *Journal of the American Ceramic Society*, 93[12] 4153-57 (2010).

- ²⁵V. Medri, P. Pinasco, A. Sanson, E. Roncari, S. Guicciardi, and A. Bellosi, "ZrB₂-Based Laminates Produced by Tape Casting," *International Journal of Applied Ceramic Technology*, 9[2] 349-57 (2012).
- ²⁶S. L. Natividad, V. R. Marotto, L. S. Walker, D. Pham, W. Pinc, and E. L. Corral, "Tape Casting Thin, Continuous, Homogenous, and Flexible Tapes of ZrB₂," *Journal of the American Ceramic Society*, 94[9] 2749-53 (2011).
- ²⁷R. He, X. Zhang, P. Hu, C. Liu, and W. Han, "Aqueous gelcasting of ZrB₂-SiC ultra high temperature ceramics," *Ceramics International*, 38[7] 5411-18 (2012).
- ²⁸Z. Lü, D. Jiang, J. Zhang, and Q. Lin, "Aqueous Tape Casting of Zirconium Diboride," *Journal of the American Ceramic Society*, 92[10] 2212-17 (2009).
- ²⁹Z. Lü, D. Jiang, J. Zhang, and Q. Lin, "Processing and properties of ZrB₂-SiC composites obtained by aqueous tape casting and hot pressing," *Ceramics International*, 37[1] 293-301 (2011).
- ³⁰J. L. Johnson and R. M. German, "PIM Materials," *Advanced Materials & Processes*, 161[4] (2003).
- ³¹B. C. Mutsuddy and R. G. Ford, "Ceramic Injection Molding," 1 ed. Chapman & Hall: London, (1995).
- ³²N. G. McCrum, C. P. Buckley, and C. B. Bucknall, "Principles of Polymer Engineering," 2nd ed. Oxford Science Publications, (2001).
- ³³J. P. Beaumont, R. Nagel, and R. Sherman, "Successful Injection Molding." Hanser Gardner Publications, Inc.: Cincinnati, (2002).
- ³⁴J. S. Reed, "Principles of Ceramic Processing," 2nd ed. Wiley Inter-Science, (1995).
- ³⁵V. M. Kryachek, "Injection Moulding (Review)," *Powder Metallurgy and Metal Ceramics*, 43[7] 336-48 (2004).
- ³⁶M. J. Edirisinghe, H. M. Shaw, and K. L. Tomkins, "Flow Behaviour of Ceramic Injection Moulding Suspensions," *Ceramics International*, 18 193-200 (1991).
- ³⁷R. G. Larson, "The Structure and Rheology of Complex Fluids." Oxford University Press: New York, (1999).
- ³⁸V. N. Shukla and D. C. Hill, "Binder Evolution from Powder Compacts: Thermal Profile for Injection-Molded Articles," *Journal of the American Ceramic Society*, 72[10] 1797-803 (1989).
- ³⁹M. Takahashi, S. Suzuki, H. Nitanda, and E. Arai, "Mixing and Flow Characteristics in the Alumina/Thermoplastic Resin System," *Journal of the American Ceramic Society*, 71[12] 1093-99 (1988).
- ⁴⁰Y. Luting, S. Wenjie, X. Tao, and M. Hezhuo, "Preparation of CIM Feedstock of Al₂O₃-SiC Nanocomposite," *Key Engineering Materials*, 280-283 1089-92 (2005).

- ⁴¹R. E. F. Q. Nogueira, A. C. Bezerra, F. C. dos Santos, M. R. de Sousa, and W. Acchar, "Low-Pressure Injection Molding of Alumina Ceramics Using a Carnauba Wax Binder: Preliminary Results," *Key Engineering Materials*, 189-191 67-72 (2001).
- ⁴²M. J. Edirisinghe and J. R. G. Evans, "Review: Fabrication of engineering ceramics by injection moulding. I. Materials selection," *International Journal of High Technology Ceramics*, 2[1] 1-31 (1986).
- ⁴³W. J. Tseng, "Influence of surfactant on rheological behaviors of injection - molded alumina suspensions," *Materials Science and Engineering A*, 289 116-22 (2000).
- ⁴⁴M. A. Janney, O. O. Omatete, C. A. Walls, S. D. Nunn, R. J. Ogle, and G. Westmoreland, "Development of Low-Toxicity Gelcasting Systems," *J. Am. Ceram. Soc.*, 81[3] 581-97 (1998).
- ⁴⁵R. J. Huzzard and S. Blackburn, "A water-based system for ceramic injection moulding," *Journal of the European Ceramic Society*, 17[2-3] 211-16 (1997).
- ⁴⁶A. J. Fanelli, R. D. Silvers, W. S. Frei, J. V. Burlew, and G. B. Marsh, "New Aqueous Injection Molding Process for Ceramic Powders," *Journal of the American Ceramic Society*, 72[10] 1833-36 (1989).
- ⁴⁷D. V. Rosato, D. V. Rosato, and M. G. Rosato, "Injection Molding Handbook (3rd Edition)." in Springer - Verlag, 2000.
- ⁴⁸W. M. Sigmund, N. S. Bell, and L. Bergstrom, "Novel Powder-Processing Methods for Advanced Ceramics," *J. Am. Ceram. Soc.*, 83[7] 1557-74 (2000).
- ⁴⁹C. Karatas, A. Kocer, H. I. Unal, and S. Saritas, "Rheological properties of feedsstocks prepared with steatite powder and polyethylene-based thermoplastic binders," *Journal of Materials Processing Technology*, 152 77-83 (2004).
- ⁵⁰X. Du, M. Qin, I. S. Humail, P. Feng, and X. Qu, "Effects of Different Debinding Atmosphere on the Properties of Powder Injection Molded AlN Ceramics," *Key Engineering Materials*, 336-338 1028-30 (2007).
- ⁵¹L. Matrici, S. Domsa, and L. Brandusan, "Aspects Concerning Rheological Properties of the CIM's Binder Systems," *Advanced Materials Research*, 23 107-10 (2007).
- ⁵²W. J. Tseng, D.-M. Liu, and C.-K. Hsu, "Influence of stearic acid on suspension structure and green microstructure of injection-molded zirconia ceramics," *Ceramics International*, 25 191-95 (1999).
- ⁵³D. R. Dinger, "Rheology for Ceramists. " Dinger Ceramic Consulting Service, (2002).
- ⁵⁴M. Acosta, V. L. Wiesner, C. J. Martinez, J. P. Youngblood, and R. W. Trice, "Effect of Polyvinylpyrrolidone Additions on the Rheology of Aqueous, Highly Loaded Alumina Suspensions," *Journal of the American Ceramic Society*, 96[5] 1372-82 (2013).
- ⁵⁵V. L. Wiesner, J. P. Youngblood, and R. W. Trice, "Room-temperature injection molding of aqueous alumina-polyvinylpyrrolidone suspensions," *Journal of the European Ceramic Society*, 34[2] 453-63 (2014).

- ⁵⁶R. T. Vanderbilt Company, "Darvan 821A Technical Data Sheet," 2009.
- ⁵⁷A. C. Young, O. O. Omatete, M. A. Janney, and P. A. Menchhofer, "Gelcasting of Alumina," *Journal of the American Ceramic Society*, 74[3] 612-18 (1991).
- ⁵⁸M. Burke, R. Greenwood, and K. Kendall, "Experimental methods for measuring the optimum amount of dispersant for seven Sumitomo alumina powders," *Journal of Materials Science*, 33[21] 5149-56 (1998).
- ⁵⁹ASTM C 1323-10, "Standard Test Method for Ultimate Strength of Advanced Ceramics with Diametrically Compressed C-Ring Specimens at Ambient Temperature." ASTM International: West Conshohocken, PA, (2010).
- ⁶⁰R. J. Hunter, "Introduction to Modern Colloid Science." Oxford Science Publications: New York, (2003).
- ⁶¹C. H. Schilling, M. Sikora, P. Tomasik, C. Li, and V. Garcia, "Rheology of alumina-nanoparticle suspensions: effects of lower saccharides and sugar alcohols," *Journal of the European Ceramic Society*, 22[6] 917-21 (2002).
- ⁶²L. B. Garrido and A. N. Califano, "Effect of an Excess Polyelectrolyte on Viscoelastic Properties of Suspensions of Alumina and Zircon Mixtures," *Colloids and Surfaces A: Physicochemical and Engineering Aspects*, 302 24-30 (2007).
- ⁶³B. G. Liptak, "Instrument Engineers' Handbook," 4th ed. CRC Press: Boca Raton, Florida, (2003).
- ⁶⁴ASTM C 373-88, "Standard Test Method for Water Absorption, Bulk Density, Apparent Porosity, and Apparent Specific Gravity of Fired Whiteware Products." ASTM International: West Conshohocken, PA, (2006).
- ⁶⁵ASTM C 1322-05b, "Standard Practice for Fractography and Characterization of Fracture Origins in Advanced Ceramics." ASTM International: West Conshohocken, PA, (2010).
- ⁶⁶D. C. Montgomery, G. C. Runger, and N. F. Hubele, "Engineering Statistics," 4th ed. John Wiley & Sons, Inc.: New York, NY, (2007).
- ⁶⁷M. S. Subbanna, Pradip, and S. G. Malghan, "Shear Yield Stress of Flocculated Alumina-Zirconia Mixed Suspensions: Effect of Solid Loading, Composition and Particle Size Distribution," *Chem. Eng. Sci.*, 17[530] 3073-19 (1998).
- ⁶⁸R. Moreno, "Rheology." in *Encyclopedia of Materials - Science and Technology*, Vol. 1-11. Edited by K. H. J. Buschow, R. W. Cahn, M. C. Flemings, B. Ilschner, E. J. Kramer, and S. Mahajan. Elsevier, 2001.
- ⁶⁹M. Pattanaik and S. K. Bhaumic, "Adsorption Behavior of Polyvinyl Pyrrolidone on Oxide Surfaces," *Materials Letters*, 44 352-60 (2000).
- ⁷⁰J. A. Lewis, "Colloidal Processing of Ceramics," *Journal of the American Ceramic Society*, 83[10] 2341-59 (2000).

- ⁷¹N. Nagendra, S. Biswas, and S. Bandopadhyay, "Evaluation of mechanical properties of tubular LSFCE perovskite membranes at elevated temperatures in reactive environments," *Solid State Ionics*, 195[1] 16-24 (2011).
- ⁷²R. H. Carter, J. H. Underwood, J. J. Swab, A. A. Wereszczak, C. Leveritt, R. Emerson, and L. Burton, "Material Selection for Ceramic Gun Tube Liner," *Materials & Manufacturing Processes*, 21[6] 584-90 (2006).
- ⁷³J. B. Wachtman, "Mechanical Properties of Ceramics." John Wiley & Sons, Inc.: New York, (1996).
- ⁷⁴A. Krell and P. Blank, "The Influence of shaping method on the grain size dependence of strength in dense submicrometre alumina," *Journal of the European Ceramic Society*, 16[11] 1189-200 (1996).
- ⁷⁵A. Krell, E. Pippel, J. Woltersdorf, and W. Burger, "Subcritical crack growth in Al₂O₃ with submicron grain size," *Journal of the European Ceramic Society*, 23[1] 81-89 (2003).
- ⁷⁶F. Harbach and H. Nienburg, "Homogeneous Functional Ceramic Components Through Electrophoretic Deposition from Stable Colloidal Suspensions-I. Basic Concepts and Application to Zirconia," *J. Am. Cer. Soc.*, 18[6] 675-83 (1998).
- ⁷⁷J. S. Reed, "Common Raw Materials/Industrial Inorganic Chemicals," pp. 40-49. in Principles of Ceramics Processing. Wiley Interscience, 1995.
- ⁷⁸D. Hotza and P. Greil, "Review: Aqueous Tape Casting of Ceramics Powders," *Materials Science and Engineering A*, 202 206-17 (1995).
- ⁷⁹W. M. Sigmund, N. S. Bell, and L. Bergström, "Novel Powder-Processing Methods for Advanced Ceramics," *J. Am. Cer. Soc.*, 83[7] 1557-74 (2000).
- ⁸⁰R. J. Hunter, "Foundations of Colloid Science," Vol. 2. Oxford University Press: Oxford, (2001).
- ⁸¹P. Somasundaran, "Encyclopedia of Surface And Colloid Science," Vol. 7, (2006).
- ⁸²A. L. Ogden and J. A. Lewis, "Effect of Nonadsorbed Polymer on the Stability of Weakly Flocculated Suspensions," *Langmuir*, 12 3413-34 (1996).
- ⁸³R. I. Feigin and D. H. Napper, "Depletion stabilization and depletion flocculation," *Journal of Colloid and Interface Science*, 75[2] 525-41 (1980).
- ⁸⁴R. I. Feigin and D. H. Napper, "Stabilization of colloids by free polymer," *Journal of Colloid and Interface Science*, 74[2] 567-71 (1980).
- ⁸⁵R. G. Horn, "Surface Forces and their Action in Ceramic Materials," *J. Am. Cer. Soc.*, 73[5] 1117-35 (1990).
- ⁸⁶A. Dakskobler, K. Kočevár, and T. Kosmač, "Short Range Repulsive Potential Developed by the Addition of Mg(II) Ions to Aqueous Alumina Slurries," *Journal of the European Ceramic Society*, 21 2361-68 (2001).

- ⁸⁷A. Dakskobler and T. Kosmač, "Weakly Flocculated Aqueous Alumina Suspensions Prepared by the Addition of Mg(II) Ions," *J. Am. Cer. Soc.*, 83[3] 666-68 (2000).
- ⁸⁸A. Dakskobler and T. Kosmač, "Destabilization of an Alkaline Aqueous Alumina Suspension by the Addition of Magnesium Acetate," *Colloids and Surfaces A: Physicochemical and Engineering Aspects*, 195 197-203 (2001).
- ⁸⁹Zschimmer & Schwarz, "Dolapix CE 64." in. Edited by T. D. Sheet, 2012.
- ⁹⁰R. Moreno, A. Salomoni, and I. Stamenkovic, "Influence of slip rheology on pressure casting of alumina," *Journal of the European Ceramic Society*, 17[2-3] 327-31 (1997).
- ⁹¹S. Novak and K. König, "Fabrication of alumina parts by electrophoretic deposition from ethanol and aqueous suspensions," *Ceramics International*, 35[7] 2823-29 (2009).
- ⁹²S. Novak, G. Dražić, and S. Macek, "A study of ceramic-suspension solidification using complex-impedance spectroscopy," *Journal of the European Ceramic Society*, 21[10-11] 2081-84 (2001).
- ⁹³G. Tari, J. M. F. Ferreira, A. T. Fonseca, and O. Lyckfeldt, "Influence of particle size distribution on colloidal processing of alumina," *Journal of the European Ceramic Society*, 18[3] 249-53 (1998).
- ⁹⁴S. Gaydardzhiev and P. Ay, "Characterization of Aqueous Suspensions of Fumed Aluminum Oxide in the Presence of Two Dolapix Surfactants," *J. Mater. Sci.*, 41 5257-62 (2006).
- ⁹⁵I. Száraz and W. Forlsing, "PVP and Azelaic Acid Adsorption on γ -alumina Studied by FT-IR Spectroscopy," *Vibrational Spectroscopy*, 29 15-20 (2002).
- ⁹⁶C. Maltesh, P. Somasundaran, R. A. Kulkarni, and S. Gundiah, "Polymer-Polymer Complexation in Dilute Aqueous Solutions: Poly(acrylic acid)-Poly(ethylene oxide) and Poly(Acrylic acid)-Poly(vinylpyrrolidone)," *Langmuir*, 7 2108-11 (1991).
- ⁹⁷K. Esumi, "Adsorption of Polymer and Surfactant from Their Binary Mixtures on Alumina," pp. 138-52. in *Surfactant Adsorption and Surface Solubilization*, Vol. 615. *ACS Symposium Series*. American Chemical Society, 1996.
- ⁹⁸M. S. Ali, M. Suhail, G. Ghosh, M. Kammil, and Kabir-ud-Din, "Interactions Between Cationic Gemini/Conventional Surfactants with Polyvinylpyrrolidone: Specific Conductivity and Dynamic Light Scattering Studies," *Colloids and Surfaces A: Physicochemical and Engineering Aspects*, 350 51-56 (2009).
- ⁹⁹H. M. Wyss, E. V. Tervoort, and L. J. Gauckler, "Mechanics and Microstructures of Concentrated Particle Gels," *J. Am. Cer. Soc.*, 88[9] 2337-48 (2005).
- ¹⁰⁰J. A. Lewis, "Colloidal Processing of Ceramics," *J. Am. Cer. Soc.*, 83[10] 2341-59 (2000).

- ¹⁰¹M. Pradhan and P. Bhargava, "Influence of Sucrose Addition on the Rheology of Alumina Slurries Dispersed with Polyacrylate Dispersant," *J. Am. Cer. Soc.*, 88[4] 833-38 (2005).
- ¹⁰²J. Israelachvili, "Intermolecular and Surface Forces," pp. 450 Second ed. Academic Press: Oxford, UK, (1991).
- ¹⁰³P. J. Flory, "Statistical Mechanics of Chain Molecules." Hanser Gardner Pubns, (1989).
- ¹⁰⁴R. J. Flatt and P. Bowen, "Yodel: A Yield Stress Model for Suspensions," *Journal of the American Ceramic Society*, 89[4] 1244-56 (2006).
- ¹⁰⁵E. Tarassova, V. Aseyev, H. Tenhu, and S. Klenin, "Poly(vinyl pyrrolidone)-C70 complexes in aqueous solutions," *Polymer*, 44[17] 4863-70 (2003).
- ¹⁰⁶J. K. Armstrong, R. B. Wenby, H. J. Meiselman, and T. C. Fisher, "The Hydrodynamic Radii of Macromolecules and Their Effect on Red Blood Cell Aggregation," *Biophysical Journal*, 87[6] 4259-70 (2004).
- ¹⁰⁷W. B. Russel, "Review of the Role of Colloidal Forces in the Rheology of Suspensions," *Journal of Rheology*, 24[3] 287-317 (1980).
- ¹⁰⁸J. E. Seebergh and J. C. Berg, "Depletion flocculation of aqueous, electrosterically-stabilized latex dispersions," *Langmuir*, 10[2] 454-63 (1994).
- ¹⁰⁹A. L. Ogden and J. A. Lewis, "Effect of Nonadsorbed Polymer on the Stability of Weakly Flocculated Suspensions," *Langmuir*, 12[14] 3413-24 (1996).
- ¹¹⁰L. Bergström, "Hamaker constants of inorganic materials," *Advances in Colloid and Interface Science*, 70[0] 125-69 (1997).
- ¹¹¹B. Vincent, J. Edwards, S. Emmett, and A. Jones, "Depletion flocculation in dispersions of sterically-stabilised particles ("soft spheres")," *Colloids and Surfaces*, 18[2-4] 261-81 (1986).
- ¹¹²D. H. Napper, "Polymeric Stabilization of Colloidal Dispersions." Academic Press Inc.: New York, (1983).
- ¹¹³T. van den Boomgaard, T. A. King, T. F. Tadros, H. Tang, and B. Vincent, "The influence of temperature on the adsorption and adsorbed layer thickness of various molecular weight fractions of poly(vinyl alcohol) on polystyrene latex particles," *Journal of Colloid and Interface Science*, 66[1] 68-76 (1978).
- ¹¹⁴R. Hogg, T. W. Healy, and D. W. Fuerstenau, "Mutual coagulation of colloidal dispersions," *Transactions of the Faraday Society*, 62[0] 1638-51 (1966).
- ¹¹⁵J. Cesarano III and I. A. Aksay, "Processing of Highly Concentrated Aqueous alpha-Alumina Suspensions Stabilized with Polyelectrolytes," *Journal of the American Ceramic Society*, 71[12] 1062-67 (1988).
- ¹¹⁶Y. Mao, M. E. Cates, and H. N. W. Lekkerkerker, "Depletion force in colloidal systems," *Physica A: Statistical Mechanics and its Applications*, 222[1-4] 10-24 (1995).

- ¹¹⁷B. Vincent, P. F. Luckham, and F. A. Waite, "The effect of free polymer on the stability of sterically stabilized dispersions," *Journal of Colloid and Interface Science*, 73[2] 508-21 (1980).
- ¹¹⁸T. Kuhl, Y. Guo, J. L. Alderfer, A. D. Berman, D. Leckband, J. Israelachvili, and S. W. Hui, "Direct Measurement of Polyethylene Glycol Induced Depletion Attraction between Lipid Bilayers," *Langmuir*, 12[12] 3003-14 (1996).
- ¹¹⁹P. Jenkins and M. Snowden, "Depletion flocculation in colloidal dispersions," *Advances in Colloid and Interface Science*, 68[0] 57-96 (1996).
- ¹²⁰M. Acosta, "Design and Manufacture of Ultra-High Temperature Ceramics with Oriented Strengthening and Toughening Phases," Ph.D. Dissertation, Purdue University, West Lafayette, IN, 2012.
- ¹²¹A. Krell, P. Blank, H. Ma, T. Hutzler, and M. Nebelung, "Processing of High-Density Submicrometer Al₂O₃ for New Applications," *Journal of the American Ceramic Society*, 86[4] 546-53 (2003).
- ¹²²T. Huang, G. E. Hilmas, W. G. Fahrenholtz, and M. C. Leu, "Dispersion of Zirconium Diboride in an Aqueous, High-Solids Paste," *International Journal of Applied Ceramic Technology*, 4[5] 470-79 (2007).
- ¹²³P. S. Kisliy, M. A. Kuzenkova, and O. V. Zaveruha, "On the Sintering Process of Zirconium Diboride with Tungsten," *Phys. Sint.*, 3[1] 29-44 (1971).
- ¹²⁴S. C. Zhang, G. E. Hilmas, and W. G. Fahrenholtz, "Improved Oxidation Resistance of Zirconium Diboride by Tungsten Carbide Additions," *Journal of the American Ceramic Society*, 91[11] 3530-35 (2008).
- ¹²⁵W. D. Callister and D. G. Rethwisch, "Materials Science and Engineering: An Introduction." John Wiley & Sons Canada, Limited, (2009).
- ¹²⁶A. L. Chamberlain, W. G. Fahrenholtz, G. E. Hilmas, and D. T. Ellerby, "High-Strength Zirconium Diboride-Based Ceramics," *Journal of the American Ceramic Society*, 87[6] 1170-72 (2004).
- ¹²⁷F. Monteverde, "The addition of SiC particles into a MoSi₂-doped ZrB₂ matrix: Effects on densification, microstructure and thermo-physical properties," *Materials Chemistry and Physics*, 113[2-3] 626-33 (2009).
- ¹²⁸F. Monteverde, S. Guicciardi, and A. Bellosi, "Advances in microstructure and mechanical properties of zirconium diboride based ceramics," *Materials Science and Engineering: A*, 346[1-2] 310-19 (2003).
- ¹²⁹W. G. Fahrenholtz, G. E. Hilmas, I. G. Talmy, and J. A. Zaykoski, "Refractory Diborides of Zirconium and Hafnium," *Journal of the American Ceramic Society*, 90[5] 1347-64 (2007).
- ¹³⁰Y. Yan, Z. Huang, S. Dong, and D. Jiang, "Pressureless Sintering of High-Density ZrB₂-SiC Ceramic Composites," *Journal of the American Ceramic Society*, 89[11] 3589-92 (2006).

- ¹³¹R. M. German and A. Bose, "Injection Molding of Metals and Ceramics." Metal Powder Industries Federation: Princeton, (1997).

VITA

VITA

Valerie L. Wiesner was born in January of 1986 in Lawrence, Kansas. From 2004 to 2008 she attended Carleton College in Northfield, Minnesota, where she earned a B.A. in Physics and a concentration in Japanese Language and Literature. During her undergraduate career, Valerie actively participated in research opportunities, including NSF-sponsored internships at both Purdue University and Cornell University in Materials Science and Engineering. Additionally, at Carleton College she contributed to astrophysics research in collaboration with the National Radio Astronomy Observatory Green Bank Telescope in West Virginia for nearly three years. Upon completing her undergraduate studies, Valerie spent one year working as a primary and junior high school English teacher and translator for the Musashimurayama Board of Education in Tokyo, Japan, through the Japan Exchange and Teaching (JET) Programme sponsored by the Japanese Government.

Valerie began her graduate studies at the Purdue University School of Materials Engineering in August of 2009. She was advised by Prof. Rodney Trice and Prof. Jeffrey Youngblood on her doctoral research, which focused on developing a novel ceramic injection molding process to allow for production of complex-shaped parts at room temperature in an environmentally friendly, low-cost way. She has presented ten conference talks at international conferences as well as has two publications stemming

from her graduate research. She has received several awards, including the Graduate Excellence in Materials Science (GEMS) Diamond Award presented by the American Ceramic Society (ACerS) at the 2013 Materials Science & Technology (MS&T) Conference in Montréal, Québec, Canada. She was selected to participate in the NASA Pathways Program to work at the Ceramics Branch located at NASA Glenn Research Center in Cleveland, Ohio, during the summer of 2013.

In addition to research, Valerie was actively involved in teaching, mentoring, outreach and recruitment activities within Purdue University and the ceramics field. She held several leadership positions, including Recruitment Chair (2013) for the American Ceramic Society's President's Council of Student Advisors (ACerS' PCSA), Purdue University Women in Engineering Graduate Mentoring Program (GMP) Leadership Team Member (2011-13) as well as Secretary (2010-11) and Recruitment Chair (2012-2013) for the Purdue University Materials Science and Engineering Graduate Student Association (MSEGSA), during her tenure as a graduate student. She participated in and led numerous outreach activities for the School of Materials Engineering, College of Engineering and Women in Engineering Program. Valerie was recognized for her efforts as the recipient of the 2013 Purdue University School of Materials Engineering Outstanding Graduating Graduate Student Award and the 2013 Purdue University College of Engineering Outstanding Service Award. After graduation, Valerie will join the Ceramics Branch at NASA Glenn Research as a Materials Engineer.

PUBLICATIONS

PUBLICATIONS

- V. L. Wiesner, J. P. Youngblood and R. W. Trice, "Room-temperature injection molding of aqueous alumina-polyvinylpyrrolidone suspensions," *Journal of the European Ceramic Society*, 34[2] 453-63 (2014).
- M. Acosta, V. L. Wiesner, C. J. Martinez, J. P. Youngblood and R. W. Trice, "Effect of Polyvinylpyrrolidone Additions on the Rheology of Aqueous, Highly Loaded Alumina Suspensions," *Journal of the American Ceramic Society*, 96[5] 1372-82 (2013).